CHALMERS

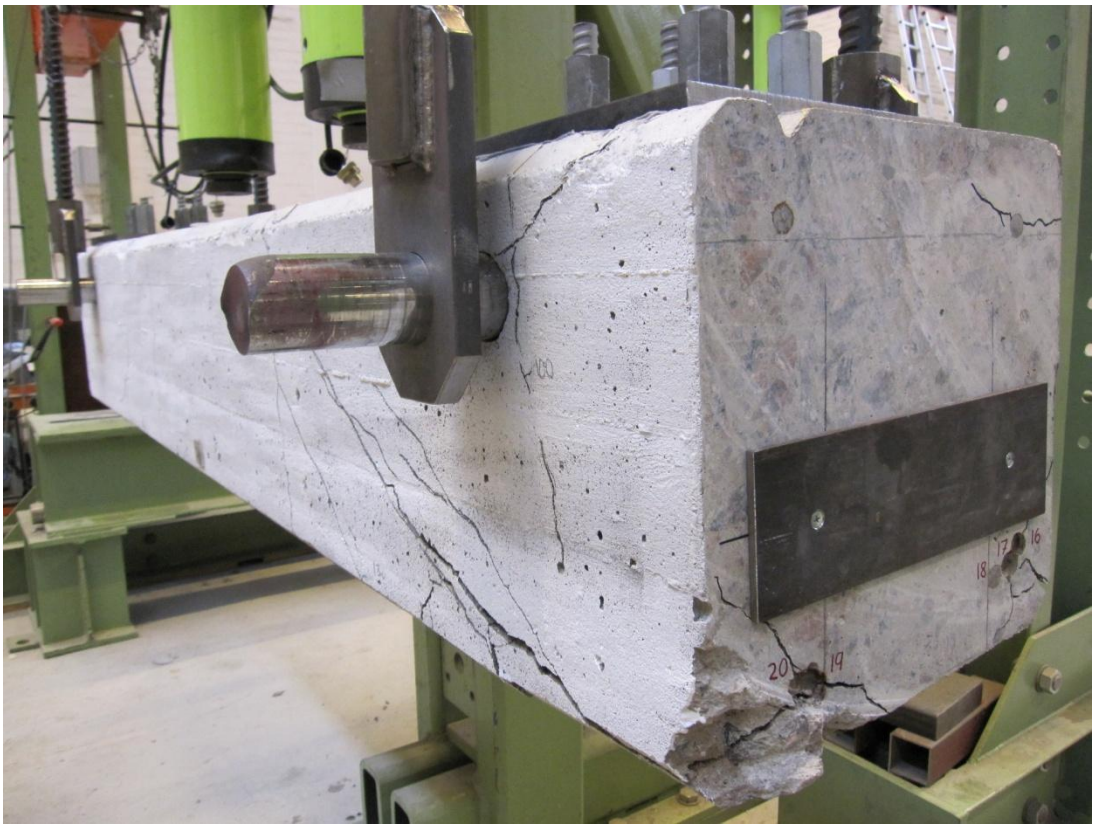

# Design of Test Set-up using FEM

## Pilot Tests on Anchorage of Naturally Corroded Reinforcement

*Master of Science Thesis in the Master's Programme Structural Engineering and Building Performance Design*

FREDRIK BERG
DAVID JOHANSSON

Department of Civil and Environmental Engineering
*Division of Structural Engineering*
*Concrete Structures*
CHALMERS UNIVERSITY OF TECHNOLOGY
Göteborg, Sweden 2011
Master's Thesis 2011:33

MASTER'S THESIS 2011:33

# Design of Test Set-up using FEM

Pilot Tests on Anchorage of Naturally Corroded Reinforcement

*Master of Science Thesis in the Master's Programme Structural Engineering and Building Performance Design*

FREDRIK BERG

DAVID JOHANSSON

Department of Civil and Environmental Engineering
*Division of Structural Engineering*
*Concrete Structures*
CHALMERS UNIVERSITY OF TECHNOLOGY
Göteborg, Sweden 2011

Design of Test Set-up using FEM
Pilot Tests on Anchorage of Naturally Corroded Reinforcement

*Master of Science Thesis in the Master's Programme Structural Engineering and Building Performance Design*

FREDRIK BERG
DAVID JOHANSSON



Examensarbete / Institutionen för bygg- och miljöteknik,
Chalmers tekniska högskola 2011:33

Department of Civil and Environmental Engineering
Division of Structural Engineering
Concrete Structures
Chalmers University of Technology
SE-412 96 Göteborg
Sweden
Telephone: + 46 (0)31-772 1000

Cover:
Anchorage failure of an edge beam specimen from Stallbackabron. Photograph taken by Fredrik Berg: 18 May 2011.

Reproservice, Chalmers University of Technology
Göteborg, Sweden 2011

Design of Test Set-up using FEM
Pilot Tests on Anchorage of Naturally Corroded Reinforcement

*Master of Science Thesis in the Master's Programme Structural Engineering and Building Performance Design*

FREDRIK BERG
DAVID JOHANSSON
Department of Civil and Environmental Engineering
Division of Structural Engineering
Concrete Structures
Chalmers University of Technology

## ABSTRACT

Corrosion of reinforcement is one of the most common causes of deterioration in reinforced concrete structures. So far, most of the knowledge about the structural behaviour of corroded reinforced concrete structures is based on experimental investigations of artificially corroded concrete specimens. This constitutes the base for existing analytical and numerical models. In order to investigate their reliability and representativeness in comparison to field conditions, tests on naturally corroded concrete structures are essential. The aim of this thesis is to design a test set-up using a non-linear finite element method so that an anchorage failure takes place in experiments of edge beams taken from Stallbackabron; a composite bridge with steel beams and a concrete deck, located outside Trollhättan in Sweden. The specimens showed different extent of corrosion induced damage, from no sign of corrosion to extensive cover cracking resulting in spalling of the concrete cover. A four point bending test, indirectly supported with suspension hangers, was considered to be the most promising test set-up. Details of the configuration were designed by conducting a parametric study by simulating the test set-up using non-linear finite element analysis prior to actual testing. Several parameters were investigated: the location of the suspension hole, the position of the loads and the effects of notches. It was found that the edge beams needed to be strengthened; hence, strengthening became an additional parameter in the design. The finite element software DIANA, together with the pre- and post-processor FX+ was used for the analyses. Simulations of the test set-ups were first done in two dimensions. However, this showed to be insufficient for describing anchorage failure; hence, more advanced, three-dimensional, simulations were conducted. From the three-dimensional analyses a promising test set-up was established; this was later validated in two pilot tests carried out at the laboratory of Structural Engineering at Chalmers University of Technology. The first pilot test resulted in local failure of the suspension hole, due to insufficient detailing of the strengthening. The detailing was improved in the second pilot test in a successful manner; thus, the second pilot test confirmed that the test configuration, established through non-linear finite element method, captured anchorage failure as intended.

Key words: Naturally corrosion, anchorage, design of test set-up, non-linear finite element method, experiments

Utformning av provuppställning genom tillämpning av FEM
Pilotförsök av förankring hos naturligt korroderad armering
Examensarbete inom Structural Engineering and Building Performance Design
FREDRIK BERG
DAVID JOHANSSON
Institutionen för bygg- och miljöteknik
Avdelningen för Konstruktionsteknik
Betongbyggnad
Chalmers tekniska högskola

## SAMMANFATTNING

Korrosion är en av de vanligaste nedbrytningsmekanismerna av armerade betongkonstruktioner. Kunskapen om dess nedbrytande effekt av de konstruktionstekniska egenskaperna baseras främst på experimentella undersökningar av artificiellt korroderade provkroppar. Analytiska, såväl som numeriska, modeller har utvecklats utifrån sådana undersökningar. Försök med naturligt korroderade betongkonstruktioner är nödvändiga för att avgöra och bedöma de empiriska modellernas tillförlitlighet och representativitet. Syftet med detta examensarbete är att utforma en provuppställning, med hjälp av en olinjär finit elementmetod, så att förankringsbrott erhålls i försök med kantbalkar tagna från Stallbackabron; en samverkansbro med stålbalkar och betongplatta, lokaliserad utanför Trollhättan i Sverige. Provkropparna visade olika grad av korrosionsinducerade skador, från inga tecken av korrosion till omfattande sprickbildning som lett till spjälkning av betongen. Ett upphängt fyrpunktstest med indirekta stöd ansågs vara den mest lovande provuppställningen för försöken. Detaljer i uppställningen utformades i en parameterstudie. Flera parametrar undersöktes: placering av upphängningshålet, lasternas position och inverkan av urholkning eller utskurna jack. Det kunde konstateras att kantbalkarna behövde förstärkas; förstärkningen tillkom då som en parameter i studien. DIANA, ett finit elementprogram, användes för att genomföra analyserna tillsammans med modellerings– och resultathanteringsprogrammet FX+. Simuleringar av provuppställningar utfördes först i två dimensioner. Detta visade sig dock vara otillräckligt för att beskriva förankringsbrott, därför kom en mer avancerad tredimensionell simulering att genomföras. Från de tredimensionella analyserna fastställdes en lovande provuppställning. Denna validerades efter två pilotförsök, utförda i laboratoriet tillhörande avdelningen för konstruktionsteknik, institutionen för bygg- och miljöteknik, vid Chalmers tekniska högskola. Det första pilotförsöket uppvisade lokalt brott vid upphängningshålet, till följd av bristfällig utformning av förstärkningen. Utformningen förbättrades vilket medförde att det andra pilotförsöket lyckades. Därmed kunde det bekräftas att provuppställningen, erhållen genom den olinjära finita elementmetoden, gav upphov till förankringsbrott.

Nyckelord: Naturlig korrosion, förankring, utformning av provuppställning, olinjär finite element metod, experiment

# Contents

# Preface

The work in this thesis was carried out from December 2010 to May 2011 at the Department of Civil and Environmental Engineering, Division of Structural Engineering, Concrete Structures, Chalmers University of Technology.

It was a great privilege to do research at Chalmers under the supervision of Ph.D Kamyab Zandi Hanjari, Associate Professor Mario Plos and Associate Professor Karin Lundgren, who also was the examiner. They all inspired us by showing great interest in our work and by their never ceasing engagement and support. It cannot be stated how much they have contributed to this thesis; their experience and knowledge were invaluable! Thank you!

We also would like to thank Ph. D. Jonas Magnusson, Professor Björn Engström and Professor Mohammad Al-Emrani, for taking interest in our work and offering their knowledge and experience.

It should be noted that the investigation of promising concrete structures for this thesis were done by Zandi Hanjari and Plos. Their major effort in finding the naturally corroded specimens deserves all gratitude!

Ph.D. Zandi Hanjari is also highly appreciated for always helping and guiding us in our work with the FE modelling.

We would also like to thank our opponents, Paulina Nenonen and Johanna Ruul; their brilliant comments of the work were highly appreciated.

Finally, we would like to address our gratitude to Lars Wahlström, Engineer at the laboratory of Structural Engineering at Chalmers University of Technology, for all his work with the experimental tests and for sharing his experience from practice.

Göteborg, May, 2011

Fredrik Berg & David Johansson

# Notations

### Roman upper case letters

| | |
|---|---|
| $A_s$ | Cross section area of reinforcement |
| $A_{st,\ min}$ | Minimum total stirrup area |
| $D_{11}$,$D_{22}$,$D_{33}$ | Stiffness variables |
| $E_c$ | Modulus of elasticity for concrete |
| $E_s$ | Modulus of elasticity for steel reinforcement |
| $G_f$ | Fracture energy |
| $F_1$,$F_2$ | Yield functions |

### Roman lower case letters

| | |
|---|---|
| $a$ | Clear spacing |
| $c_{min}$ | Minimum concrete cover |
| $f_{cc,cyl}$ | Concrete compression strength according to cylinder test |
| $f_{cc,hammer}$ | Concrete compression strength according to hammer test |
| $f_{ck}$ | Concrete compression strength, characteristic |
| $f_{ct}$ | Concrete tension strength |
| $f_{cc}$ | Concrete compression strength |
| $f_{su}$ | Ultimate strength of reinforcement |
| $f_{sy}$ | Yield strength of reinforcement |
| $n$ | Quantity, e.g. reinforcement bars |
| $p$ | Transverse pressure |
| $s_y$ | Slip at yielding |
| $s_1$,$s_2$,$s_3$,$s_4$,$s_5$ | Slip |
| $t_n$ | Normal stress |
| $t_r$ | Radial stress |
| $t_t$ | Bond stress |
| $u_n$ | Relative normal displacement |
| $u_t$ | Slip |

### Greek letters

| | |
|---|---|
| $\alpha$ | Exponent for ascending bond stress |
| $\varepsilon_{su}$ | Yield strain of reinforcement |
| $\varepsilon_{sy}$ | Ultimate strain of reinforcement |
| ø | Diameter |
| $\tau_{max}$ | Maximum bond stress |
| $\tau_y$ | Bond stress when reinforcement yield |
| $\tau_f$ | Bond stress at failure |
| $\tau_{y,pl}$ | Bond stress at plastic stage of reinforcement |

# 1 Introduction

## 1.1 Background

Deep understanding of the effects of deterioration is essential in the development of models which can be used to study the structural behaviour of deteriorated concrete structures. Corrosion of reinforcement is one of the most common causes of deterioration in reinforced concrete structures due to environmental impacts. Analytical and numerical models have been developed based on experimental investigations of artificially corroded specimens. Hence, methods devised to analyze and subsequently predict the mechanical behaviour of reinforced concrete structures with an observed and measured level of deterioration, can be developed.

Anchorage, in prior to shear and bending moment resistance, stands for the main uncertainties in the evaluation of the structural behaviour of a corroded reinforced concrete structures. The bond behaviour, i.e. the interaction between the steel reinforcement and the surrounding concrete, is decisive for both the load bearing capacity and the ductility in the ultimate state, as well for the stiffness distribution and the crack pattern in the service state.

There are reasons to believe that the deterioration caused by natural corrosion does not have the same effects on the structural behaviour as the deterioration caused by artificial corrosion. In order to validate the empirical models based on investigations of artificially corroded concrete members, and determine their reliability and representativeness in field conditions, tests on naturally corroded concrete structures are essential.

The edge beams of Stallbackabron, a composite bridge with steel beams and a concrete deck, located outside Trollhättan in Sweden, have shown different extent of corrosion induced damage, from no sign of corrosion to extensive cover cracking resulting in spalling of concrete cover. At this moment, the bridge goes through an extensive rehabilitation which consists of replacing the outermost slabs and the edge beams; this gave an exclusive opportunity to do research on very promising naturally corroded concrete members.

## 1.2 Aim, method and limitations

The aim of this thesis is to design a test-set up using non-linear finite element method so that anchorage failure occurs in experiments of edge beams from Stallbackabron. Furthermore, a few pilot tests should be carried out in order to validate the established test configuration.

## 1.3 Outline of contents

In Chapter 1, the aim, method and limitations of the work are given. Chapter 2 presents an overview of bond and anchorage of ribbed bars in concrete members. Chapter 3 deals with the test specimens used in the experiments. The choice and design of test set-up, using non-linear finite method, are discussed in Chapter 4. Chapter 5 deals with the experiments. The main conclusions are given in Chapter 6 and recommendations and suggestions for further research are presented in Chapter 7.

# 2 Bond behaviour of ribbed bars

In common design of reinforced concrete structures, such as beams, the tension caused by bending moment is mainly resisted by the steel reinforcement, while the concrete alone is usually capable of resisting the corresponding compression. If the reinforcement is going to be able to resist the tensile forces, it needs to be anchored to the concrete. To achieve a sufficient anchorage, a certain transmission length where bond action can take place is needed. The required transmission length is often denoted the anchorage length.

The bond, i.e. the interaction between concrete and the steel reinforcement bars, is influenced by several parameters such as the type of concrete and reinforcement, as well by the state of stress in the two materials. The type of concrete and reinforcement basically refers to their material properties, such as compressive and tensile strength, and their geometry, especially the bar diameter and the rib shape of the reinforcing steel. Yielding of the reinforcing steel strongly affects the bond behaviour, see CEB (2000); this will later be described more in detail. External pressure, both lateral and transversal, acting on the structure along the anchorage length also have a significant influence on the bond action.

Bond properties are influenced by many other aspects, such as concrete cover, spacing of the longitudinal and transverse reinforcement, splices and cut-off of reinforcement, number of bar layers, casting direction with respect to the free surface of the fluid concrete and bar position during casting, see CEB (2000). Time and environmental effects, such as load history, temperature fluctuation, shrinkage, creep, corrosion and frost deterioration, also influence the bond behaviour. More detailed information about many of these and other parameters that affect the bond action can be found in CEB (2000) and Sæther (2010).

The resistance of the bond is generated through three mechanisms or joint actions: chemical adhesion, friction and mechanical interlocking. The mechanism that will be dominant or decisive depends on the state of stresses in the two materials.

Low bond stresses ($\tau \leq 0.2\text{-}0.8\ f_{ct}$ , where $f_{ct}$ represents the concrete tensile strength) are resisted mainly by chemical adhesion. In this stage, no slip of the bar takes place, but highly localized stresses arise close to the rib tips, see CEB (2000). Note that the relative displacement, i.e. the slip, of the bar is always measured with reference to the undisturbed concrete and consists of two parts: the relative slip at the interface due to the difference in steel and concrete strains, and the shear deformations in the concrete involving cracking and crushing of the concrete in the surrounding area of the ribs, see CEB (2000).

For higher bond stress values ($\tau > 0.2\text{-}0.8\ f_{ct}$) the chemical adhesion breaks down and friction takes a larger role in the resistance. Further, large bearing stresses in the concrete are induced from the ribs, causing local crushing of the porous concrete-layer around the ribs, and transverse micro cracks, i.e. bond cracks, originate at the tips of the ribs, see Figure 2.1. This allows the bar to slip, but the bearing stress from the ribs remains limited and there is no concrete splitting, see CEB (2000).

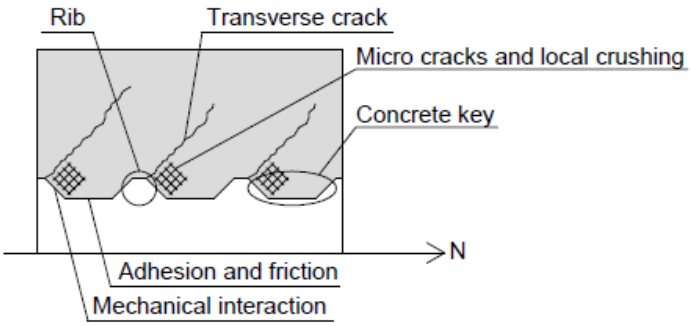


*Figure 2.1 Bond between a ribbed bar and the surrounding concrete, modified from Magnusson (2000).*

For even higher bond stress values ($\tau$ > 1-3 $f_{ct}$), longitudinal cracks, i.e. splitting cracks, spread radially, see Figure 2.2. The outward strut of the bearing stress is more or less spread normally from the surface of the ribs, depending on the rate of crushed concrete stuck to the front of the ribs. The strut can be divided into two components, i.e. longitudinal bond stress and normal splitting stress, see Figure 2.3. The inclined compressive stresses radiating from the ribbed bar is mainly balanced by circumferential tensile stresses in the surrounding concrete, see Figure 2.4, resulting in an interlocking mechanism with compressive struts between the reinforcement and the undamaged concrete, see Tepfer (1973). The bearing stresses acting on the steel reinforcement and the concrete are equal and opposite. Failures of these rings in tension give arise to the longitudinal cracks. The bond in this stage is transferred by a combination of bearing stresses, in form of the interlocking mechanism, and friction. The interlocking mechanism, with the ribs of the bar pushing against the surrounding concrete, is sometimes denoted the wedging action.

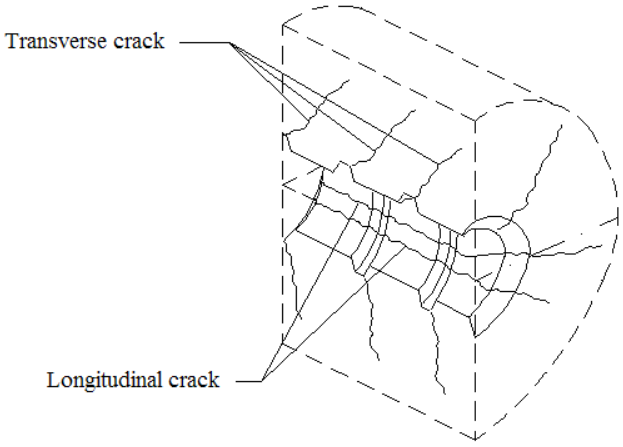


*Figure 2.2 Longitudinal and transverse cracks caused by bond, modified from CEB (2000).*

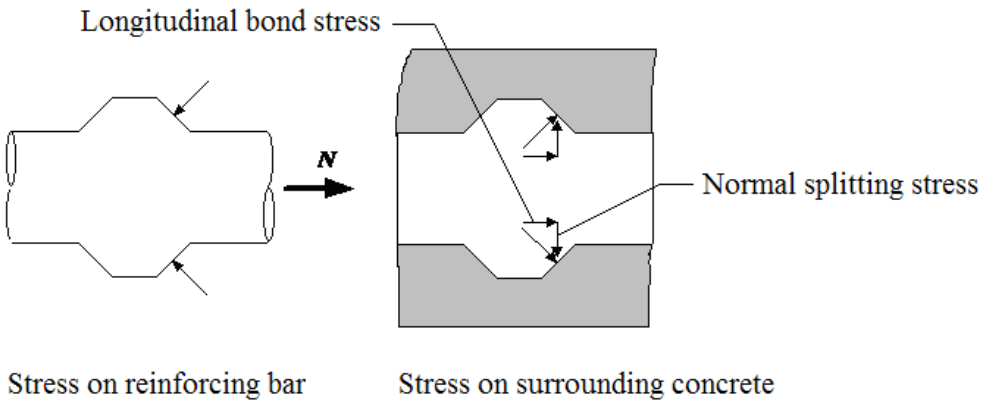


*Figure 2.3 Bond between a ribbed bar and the surrounding concrete by mechanical interlocking, modified from Magnusson (2000).*

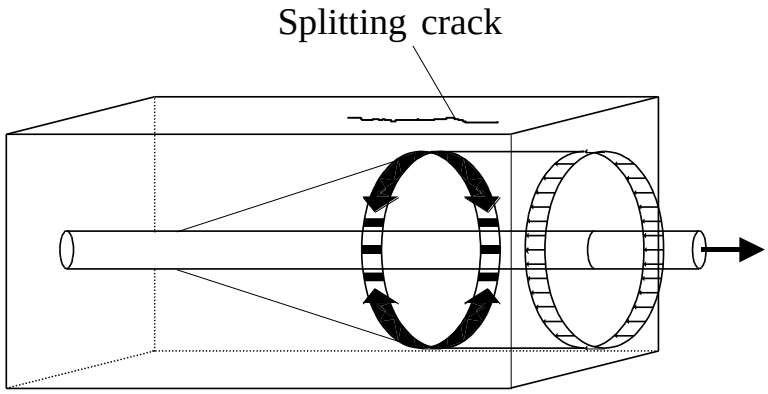


*Figure 2.4 Tensile ring stresses in the anchorage zone, adopted from Tepfers (1973).*

Note that the splitting is not only caused by the radial component of the rib bearing stresses alone. For large bar diameters, the dowel action in the shear span and the flexural stiffness of the bars in overlap splices contribute to the splitting effect, see Magnusson (2000).

Additional bond stresses lead to either a pull-out failure or a splitting failure, see Figure 2.5, depending on the level of confinement. The confinement efficiency depends on: concrete cover, bar spacing, transverse reinforcement, transverse and lateral pressure and on crack cohesion, strongly associated with concrete toughness, which is one of the many aspects of concrete fracture behaviour, see Magnusson (2000).

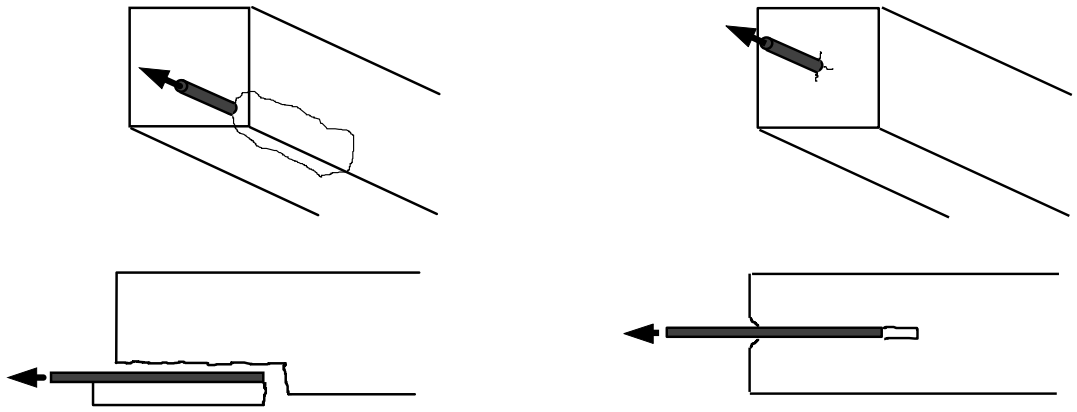

Splitting failure

Pull-out failure

*Figure 2.5 Main types of anchorage failure, modified from Engström (1995).*

Concrete is considered unconfined when $c_{min} \leq ø$ and $A_{st,\,min} \leq 0.25 \cdot n \cdot A_s$ are fulfilled, see CEB (2000); where $c_{min}$ is the minimum concrete cover, $A_{st,\,min}$ is the minimum total area of two-legged stirrups over a length equal to the anchorage length, $ø$ is the dimension of the main bars respectively, $n$ is the number of main bars and $A_s$ is the cross-section area of the main bars. Concrete is though considered well confined when $c_{min} \geq 5ø$ , $a \geq 10\,ø$, and $A_{st,\,min} \geq n \cdot A_s$; or when a high transverse pressure is present, $p \geq 7.5\ MPa$, see CEB (2000); where $a$ represents the clear spacing between the reinforcement bars. Hence, the edge beams in this study, described in Chapter 3, are treated to be in an intermediate level, between confined and well confined.

Roughly, an unconfined concrete structure under loading results in a splitting failure, while a confined concrete structure results in pull-out failure. The reality is though more complex than that.

An unconfined concrete structure has in general a small concrete cover, relative to the bar diameter, and is often provided with light-to-medium transverse reinforcement; the longitudinal cracks then tend to break out through the whole cover, reaching the outer surface, and between the longitudinal bars. The outbreak of splitting cracks through the entire concrete cover and bar spacing may lead to a brittle collapse mechanism when the bond capacity abruptly vanishes.

However, a confined concrete structure has in general a large concrete cover and heavy transverse reinforcement; cover splitting is prevented by the confining action and it remains limited to a cracked core around the bar leading to pull-out failure. In the pull-out failure, the bond stress increases until the concrete keys between the ribs are sheared-off or completely crushed, see Figure 2.1. The reinforcing bar then slides inside a concrete pipe with a rough surface and the stresses transfer through friction, see Magnusson (2000). The definitions of small and large concrete cover, together with the definitions of light, medium and heavy transverse reinforcement, are given in CEB (2000).

However, the development of a splitting crack along the transmission length does not necessarily lead to a sudden splitting failure. Provided that the confinement is sufficient, the splitting crack can develop in a stable manner along the entire transmission length. At the occurrence of longitudinal splitting cracks, the bond stresses can be redistributed more uniformly before failure. The bar is then pulled out.

Hence, the bond failure may be defined as "splitting induced pull-out failure", see Magnusson (2000); and can be seen as an intermediate failure mode of splitting and pull-out failure.

To summarize, the decisive bond mechanism depends on the bond stress and the confinement. Splitting failure and pull-out failure constitute the two main types of anchorage failure. The former mode shows a brittle behaviour in comparison to the latter mode with a ductile behaviour. More information about bond behaviour can be found in Magnusson (2000) and CEB (2000). Information about material and bond properties, together with the mechanical behaviour, of frost- and corrosion-damaged concrete, and their effect on the load-carrying capacity of the concrete structures, can be found in Zandi Hanjari (2010).

# 3 Test specimens

The test specimens were taken from the edge beams of Stallbackabron, a composite bridge with steel beams and a concrete deck, located outside Trollhättan in Sweden. Stallbackabron, 1.392 km long, crosses lake Göta Älv and is a part of road 44/E45. It opened for service in 1981. All information and technical data of Stallbackabron were provided by Trafikverket, The Swedish Transport Administration.

A rehabilitation of the bridge started in August 2010 and is planned to be finished in August 2012. The rehabilitation consists of replacing the outermost slabs and the edge beams. The edge beams were found to be very promising in this research since they were naturally corroded and showed different extent of corrosion induced damages, from no sign of corrosion to extensive cover cracking resulting in spalling of the concrete cover. Thereto, they were reinforced, both longitudinally and transversally, with deformed bars, i.e. ribbed bars. The geometry of the edge beams was also suitable for bending tests in order to evaluate the anchorage behaviour at a structural level. In total 25 specimens have been cut and kept for research from the south cantilever of the bridge; all of them are not assigned for this study, but saved for future research. There are also plans to take the same number of specimens from the north cantilever in August 2011.

At the construction site, the edge beams were cut and removed from the bridge deck in lengths of 3.6 meters, see Figure 3.1. To be able to transport the specimens within the laboratory facilities at Chalmers University of Technology, the edge beams needed to be shorten to 2.3 meters. How the edge beams were shortened, see the hatched area in Figure 3.1. With regard to the load-bearing capacity, it was considered to be important to leave a stirrup close to the end, see Figure 3.5. Except the location of the stirrups close to the ends, the shortening cut was also adopted so that the specimen only would contain one guard rail.

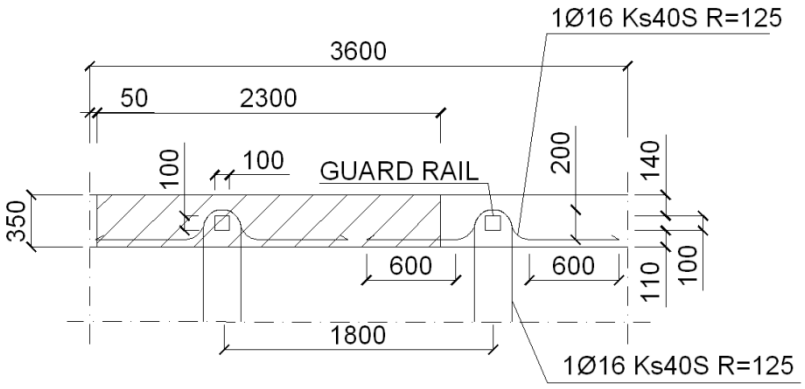


*Figure 3.1 Plan of the edge beam and the outermost slab.*

It is important to note that structures exposed to aggressive environment are susceptible to different types of deterioration, e.g. corrosion, frost, sulphate attack, etc. In case of Stallbackabron, although, corrosion has been the main cause of deterioration. The bridge also shows signs of frost deterioration; however, this has not been studied in this thesis. The severity of the deterioration has been enhanced by poor design of the bridge. The outermost slabs were too slender and lack of transverse reinforcement in the slab forced the edge beams to work as a load distributer, carrying more load than they were designed for. Loaded structures always crack, the edge

beams are no exception. The cracks enhance the chloride penetration of de-icing salts and the open cracks store up free water that increase the risk of severe frost damages. Transverse cracks in the joints of the slab accelerated the chloride penetration.

The edge beams, cut and saved for research, showed different extent of corrosion induced damage, as mentioned in previous paragraph. Hence, a classification system was introduced, see Figure 3.2.

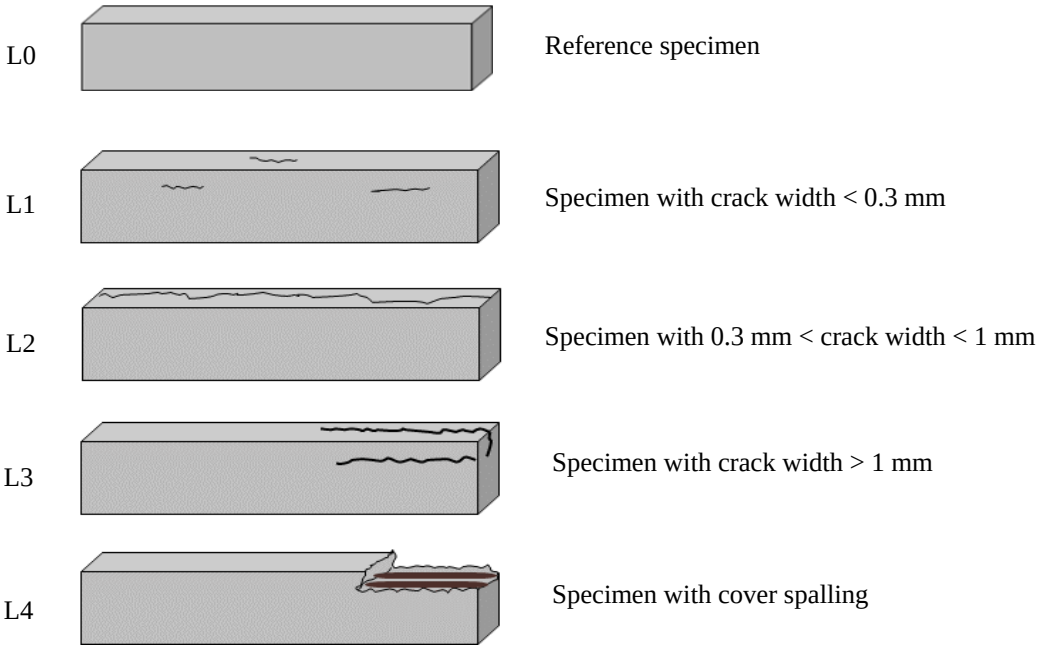


*Figure 3.2 Classification based on different extent of corrosion induced damage.*

Modified construction drawings of the bridge are depicted in Figure 3.1 and Figures 3.3-3.5. All ribbed longitudinal reinforcement bars were of Swedish type Ks60 and had a dimension of ø 16 mm. The stirrups, of Swedish type Ks40, had a dimension of ø 10 with a spacing of s300 mm. The edge beams were also provided with guard rails with a spacing of 1.8 m. Around every guard rail, the edge beams were supplied with 1ø16 Ks40S R=125 in both longitudinal and transverse directions. Bars, in transverse direction of the bridge deck, continue from the slab into the edge beams. They have the dimensions ø10 and ø12 with a quality of Ks60 and a spacing of s300. The concrete was of type K400 according to the drawings; this corresponds in the present nomenclature to K40. No complete information about the composition of the concrete and the mixing procedure was given.

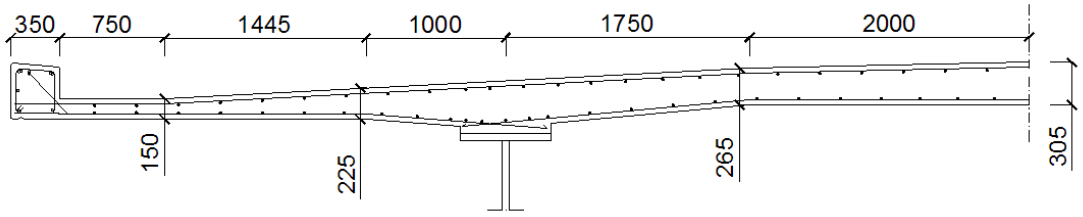


*Figure 3.3 Cross-section of the bridge deck.*

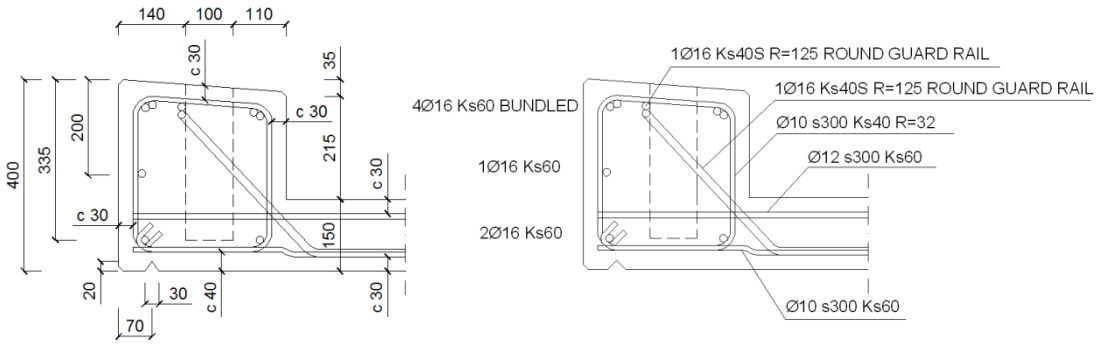


*Figure 3.4 Detail of the edge beam.*

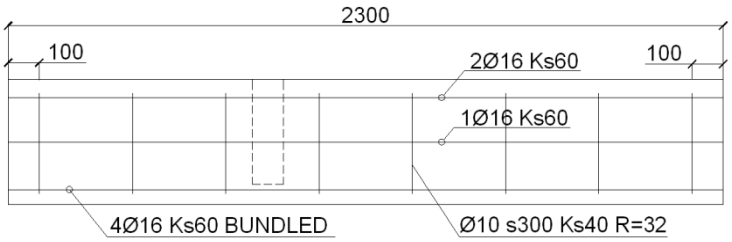


*Figure 3.5 Elevation after shortening.*

The actual specimens diverged in many aspects from the drawings, due to altering accuracy and precision in workmanship during erection of the bridge. The specimens showed varying amount and position of the longitudinal reinforcement, together with shifting spacing distance between the transverse reinforcement, i.e. the stirrups. The concrete cover also varied. To that, there was no information available about the location of the reinforcement bars going around the guard rails, see bars denoted 1ø16 Ks40S R=125 in Figure 3.1 and Figure 3.4. There was also lack of information regarding the location of the bars going from the slab into the edge beam. Furthermore, there was no information about how the longitudinal reinforcement were spliced. The edge beams could not be completely separated from the slab during cutting, so the specimens are given an extra "heel" of concrete, see top left picture in Figure 3.6.

The longitudinal reinforcement bars, closest to the upper inclined surface of the edge beams, were more damaged than the other longitudinal bars and therefore more interesting in the investigation of bond and anchorage behaviour. The higher extent of corrosion induced damage is reasonable since the upper bars during its service life time were most exposed to de-icing salts. In the experiments, described in Chapter 5, the beams were positioned upside down so that the most corroded bars were loaded in tension. The rotation of the edge beams facilitated the loading, since the load worked on a flat surface instead of a surface with an inclination.

*Figure 3.6 The actual specimens from Stallbackabron.*

# 4 Design of test set-up

Different test set-ups were examined and evaluated. The most promising test configuration was later designed in detail by using non-linear finite element method.

## 4.1 Choice of test set-up

To secure anchorage failure, for beams with various corrosion damage levels, in one common test set-up, the test configuration had to be thoroughly evaluated. To capture anchorage failure without influencing and disturbing the natural damages of the edge beams, was of great interest. In other words, it was of great importance to avoid any damage to the beams during preparation.

Four different test configurations were considered in the choice of a test set-up: a four point bending test, indirectly supported; a four point bending test, directly supported; a pull- out test; and a beam-end test. They are all illustrated in Figure 4.1.

The four point bending test indirectly supported with suspension hangers, proved to be the best choice with least disturbance and influence on the natural damages of the edge beams while capturing the structural behaviour.

The four point bending test is a stable and simple test set-up, and it is commonly used in experimental tests of shear and anchorage capacities. Concentrated loads, in comparison to distributed loads, result in better defined conditions with respect to the load effects. At the same time, with a distributed load, the load set-up would be very complicated as the deflection of the beam may vary the distribution of the load during the test.

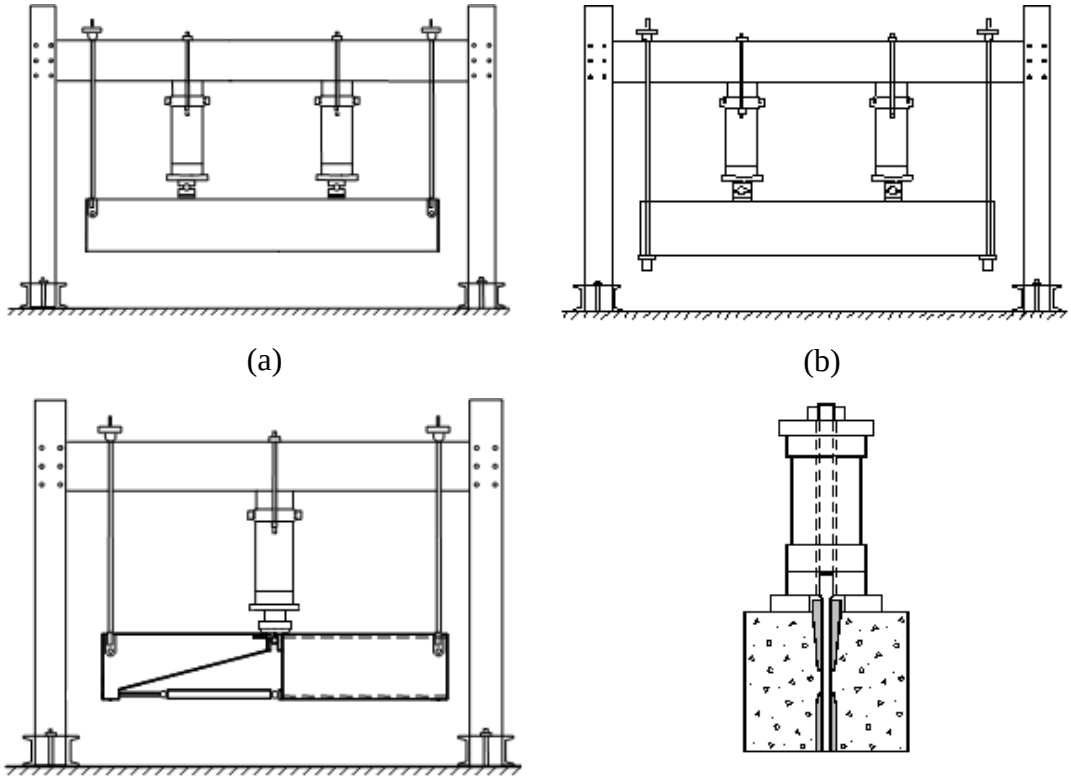


*Figure 4.1 Examples of test set-ups: (a) beam test: four point bending, indirectly supported; (b) beam test: four point bending, directly supported; (c) beam-end test; and (d) pull-out test.*

The pull-out test was excluded since it would have been very difficult to grab bundled bars. The eccentric position of the bars would have made it even harder to carry out the test. Finally, preparation of specimens for pull-out test would also have disturbed the region around the bars and influenced the bond properties. Depending on how the pull-out test would have been designed, there was a risk that the specimens would be subjected to transverse or lateral pressure, i.e. another reason for not choosing that test configuration. The pull-out test would otherwise have been favourable as it gives a well defined anchorage length. In a beam-end test, the edge beams would have been cut with an inclined angle representing the critical shear crack. The angle lies within interval $21.8^{o}$ - $45^{o}$, depending on the design of the transverse reinforcement, see Al-Emrani *et al* (2008a). The beam-end test has a well defined anchorage length and represents the structural behaviour in a better way than the pull-out test. However, the beam-end test, like the pull-out test, includes the difficulty of gripping the reinforcement bars. It also has a large impact on the natural damages which should be avoided; thus, the configuration is not an option. The angle used when cutting the beam may as well not represent the real behaviour of the edge beam, i.e. not represent the actual critical shear crack. The four point bending test, directly supported, was left out because of the support pressure which influences the anchorage behaviour to a large extent. With external transverse pressure acting in the anchorage region, i.e. along the transmission length, both bond stiffness and strength increase, see Zandi Hanjari (2010); in other words, the transverse pressure from the supports in the directly supported specimens gives rise to a more favourable stress state and favour bond action, and thus provides an anchorage capacity greater than that of the indirectly anchorage capacity which is not desirable. For severely damaged members with cover spalling in the end regions, a test configuration with direct support would thereto not be viable. Direct support, however, is expected to show higher shear capacity than an indirect support, see Magnusson (2000), and often result in well defined anchorage length in comparison to the indirect support; this is because inclined shear cracks often propagate to the support. The advantages does not weight heavier than the disadvantages though.

## 4.2 Finite Element Method-FEM

The four point bending test, indirectly supported with suspension hangers, was designed in detail so that an anchorage failure took place. This was done in a parametric study by simulating the test set-up using non-linear finite element method, prior to actual testing. Several parameters were investigated: the location of the suspension hole, the position of the concentrated loads and the influences of notches. Notches were included in the study since they were considered to be a tool that could be used in controlling the anchorage length, so that it would become well defined. The parametric study is schematically shown in Figure 4.2.

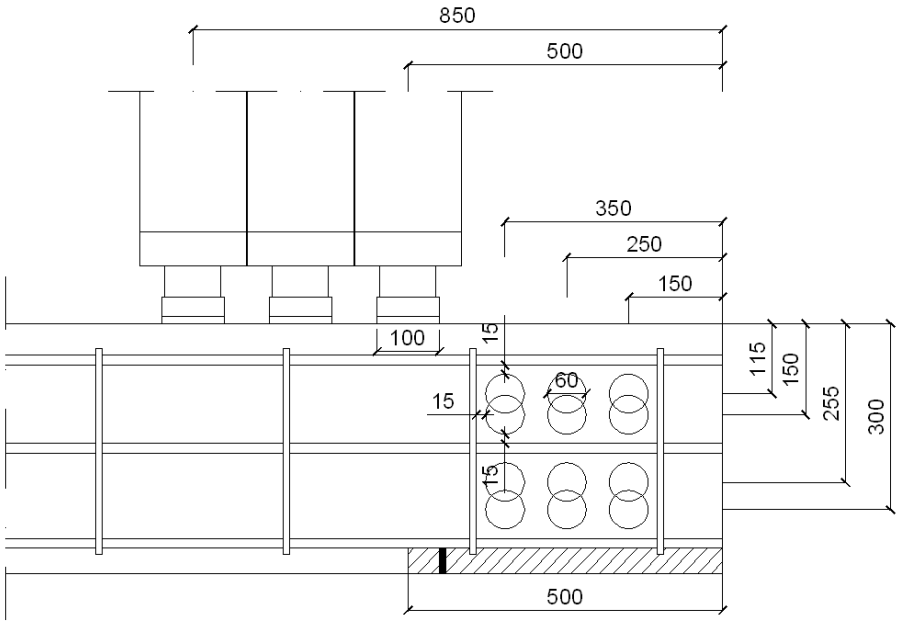


*Figure 4.2 Schematic illustration of the parametric study.*

As the drilling should have been carried out so that no reinforcement were cut-off; there were some constraints regarding where the suspension hole could be placed. Twelve main locations were studied, see Figure 4.2. They all have a safety margin of 15 mm to the closest reinforcing bar. Figure 4.2 does not though represent all locations of the suspension hole that were investigated; some suspension holes, better adopted to the real geometry of the edge beams, were also examined. Each location of the suspension hole was tested with three different positions of the concentrated loads. and in some cases, also with notches. The load was positioned within a region of 500-850 mm, counted from the free end. With respect to the shear capacity, it was considered to be important to place the load so that the load path crosses at least one stirrup. The concentrated loads were simulated to be distributed over 100 mm, which later where verified to be a good estimation considering the real dimensions of the hydraulic jacks. The hatched area in Figure 4.2, represents within what region the notches were defined. The notches were designed as a cut of a thin slot, see black solid hatched area, or as cuts of whole blocks, see dashed hatch area. The position of the slot and the extension of the blocks were varied in the domain area. The dimension of the suspension hole was more or less limited by the design of the steel rod going through the hole. Using high quality steel the minimum required diameter of the rod was in the range of 60 mm.

Data of the material properties corresponding to the ribbed hot-rolled reinforcement bars, Ks40 and Ks60, were received from old tests at Chalmers University of Technology, from the time when Stallbackabron was built. The data, given in Table 4.1 and Appendix A, should be seen as an initial qualified assumption of the real material properties. The national classification of the concrete, i.e. K40, represents the uniaxial compressive strength of a concrete cube. In the numerical analyses, the cylinder compressive strength was used. Translation of the strength classification, from cube to cylinder compressive strength, was then essential. The relationship, between the cylinder and the cube compressive strength, according to EN-standard, are different depending on how the specimens have been cured after casting. For more detailed information, see Al-Emrani *et al* (2008a). To be conservative, the relationship resulting in lowest possible cylinder compressive strength was used. K40 was then

replaced by C30. The mechanical properties of the concrete, according to Eurocode 2, see EN 1992-1-1 (2004), are given in Table 4.2. The fracture energy was determined from the compressive strength according to CEB-FIB Model Code 1990, see CEB (1993).

*Table 4.1 Mechanical properties of the reinforcement received from old tensile tests at Chalmers University of Technology.*

| | $f_{sy}$ [MPa] | $f_{su}$ [MPa] | $\varepsilon_{sy}$ [‰] | $\varepsilon_{su}$ [‰] | $E_s$ [GPa] |
|---|---|---|---|---|---|
| Longitudinal reinforcement, Ks60 | 693 | 907 | 0.312 | 1.25 | 222 |
| Transverse reinforcement, Ks40 | 468 | 638 | 0.227 | 1.14 | 206 |

*Table 4.2 Mechanical properties of the concrete according to Eurocode 2, see EN 1992-1-1 (2004):*

| | $f_c$ [MPa] | $f_t$ [MPa] | $E_c$ [GPa] | $G_f$ [N/m] |
|---|---|---|---|---|
| Concrete | 38 | 2.9 | 33 | 79.2 |

The finite element program DIANA, version 9.4.3, together with the pre- and post-processor FX+, version 3.0.0, was used for the analyses.

The beams were studied at a structural level and due to symmetry only a half-member was analysed. Several simplifications have been made, such as neglecting the deterioration of corrosion and frost. The result of this is conservative, i.e. on the safe side. Transverse reinforcement from the slab going into the edge beams and the guard rails, together with the reinforcement positioned round the rails, have not been accounted for in the FE simulation. Deviations of the position and the varying amount of the longitudinal and transverse reinforcement have not been accounted for either; neither the deviation of the concrete cover.

The numerical models were verified with simple analytical calculations of the bending moment capacity, the shear capacity and the anchorage capacity. The analytical calculations, all according to Eurocode 2, showed that the shear capacity is critical, due to large spacing between the transverse reinforcement, i.e. the stirrups. In order to predict the applied load in the ultimate limit state, a strut and tie model was set up. The strut and tie model showed though to be statically indeterminate; hence, no results were received. However, the model gave an estimation of the load path and the corresponding stress field.

### 4.2.1 Two-dimensional simulation

An example of a finite element model in two dimensions is illustrated in Figure 4.3.

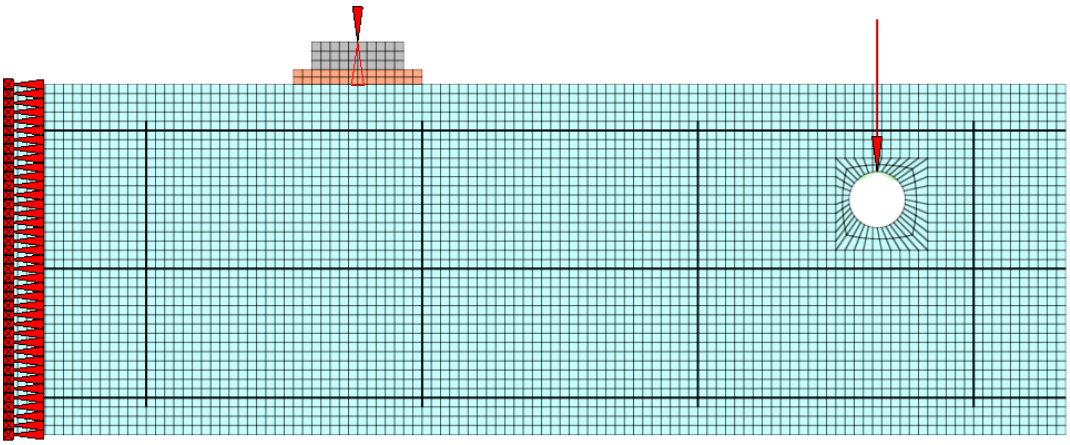

*Figure 4.3 An example of a finite element model in two dimensions.*

The concrete was modelled using four-node quadrilateral plane stress elements, see Q8MEM in DIANA (2010). The concrete was modelled with a constitutive model based on non-linear fracture mechanics using a smeared rotating crack model, see DIANA-option "ROTATE" in DIANA (2010). A uniaxial stress-strain relation, based on secant stiffness, expresses the softening response in the fracture zone, i.e. the crack. The behaviour in tension was described as linear elastic until the uniaxial tensile strength was reached. The tensile response of concrete was taken into account according to Hordijk model, see DIANA-option "HORDYK" in DIANA (2010). The crack band width, in which cracks localize, was assumed to be equal to the element size. This was later verified to be a good approximation of the localization zone in the analyses. The response of concrete in compression was taken into account according to Thorenfeldt model, see DIANA-option "THOREN" in DIANA (2010).

The longitudinal tensile reinforcement, i.e. the main reinforcement, was modelled by two-node straight truss elements, see L2TRU in DIANA (2010). Interaction between the reinforcement and the concrete was modelled with 2+2 node line interface elements, see L8IF in DIANA (2010). The interface elements, used at the surface between the reinforcement bars and the concrete, described the bond-slip behaviour in terms of a relation between the tractions and the relative displacements. The elements had, initially, a thickness of zero. For this type of modelling, the use of predefined bond stress versus slip relation is necessary, the bond stress-slip relationship according to CEB-FIP Model Code 1990, see CEB (1993), was adopted in the analyses. Data corresponding to "confined" and "good conditions" were obtained, see Figure 4.4 and Table 4.3. Hence, desired pull-out failure was assumed.

Engström (1992) showed that the bond stress-slip relationship is significantly affected by yielding of the reinforcement. Engström concluded that, due to the drastic increase of axial strains and the contraction of the bar caused by yielding, the interlocking effect between the steel ribs and the concrete was drastically reduced. He proposed that the local bond stress-slip model should be modified when the steel is in the plastic stage, see Figure 4.4 and Table 4.4. A non-linear descending branch in the bond-slip relationship starts at the very onset of yielding. Hence, the bond stress-slip relationship can be influenced not only by the softening of the surrounding concrete, but also by the softening of the steel at yielding. More information about yielding of

reinforcement and its effect on the bond is given in Shima *et. al.* (1987a,b,c), Bigaj (1995) and Huang *et al.* (1996).

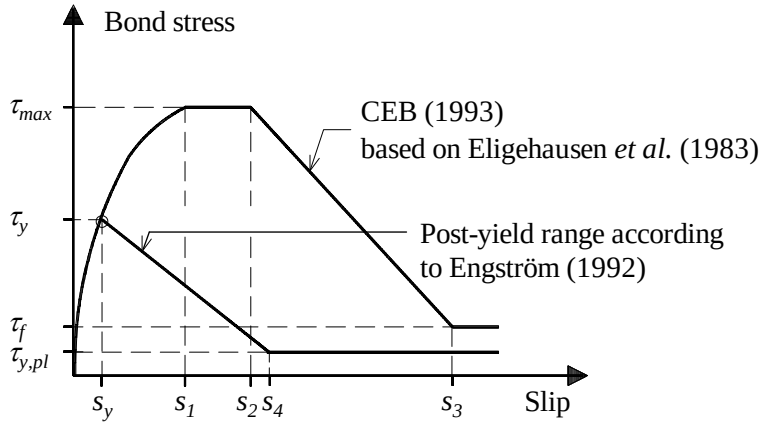


*Figure 4.4* *Bond stress-slip relationship according to CEB (1993) based on Eligehausen et al. (1983), and a modified model in the post-yield range of the steel according to Engström (1992); modified from Magnusson (2000).*

*Table 4.3* *Parameters defining the local bond stress-slip relationship in Figure 4.4 according to CEB (1993).*

| Parameters | Unconfined concrete [1] | | Confined concrete [2] | |
|---|---|---|---|---|
| | Bond conditions | | Bond conditions | |
| | Good | All other cases | Good | All other cases |
| $s_1$ | 0.6 mm | 0.6 mm | 1.0 mm | 1.0 mm |
| $s_2$ | 0.6 mm | 0.6 mm | 3.0 mm | 3.0 mm |
| $s_3$ | 1.0 mm | 2.5 mm | Clear rib spacing | Clear rib spacing |
| $\alpha$ | 0.4 | 0.4 | 0.4 | 0.4 |
| $\tau_{max}$ | $2.0(f_{ck})^{0.5}$ | $1.0(f_{ck})^{0.5}$ | $2.5(f_{ck})^{0.5}$ | $1.25(f_{ck})^{0.5}$ |
| $\tau_{.f}$ | $0.15\,\tau_{max}$ | $0.15\,\tau_{max}$ | $0.40\,\tau_{max}$ | $0.40\,\tau_{max}$ |

1) Failure by splitting of the concrete

2) Failure by shearing off the concrete between the ribs

*Table 4.4* *Parameters defining the local bond stress-slip relationship used in Figure 4.4 in the plastic stage of the steel, according to Engström (1992).*

| Parameters | Confined concrete |
|---|---|
| $\tau_{y.pl}$ | $0.5\,\tau_f$ |
| $s_4$ | $0.5s_3$ |

To have an accurate model with interface elements, yielding of the reinforcement have been avoided to the largest extent possible. It was later validated that no reinforcement yield until the very last increment load step, therefore the local bond stress-slip model according to CEB-FIB Model Code 1990 could be fully used, without considering modifications suggested by Engström.

Provided that the local bond-slip relationship is identified, it is possible to predict the deviation of steel stresses, bond stresses and local slip along an anchored bar ; all this done by using equilibrium conditions, compatibility conditions and constitutive relationships, such as stress-strain relationships for steel and concrete, see Magnusson (2000).

The compressive reinforcement and the transverse reinforcement were modelled as embedded in the concrete elements, i.e. assuming perfect bond or complete interaction between the reinforcement and the concrete. In the modelling of the embedded reinforcement, the reinforcement does not have separate degrees of freedom; instead, higher strength and stiffness are adopted to the concrete elements in the direction of the embedded reinforcement. Interaction between the compressive reinforcement and the transverse reinforcement at the corners was not counted for in the model. Neither, interaction between the tensile reinforcement, described in earlier paragraph, and the transverse reinforcement was modelled.

Due to symmetry, only half of the beam needed to be modelled. All nodes on the symmetry line, except those belonging to embedded reinforcement, had their displacements along the longitudinal axis and the axis out of plane, i.e. in lateral direction, supported. Boundary conditions were also applied on the top node, of those located on the circumference of the suspension hole, by supporting the displacement in the transverse direction. Other nodes on the circumference were linked to the node with the translation constraint, in terms of tyings, identified as slave nodes and master node respectively, see Figure 4.5. The DIANA-option “ECCENT” was used for the tyings, see DIANA (2010). This option allowed the linked elements to rotate in the plane while their relative distances were kept intact, i.e. the tied nodes were forced to remain in a straight line but the line was allowed to rotate. A loading plate in steel, together with a fibreboard, were modelled in between the hydraulic jack and the edge beam; this in order to simulate a realistic stress field and load path. The center node of the steel plate was supported for displacement in the loading direction. The boundary conditions are represented by red solid arrows in Figure 4.3, while the load is signified by a red hollow arrow. It should be mentioned that the loading plate first was modelled with tyings, infinitely stiff, but this resulted in local crushing of the edge beam close to the loading plate. It was therefore not used in a larger extent.

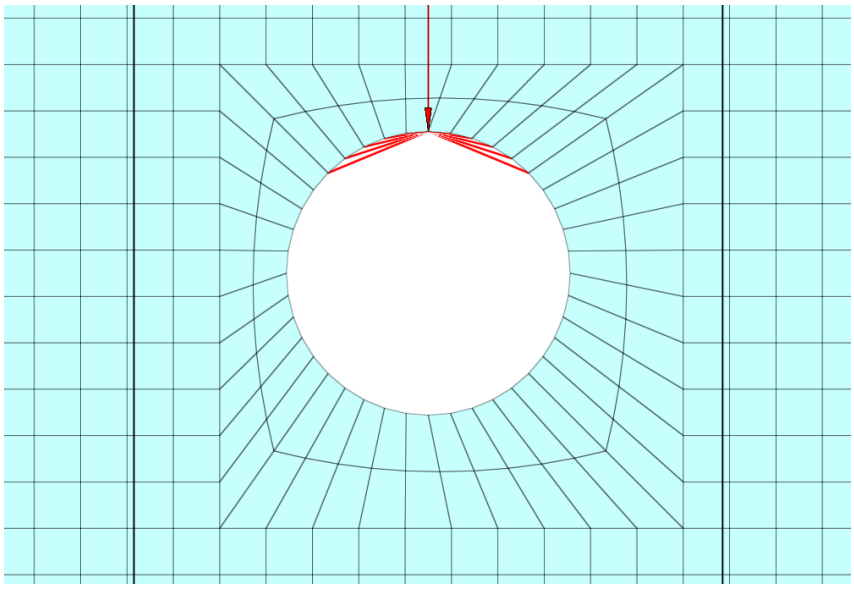

*Figure 4.5 Detail of the suspension hole showing the master node, the slave nodes and the links between them.*

One dummy beam were attached to the model in order to add degrees of freedom in one specific node, to be more exact, at the top node of those located on the circumference of suspension hole. The dummy beams were modelled using two-node straight line elements, see L6BEN in DIANA (2010). The dummy beam with its additional degrees of freedom, two translations and one rotation in each node, made it possible to use the option "ECCENT". The dummy beam is depicted as a red continuous line in Figure 4.3.

The numerical solution approach for the non-linear calculations was based on a two-phase analysis. In the first phase, the self-weight was applied as a body load in one single step. The second phase represents the variable point loads, with user defined load steps. The monotonically increasing load was applied as displacements. Regular Newton-Raphson method was used as iteration scheme in order to find equilibrium within each displacement increment.

The two-dimensional model consisted of about 5200 elements with an element size of 12 mm, and the analysis had an execution time of about 30 min. The data files and the command files are given in Appendices B-C.

#### 4.2.1.1 Results

None of the two-dimensional simulations were considered to be sufficient for describing anchorage failure. All the cases with the suspension hole in the upper half of the beam, above the mid reinforcement, ended up in a local failure of the suspension hole; while all the cases with notches ended up in shear failure. The failure modes of those cases could often be detected just by evaluation of the crack pattern, in terms of maximum principle strains, see Figure 4.6. However, some cases with the suspension hole in the lower half of the beam, under the mid reinforcement, showed a crack pattern indicating anchorage failure. The anchorage length was difficult to distinguish in all cases with promising crack pattern. The shear and bending cracks, within the shear span, did not propagate close to the section of the support; hence, the anchorage lengths ended up long and not well defined.

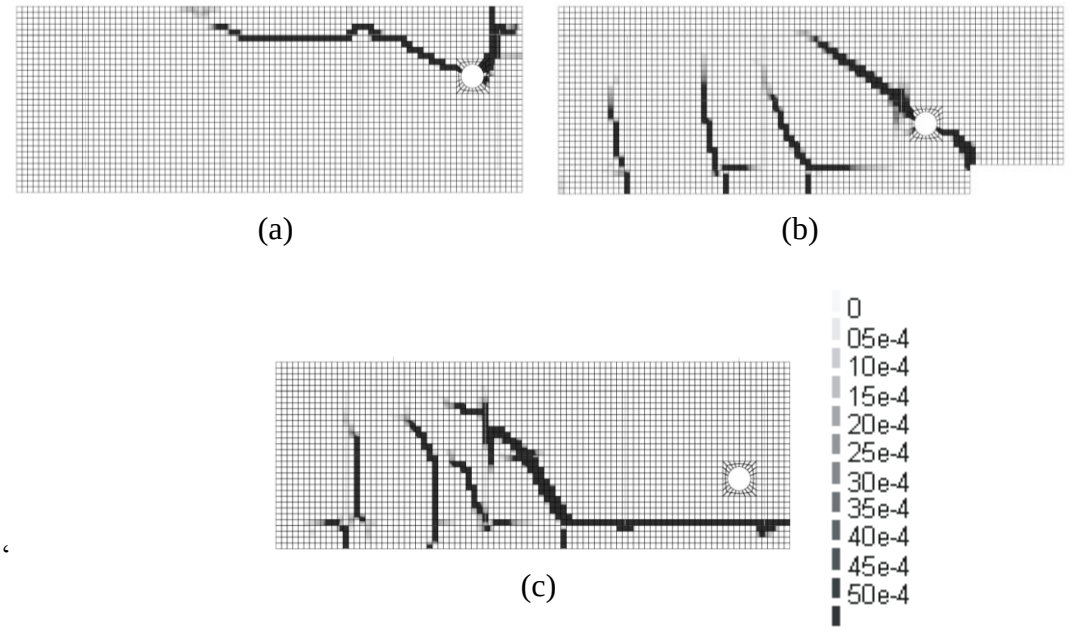


‘

*Figure 4.6 Crack pattern in terms of maximum principle tensile strains from two-dimensional numerical analyses: (a) suspension hole in the upper half of the beam; (b) beam supplied with notch; and (c) suspension hole in the lower half of the beam.*

The configurations with the most promising crack patterns, Figure 4.6(c), were investigated deeper by studying stresses in the reinforcement bars and relationships such as applied load vs. mid-span displacement and applied load vs. free end slip, see Figures 4.7-4.8.

The relationships show a brittle failure with no identified residual load-bearing capacity; the solution diverged and the analysis was terminated after failure. The change of stiffness indicates crack appearance. No considerable slip (0.1-0.2 mm) take place in the pre peak stage, i.e. before maximum load is reached, which indicates that an anchorage failure is unlikely the failure mode. The absence of continuous descending branch in the post peak stage of the slip curve indicates that the failure is not only sudden or abrupt, but also unstable.

Examination of the stress in the transverse and longitudinal reinforcement indicated that no yielding took place until the last increment step, i.e. the beam failed before the yield capacity of the reinforcement was reached.

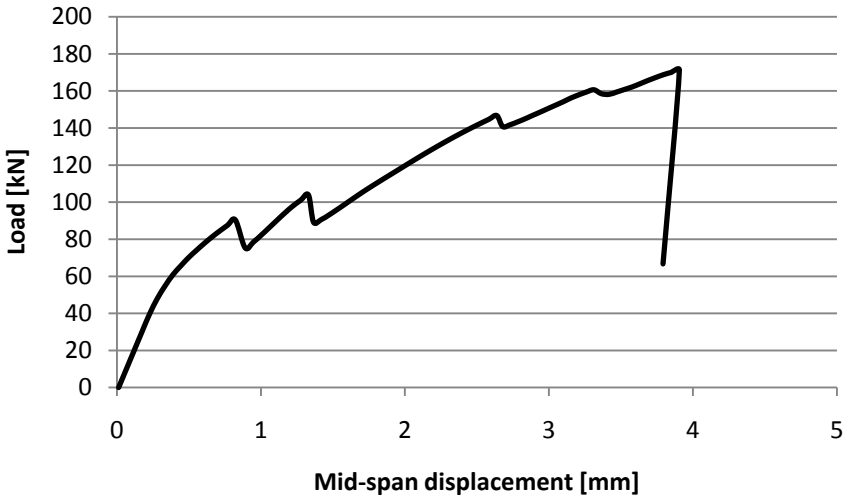


*Figure 4.7 Applied load vs. mid-span displacement.*

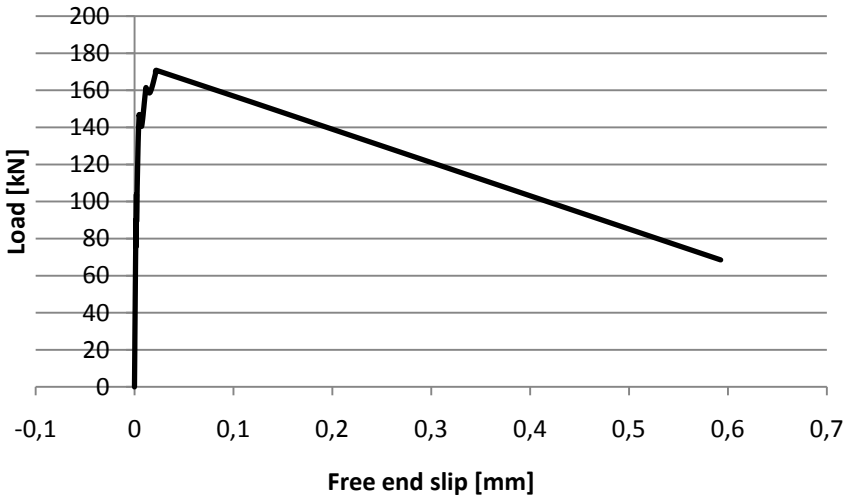


*Figure 4.8 Applied load vs. free end slip.*

Since the two-dimensional simulation was concluded to be insufficient for describing anchorage failure at a structural level, a more advanced, three-dimensional, simulation of the test set-up was considered to be necessary. The two-dimensional modelling gave though some indications in how the test-set up should be designed to capture anchorage failure. It seemed to be preferable to have a large shear span, i.e. large distance between the point load and the suspension hole. This probably due to the fact that with a larger shear span, the larger the bending moment will be, which will result in larger tensile stresses in the reinforcement. The suspension hole should be placed in the lower half of the beam, in prior to the upper half. Notches often had an unfavourable effect on the structural behaviour and should therefore be avoided. It was also concluded that the suspension hole should not be placed too far into the beam. This would just give a longer anchorage length since shear and bending cracks can only propagate within the shear span.

### 4.2.2 Three-dimensional simulation

An example of a finite element model in three dimensions is illustrated in Figure 4.9.

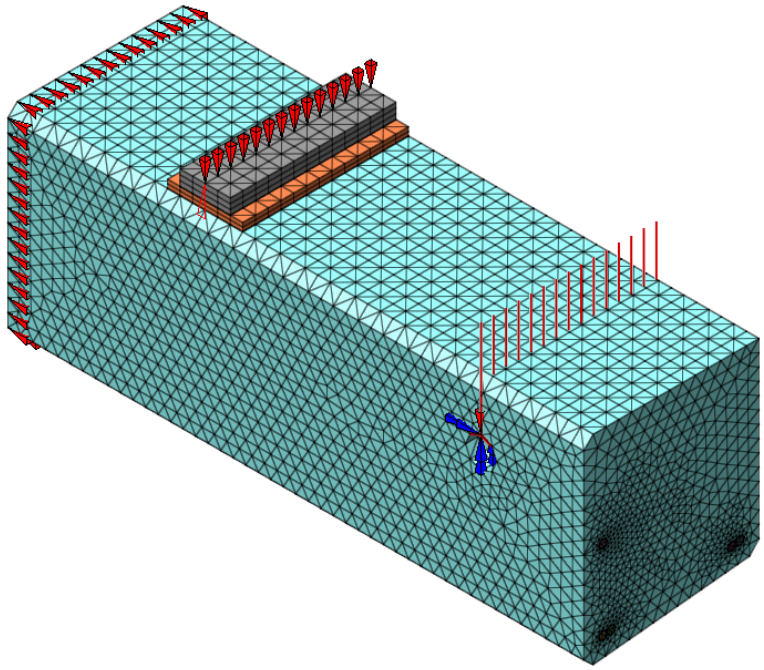

*Figure 4.9 An example of a finite element model in three dimensions.*

The concrete and the longitudinal reinforcement in the tensile zone were modelled using four-node pyramid solid elements, see TE12L in DIANA (2010). As an approximation, the cross section of the main bars was designed to have a form of an octagon. The perimeter of the octagon should have the same value as the perimeter of a real reinforcement bar of ø16. Since the cross-section area of the approximated reinforcement bar was slightly smaller than the nominal reinforcement, this had to be adjusted for in the input of the modulus of elasticity and the strength of the reinforcement, i.e. tensile and compressive strength. The adjustment was done according to Lundgren (1999); the values evaluated from the nominal area, i.e. the values in Table 4.1, were then multiplied by a factor of 1.0547. The compressive reinforcement and the transverse reinforcement were modelled as embedded in the concrete elements, i.e. assuming perfect bond between the reinforcement and the concrete. Interaction between the transverse and the longitudinal reinforcement were not included in the FE model.

The constitutive models for concrete were the same as in the two-dimensional analysis; i.e. based on non-linear fracture mechanics using a smeared rotating crack model with Hordijk and Thorenfeldt models describing tensile and compressive behaviours, respectively. The constitutive behaviour of the reinforcing steel was modelled by an elastic, perfectly plastic material model. The elastic state was limited by the von Mises yield criterion, with associated flow and isotropic strain hardening.

Interaction between the reinforcement and the concrete was modelled with a bond model, developed first in Lundgren and Gylltoft (2000). The model has been modified a number of times, the latest version is described in Lundgren (2007). The bond model was implemented as a user-supplied subroutine in DIANA. The programming

was done in FORTRAN, and the complete code can be found in Lundgren (2001). How to give input can also be found in Lundgren (2001).

In the bond model, the splitting stresses of the bond action were included. The bond stress depended not only on the slip, but also on the radial deformation or the normal stress between the reinforcement bar and the surrounding concrete. Thereby, the loss of bond at splitting failure or if the reinforcement is yielding can be simulated.

The three-dimensional simulation takes into account the real confinement conditions; this in comparison to the two-dimensional simulation where it is predefined by the user, according to CEB-FIP Model Code 1990. Hence, in the three-dimensional simulation, the bond behaviour is an output while it is an input in the two-dimensional simulation.

The model is especially suited for detailed three-dimensional finite element analysis, where both the concrete and the reinforcement are modelled with solid elements. Interface elements, used across the reinforcement and the concrete interface, describe a relation between the traction, ***t***, and the relative displacement, ***u***, in the interface. The local directions of the interface elements are of great importance; they should be orientated so that the local x-axis is normal to the plane defined by the vectors $t_n$ and $t_t$ , see Figure 4.10. The physical interpretations of variables $t_n$, $t_t$, $u_n$ and $u_t$ are shown in Figure 4.10. The interface elements were modelled using 3+3 node plane triangle elements, see T18IF in DIANA (2010). Initially, they had a thickness of zero.

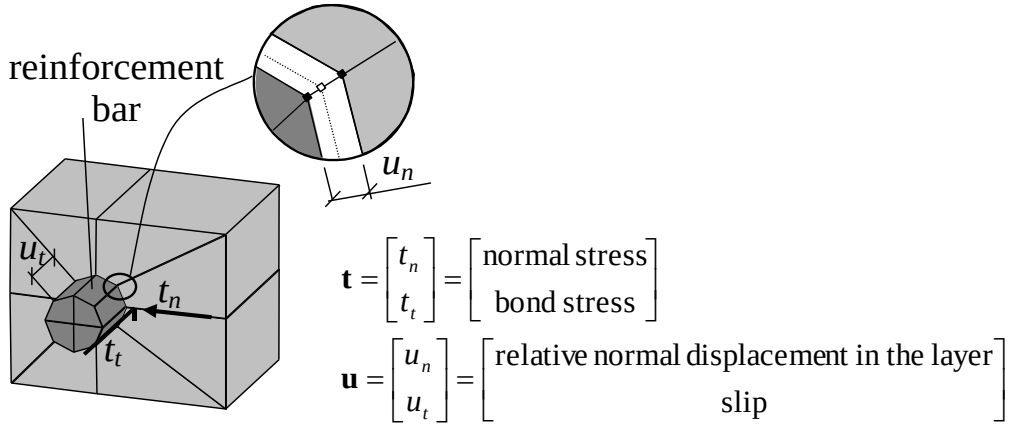


*Figure 4.10 Physical interpretation of the variables $t_n$, $t_t$, $u_n$ and $u_t$ ,adopted from Lundgren (2001).*

The bond model is a frictional model, using elasto-plastic theory to describe the relations between the stresses and the deformations. The relation between the tractions ***t*** and the relative displacements ***u*** is in the elastic range, according to equation (4.1).

$$\begin{bmatrix} t_n \\ t_t \\ t_r \end{bmatrix} = \begin{bmatrix} D_{11} & 0 & 0 \\ 0 & D_{22} & 0 \\ 0 & 0 & D_{33} \end{bmatrix} \begin{bmatrix} u_n \\ u_t \\ u_r \end{bmatrix} \tag{4.1}$$

$D_{11}$ and $D_{22}$ describe the relation between displacements and stresses in the radial and transverse directions, respectively. The third component, added for three dimensional modelling, corresponds to the stress acting in the direction around the bar, i.e. $D_{33}$ is a dummy stiffness preventing the bar from rotation around its axis. The third component was assumed to be independent of the other components.

A schematic interpretation of the model can be found by noting the two yield functions, $F_1$ and $F_2$, in Figure 4.11 The yield surface is defined by the two yield functions. The first yield line, $F_1$, describes the friction, i.e. the relation between the normal splitting stress and the bond stress, assuming that the adhesion is negligible. The second yield line, $F_2$, describes the upper limit at a pull-out failure, determined from stress in the inclined compressive struts that results from the bond action. For plastic loading along the yield function $F_2$, an associated flow rule is assumed. For the yield function, $F_1$, a non-associated flow rule is assumed.

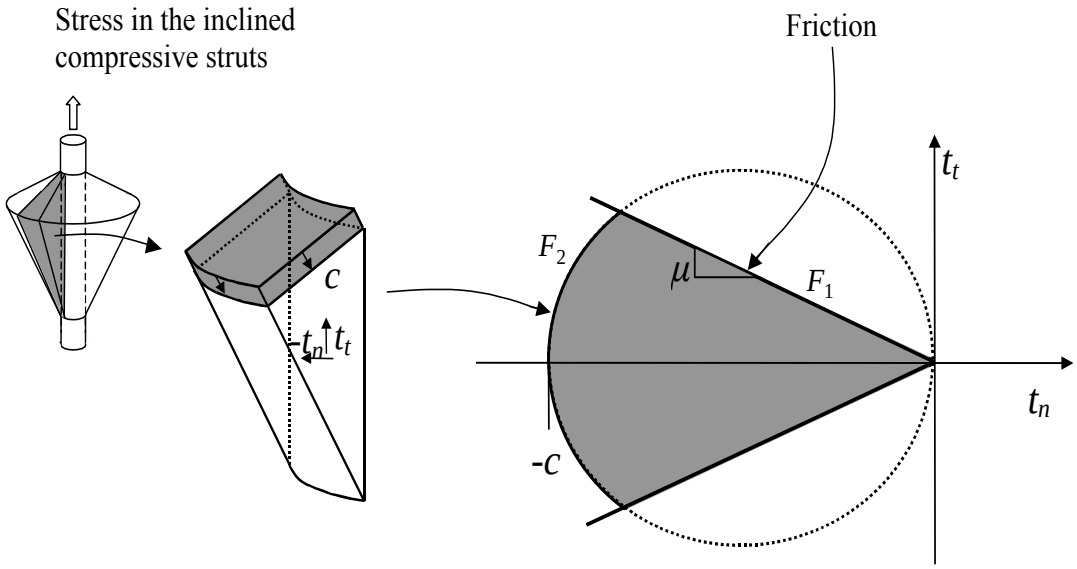


*Figure 4.11 Schematic interpretation of the model, adopted from Lundgren (2001).*

More details concerning yield functions, flow rules, and hardening rules have been given in Lundgren (2007) together with other specific information such as calibration of the model.

The boundary conditions were similar to those in the two-dimensional analysis, except some additional constraints of rotation, see Figure 4.12. The red solid arrows indicate constraints of translation, while the blue double-arrows indicate the additional constraints of rotation. During modelling, it was detected that it is of importance to support the rotation around the longitudinal axis and around the transverse axis of the beam, in those nodes belonging to the dummy beams that are in contact with the surface area of the suspension hole; this in order to reach a numerical stable model. The red continuous lines represent the dummy beams, while the green continuous lines represent the links between the master nodes and the corresponding slave nodes on the surface area of the suspension support. The load is signified by red hollow arrows.

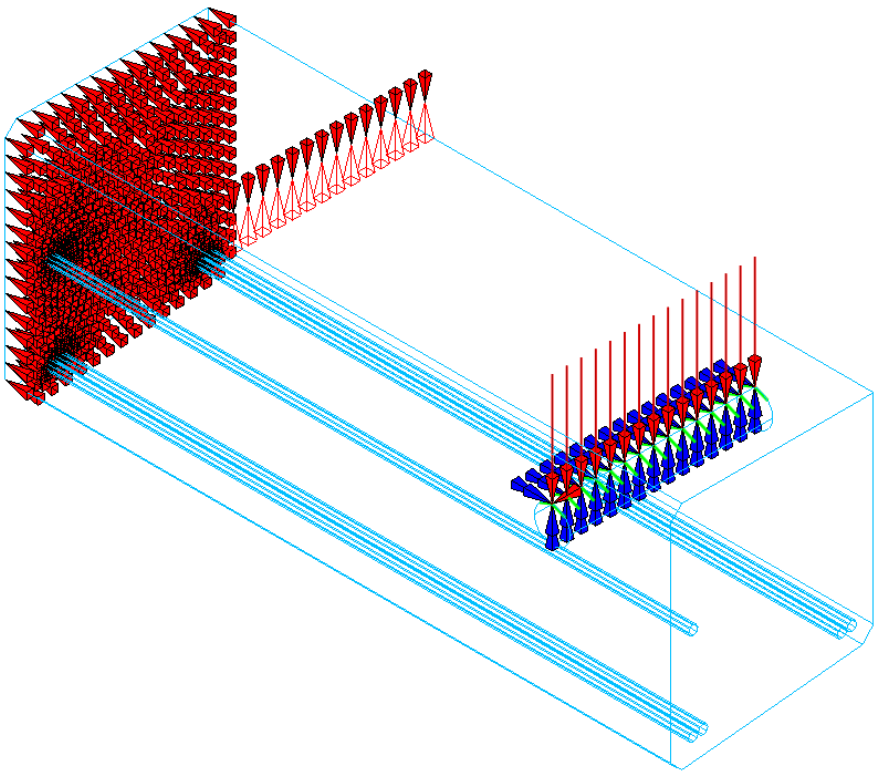

*Figure 4.12 The boundary conditions and the load.*

The numerical solution approach for the non-linear calculations was based on a two-phase analysis. In the first phase, the self-weight was applied in one single step. The second phase represents the variable point loads, with user defined load steps. The monotonically increasing load was applied as displacements. A Regular Newton-Raphson method, a non-linear solution technique, was used as iteration scheme in order to find equilibrium within each displacement increment.

The three-dimensional model consisted of about 78 400 elements with an element size of 25 mm, and the analysis had an execution time of about 7.5 hours. The data files and the command files are given in Appendices D-E.

#### 4.2.2.1 Results

The most promising test configurations, from the two-dimensional analyses, were used in the initial three-dimensional analyses. In comparison with the two-dimensional simulations with a crack pattern that indicated anchorage failure, the three-dimensional simulations indicated shear failure or local failure at the suspension hole; compare Figure 4.6(c) and Figure 4.13, having the same details of configuration. Hence, the most promising test configurations from the two-dimensional simulations were questionable; therefore, the parametric study, described in Section 4.2, had to be done from scratch in three dimensions as well. It should be noted that notches were excluded from the study, since it was considered that it always would have an unfavourable effect of the structural behaviour. In the extensive parametric study, shear failure or local failure of the suspension seemed to be critical independently of the test settings; therefore, it was concluded that the beam needed to be strengthened with transverse reinforcement.

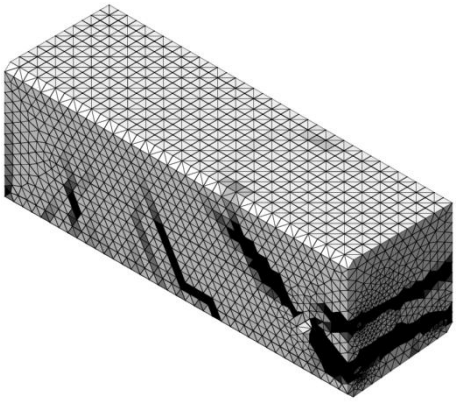

*Figure 4.13 Crack pattern in terms of maximum principle tensile strains from three-dimensional numerical analyses.*

A concrete structural member can be strengthened in several different ways in order to improve the shear capacity. This study focused on two main options, either strengthening with fibre reinforced polymer (FRP) or strengthening with steel bars.

FRP is a composite material made of polymer matrix reinforced with fibres. The fibres are usually glass, carbon or aramid, while the polymer is usually an epoxy, vinylester or polyester thermosetting plastic, see Bohlin and Olofsson (2010). The FRP is available in form of cylindrical or quadratic rods similar to elaboration of reinforcing steel, strips which are unidirectional, sheets or fabrics that are flexible with fibres in either one or least two different directions. FRP is functional in a prestressed state, pre-tensioned state to be precise, see Bohlin and Olofsson (2010).

FRP is bonded externally or internally to a concrete member. Strips, sheets or fabrics are bonded externally to the concrete surface, adhering additional reinforcement to the external faces of the structural member. For maximum efficiency of the strengthening, the FRP should be mounted with the fibre direction as parallel as practically possible to the maximum principle tensile stresses. The member can be strengthened either by side bonding, U-jacketing or wrapping, depending on practical conditions and strengthening requirements. The different arrangements are illustrated in Figure 4.14. It is also possible to mount the reinforcement internally by drilling holes in the concrete member.

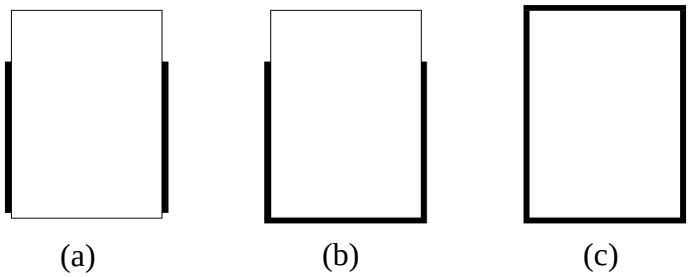


*Figure 4.14 Different arrangements when mounting FRP on the surface: (a) side bonding; (b) u-jacketing; and (c) wrapping.*

It is common to use an intermediate method to the externally and internally mounting, by applying near surface mounted reinforcement; slots are then cut by sawing in the concrete face wherein reinforcement bars are placed, usually quadric rods, and bonded using either epoxy or cement mortar, see Figure 4.15.

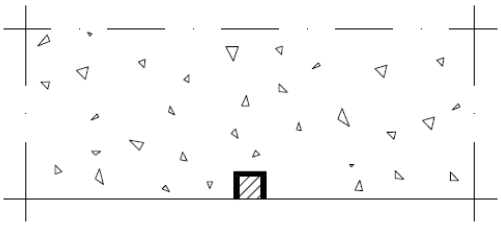

*Figure 4.15 Near surface mounting.*

Wrapping was never seen as a promising option for strengthening the beams studied in this thesis, since it would have had a large influence on the confinement with its support pressure. It is though a more efficient way of strengthening in comparison to side bonding and U-jacking with regard to anchorage. In further examination, both side bonding and U-jacking, together with near surface mounting were excluded from the list of potential ways of strengthening the edge beams; this due to the risk of insufficient transmission length of the anchorage. Thereto, the edge beams show different extent of deterioration, from no sign of corrosion to cover spalling; the latter showing poor accessibility in external and near surface mounting. The extra "heel" of concrete, described in Chapter 3, also causes practical difficulties of the establishment. In addition, external bonding require that the concrete surface is blasted which could cause more damage to the beams.

Internal mounting was considered to be the most promising option. In this method, vertical holes are drilled and reinforcing ribbed steel bars or cylindrical FRP rods are bonded using either epoxy adhesive or cement mortar. If the extra bars are internally mounted between the longitudinal bars, they do not influence the confinement considerably, but may have an effect on the splitting cracks between the main bars. Steel bars were preferred over composite FRP rods, mainly due to the deeper knowledge that exists for modelling the steel bars. Epoxy was chosen as adhesive in prior to the cement mortar, mainly due to shorter curing time and better workability. The number of reinforcing steel bars, their location, in addition with their dimension and steel quality, were determined by running a number of analyses until there was no considerable risk of yielding of the strengthening reinforcing steel, i.e. strengthening became an additional parameter in the design of the test set-up. The location of the strengthening bars were adopted to the real conditions. No bars should risk to be cut when the holes were drilled, why the location were given some constraints. The location was also adopted to replicate the design of two-legged stirrups. With respect to the load-bearing capacity, it was considered to be essential to provide the beam with pairs of strengthening bars on both sides of the suspension hole. The location of the bars was not varied that much throughout the analyses; however, the effect of the steel quality and the dimension were investigated to a larger extent. The bars, used in the strengthening, were modelled as embedded.

The most promising test configuration with respect to the location of the load and the suspension hole, together with the strengthening is depicted in Figure 4.16. The strengthening made it possible to place the suspension hole anywhere, without risking local failure of the suspension hole. However, the suspension hole was located in the upper half of the beam; cracks developing around the suspension hole could else influence and interfere the anchorage region of the main reinforcement bars.

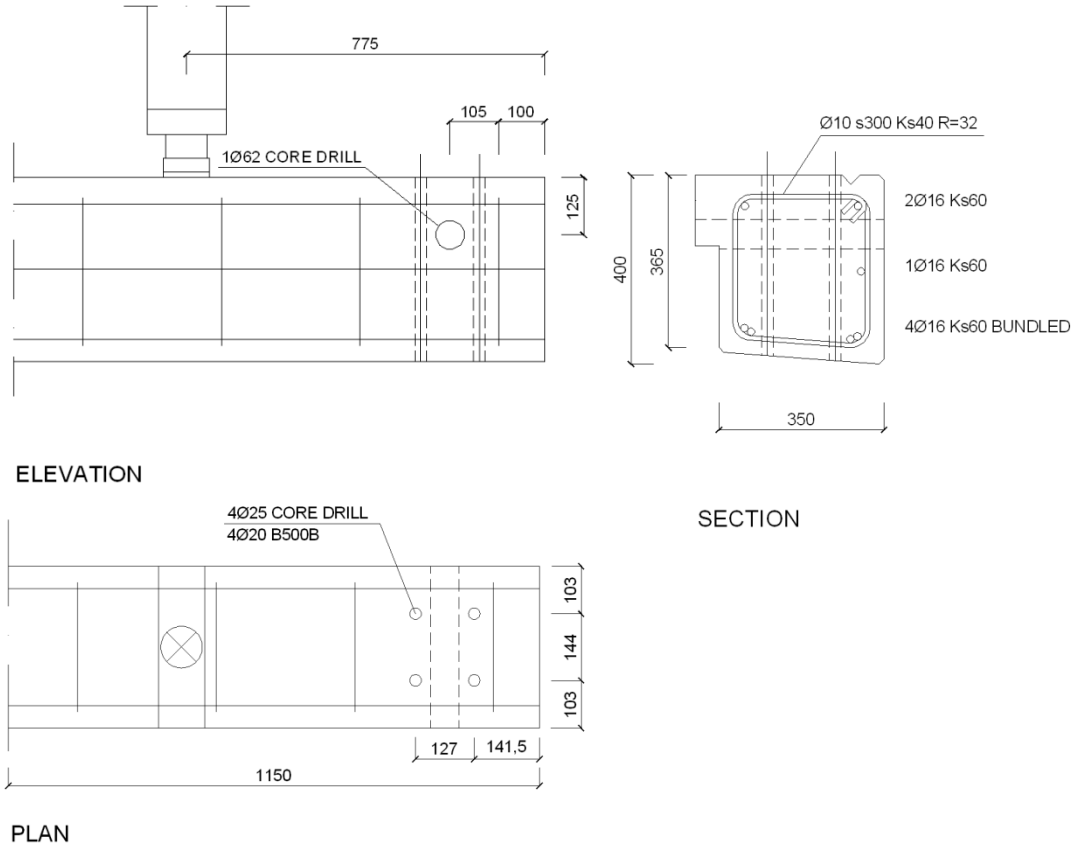


*Figure 4.16 Details of potential test.*

The beam was strengthened with 4 ø20 mm B500B steel reinforcement bars. The type, B500B, was chosen since it is the most commonly used rebar type in Sweden. The adhesive epoxy-layer around the reinforcement should preferably have a dimension of 2 mm according to Blanksvärd[1]. Accounting for the ribs of the reinforcement bars (≈ +2 mm), a core drill with a dimension of 25 mm was chosen; this resulted in an epoxy-layer of 1.5 mm which was considered to be sufficient. It should be mentioned that 4 ø16 mm bars were considered to be sufficient in strengthening the beam, carrying the entire applied load before yielding. It was though troublesome to find an appropriate dimension of a core drill with respect to the requirements of the epoxy-layer; hence, the dimension of ø16mm was not a practical solution. The reinforcement was blasted in order to achieve the best chemical adhesion possible, between the reinforcing steel and the epoxy. The holes were drilled through the depth of the beam.

There are several other ways of strengthening the structure, than those mentioned in this report. All techniques that involve external pressure in the anchorage region of the main bars should though be avoided so that the confinement is not disturbed; else there is a risk of altering the confinement conditions of the longitudinal bars in the tensile zone.

The test set-up in Figure 4.16 was analyzed in detail. Relationships such as applied load vs. mid-span displacement and applied load vs. free-end slip were studied, see Figures 4.17-4.18. Other results received from the three dimensional FE analyses

[1] Ph. D. Thomas Blanksvärd: Sto Scandinavia AB. Product Manager Nordic Countries. Civil Engineering (March 2011).

were also studied: the maximum principle strains indicating the crack pattern, see Figure 4.19, and the stresses in the reinforcement, see Figure 4.20.

The third stirrup, counted from the beam end, yielded just before maximum load was reached. The stresses in that step are given in Figure 4.20. The yield capacity of the longitudinal tensile reinforcement was not reached though; hence, no larger plastic deformations appeared and the compressive zone was not crushed, i.e. flexure failure did not occur.

Locally the tensile stresses peaked, the reason for that are the appearance and the development of cracks. In a reinforced concrete member loaded in tension, the tensile force is resisted by both the reinforcing steel and the surrounding concrete. The load transfer between the bars and the embedment is assured by the bond between them. The longitudinal load transfer is not uniform as the force in a reinforcing bar changes along its length, the same thing will occur in the concrete embedment. In the uncracked state, the concrete strain and the steel strain are equal at the same level of the reinforcement. In cracked state, the load needs to be entirely carried by the reinforcement across the cracks. Thus, the strains in a bar embedded in concrete are smaller than those in a bare bar, at all load levels. The decrease in steel strain due to the concrete may be considered as a stiffness increase of the reinforcement compared to the bare bar. This bond-related phenomenon is called tension-stiffening, see CEB (2000).

The development of cracks in the shear span was crucial in the analyses; this since the inclined shear cracks had to cross the tensile reinforcement, close to the section of suspension, for the anchorage to become critical. Due to the inclined cracks in the shear span, the tensile stresses in the main reinforcement increased; at the same time the available anchorage length decreased. The crack development, of the test set-up in Figure 4.16, indicates that the beam failed in an anchorage failure. The first cracks were of flexural type and occurred between the two concentrated loads. With increased load, flexural cracks and inclined shear cracks developed in the shear span, where the flexural cracks formed close to the stirrups and the inclined shear cracks curved towards the concentrated loads. The anchorage became more stressed when the cracks propagated towards the support. At a critical stage, the transmission length was too short in order to transfer the tensile forces in the main reinforcement bars to the surrounding concrete; i.e. the beam failed due to insufficient anchorage of the tensile reinforcement.

It should be noted that cracks also developed around the suspension hole; they never became critical though, due to the strengthening of steel reinforcement bars.

The three dimensional analysis showed no substantial, but still recognizable, residual load-bearing capacity, see plateau in Figure 4.17. The free end slip were considerable (0.1-0.2 mm) in the pre-peak stage; i.e. up to maximum load; subsequently, the free end slip increased while the load was constant, which is represented by a descending branch in Figure 4.18. The continuous descending branch in the post peak stage speaks for a stable failure. Besides the flexural and inclined shear cracks, the three dimensional crack pattern indicated transverse cracks and longitudinal splitting cracks in the anchorage zone, see Figure 4.19 (c) and Figure 4.19 (e). The failure was designated as a splitting induced pull-out failure, where concrete cover was spalled off gradually as the free end-slip increased.

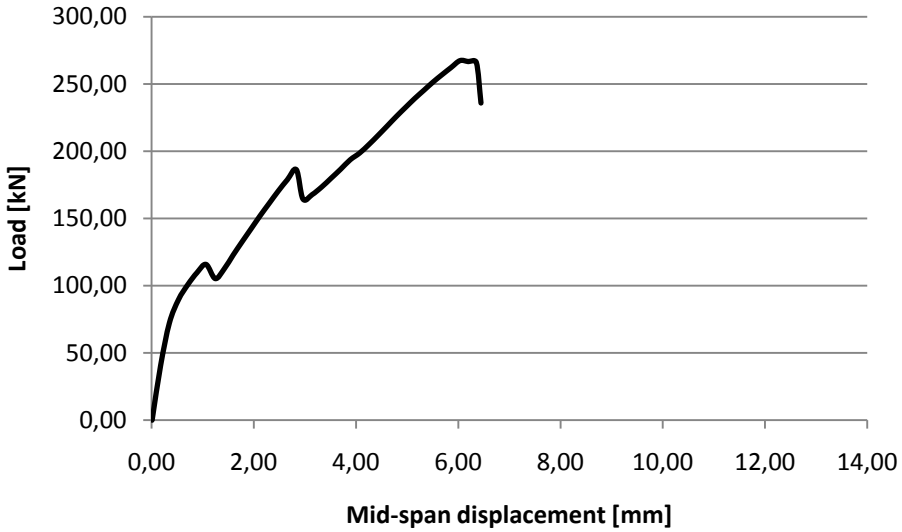


*Figure 4.17 Applied load vs. mid-span displacement from three-dimensional analysis.*

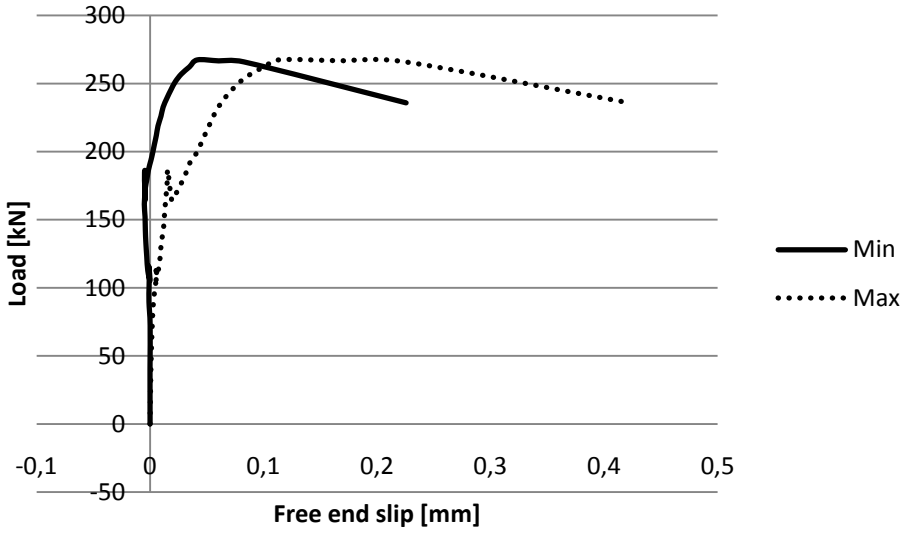


*Figure 4.18 Applied load vs. free end slip from three-dimensional analysis. Min and Max are represented by the upper and lower pair of bundled main bars respectively.*

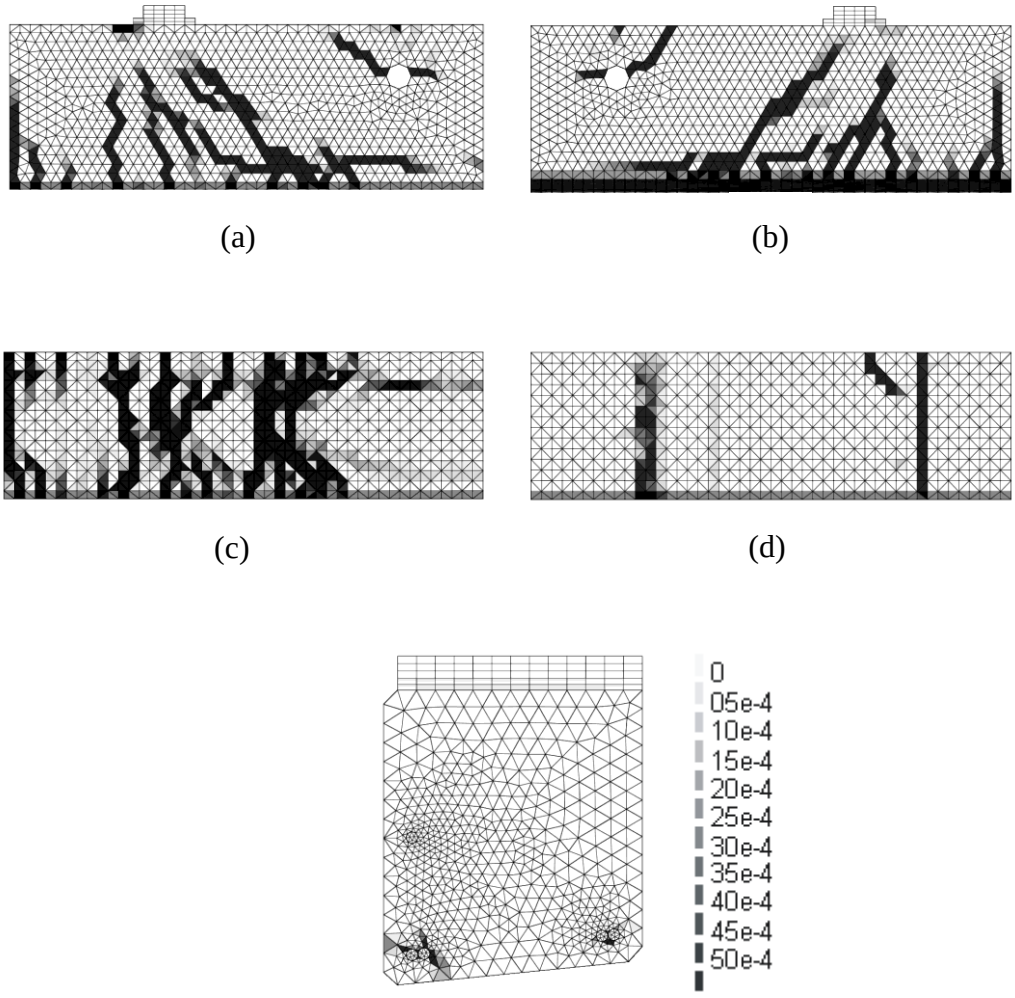


*Figure 4.19* *Crack patterns in terms of maximum principle tensile strains from three-dimensional numerical analyses: (a) front; (b) rear; (c) bottom; (d) top; and (e) free end.*

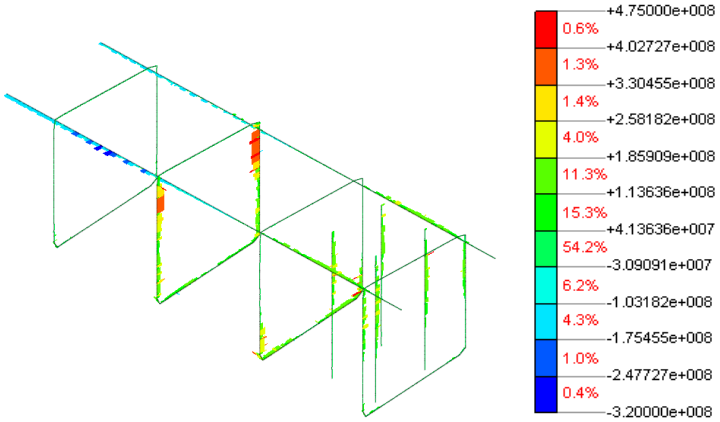


*Figure 4.20* *Stresses in embedded reinforcement one load step prior to maximum load.*

# 5 Experiments

All tests were performed at the laboratory of Structural Engineering at Chalmers University of Technology

## 5.1 Material properties

Experiments of the main and transverse reinforcement bars, together with tests of the concrete, should be carried out in order to update the numerical model with the actual data of the material properties.

### 5.1.1 Concrete

Tests of the cylindrical compressive strength ($f_{c,\ cyl}$), according to the Swedish Standard SS-EN 12390-3, were conducted. The test specimens were drilled according to Swedish Standard SS –EN 12504-1. The drilled cores had a height of 108 mm and a diameter of 54 mm. Considering the small diameter, the strength value was recalculated according to Swedish Standard SS –EN 13 72 07. All the standards are given in Swedish Standards Institute (2002). The strength value, given in Table 5.1, was determined as the mean value from series of five tests.

The compressive strength was also measured with a test hammer. The hammer was of type N with impact energy of 2,207 Nm. The test was carried out on the short face of the beam. The compressive strength in Table 5.1 shows the mean value of ten tests.

*Table 5.1 Compressive strength of concrete.*

| | $f_{cc,cyl}$ [MPa] | $f_{cc,hammer}$ [MPa] |
|---|---|---|
| Concrete | 49,5 | 44,0 |

The intention was to do additional tests in evaluation of the splitting tensile strength ($f_{t,sp}$) and the modulus of elasticity ($E$) according to the Swedish standards SS-EN 12390-6 and SS 13 72 32, but the time was short and the tests had to be excluded from this thesis.

The toughness of the concrete is also an important parameter if brittle failures are to be avoided. The toughness can be quantified by means of the fracture energy, $G_F$. Spot test in determination of the fracture energy can be made according to RILEM 50-FMC Committee (1985). The technique was though not adoptable or applicable on the concrete specimens received from Stallbackabron.

### 5.1.2 Steel reinforcement

There was no time for tests of the reinforcement. It would have been very interesting to execute tensile tests of the main bars and the stirrups, i.e. the reinforcement with the most sever deterioration due to corrosion.

## 5.2 First beam test

The test set-up was determined through extensive numerical approach, see Chapter 4. The loading arrangement and the instrumentation of the test are schematically shown in Figure 5.1. Details of the test set-up are shown in Figure 4.16. The first test was performed on a specimen of damage level L3, see Chapter 3.

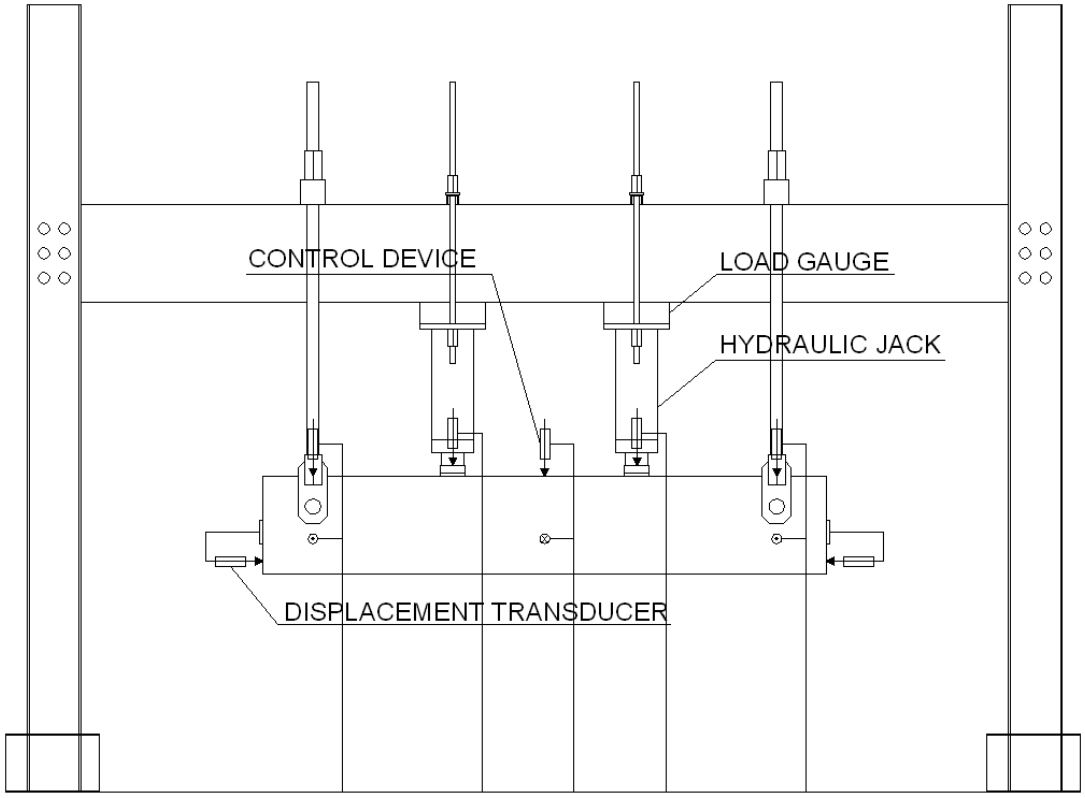


*Figure 5.1 The loading arrangement and the instrumentation of the first beam test.*

The test was conducted by displacement control with a mid-span displacement rate of about 0.1 mm/min up to maximum load. Displacement control was adopted to permit measurements in the post-peak stage. The control device was placed on top of the beam in the mid-span. The load was applied by two symmetrically placed hydraulic jacks and was measured by load gauges, i.e. load cells, placed on top of each jack. Both jacks were connected to the same pump to ensure that the loads were equal or about the same magnitude. The load was applied in the opposite direction to that of the casting of the edge beam, as it was placed upside down. To spread the stresses from the concentrated loads acting on the concrete beam and to avoid local crushing of the concrete, a steel plate (350×100×30mm) and a fibre board (350×100×12.5mm) were placed between the hydraulic jack and the concrete beam. The mid-span displacement was measured relative to the floor by a linear variable differential transformer (LVDT), i.e. displacement transducer. Furthermore, displacement transducers measured the vertical displacements relative to the floor in sections of the suspensions and the loads, two transducers at each suspension and one at each adjacent load. Two transducers in each section, located next to each long side, were desirable since the beam has a non symmetric cross section which could cause skew bending and interfere with the measurements. All transducers measuring relative to the floor were positioned by floor-stands. Displacement transducers, one per main bar, were placed on the short-face of the beam ends to measure the free end slip of the reinforcement. The end slip was measured relative to a point on the short-face of the beam end, located about 80 mm above the uppermost main reinforcement bar, see Appendix F. Due to the inclined cross section of the beam, the distance between the reference point and the measured reinforcement bar differed from bar to bar. The displacement transducers were positioned by magnetic stands attached to a steel plate, anchored on the short face. The arrangement of all displacement transducers is given in Appendix F. All of the data were continuously stored in a data-log, 1 log/s.

In addition, the crack development was continuously registered and the lateral mid-span displacement was plotted against transverse mid-span displacement on a xy-recorder. Two other displacement transducers, in the sections of the suspensions and in lateral direction, were connected to volt-meters in order to indicate if the beam tended to rotate or move in a rigid body motion. From the analyses it was shown that the beam tended to move in lateral direction. For safety reasons, in case of extensive displacements, heavy supports were placed in the mid span on each side of the beam. The actual test set-up is depicted in Figure 5.2.


*Figure 5.2 Actual test set-up.*

### 5.2.1 Results

The first beam test resulted in a local failure at the suspension hole, due to insufficient anchorage of the strengthening steel bars. The transmission length between the critical crack, initiating from the suspension hole and propagating to the adjacent concentrated load and to the free end, was too short, i.e. the chemical adhesion from the epoxy could not withstand the bond stresses. The required transmission length, i.e. the critical anchorage length, was hard to predict since few studies have been made dealing with the bond behaviour and the corresponding anchorage capacity of steel reinforcement bars, assembled to concrete structures using epoxy adhesive.

The initial crack pattern and the crack pattern after loading are given in Appendix H and Appendix I respectively. The critical cracks are marked with continuous bold solid lines. Note that the critical cracks include splitting cracks, penetrating the concrete cover around the compressive reinforcement bars and in between the bars. As a result, the longitudinal bars in the compression zone showed a considerable free end slip. Other sever cracks developed around the suspension hole, forming a wedge between the hole and the top of the beam.

The average load of the two hydraulic jacks were plotted against the mid-span displacement, see Figure 5.3. The maximum load was about 170 kN. The change of

stiffness indicates that crack appeared. Since the edge beam failed in an unwanted local failure at the suspension hole, no free end slip of the tensile reinforcement were measured and therefore not shown here.

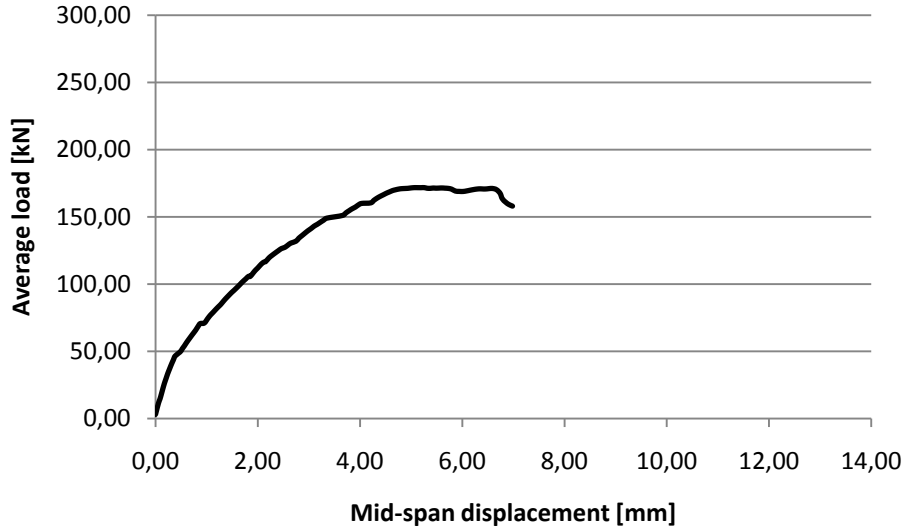


*Figure 5.3 Average load vs. mid-span displacement.*

An extra loading cycle was executed where the slip of one strengthening reinforcement bar was measured. The result is depicted in Figure 5.4. The extra load cycle confirmed that it was lack of anchorage of the strengthening reinforcement bars that caused the failure.

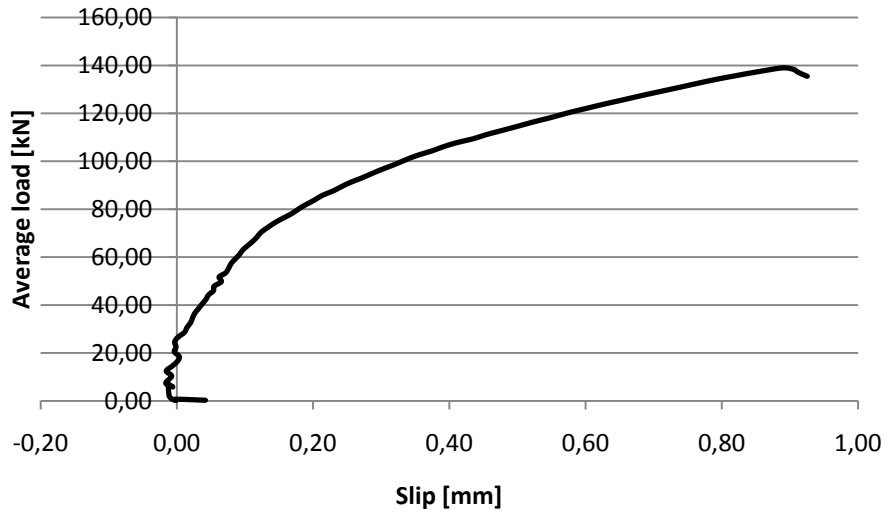


*Figure 5.4 Average load vs. free end-slip of one strengthening reinforcement bar.*

## 5.3 Second beam test

The experience gained from the first beam test led to a modification of the strengthening, shown in Figure 5.5. The strengthening bars, 4 ø16 B500B, from the first test were replaced by bars of prestressing steel (dywidags) with a diameter of 20 mm. The high yield reinforcing steel, fully threaded, were anchored at the top of the beam with hexagonal nuts and flat steel plates. The mechanical docking of the bars, by means of threaded coupling, was considered to provide the additional anchorage

needed in the first beam test. The bars were injected with epoxy, the same technique used in the first test. Epoxy was also applied in between the flat steel plate and the concrete beam in order to obtain even pressure. The specimen used in the second test had a damage level of L1, see Chapter 3. Besides that the suspension hangers were equipped with strain gauges, the test method used was about the same as for the first beam, see Section 5.2. The arrangement of the strain gauges and all the displacement transducers is given in Appendix G.

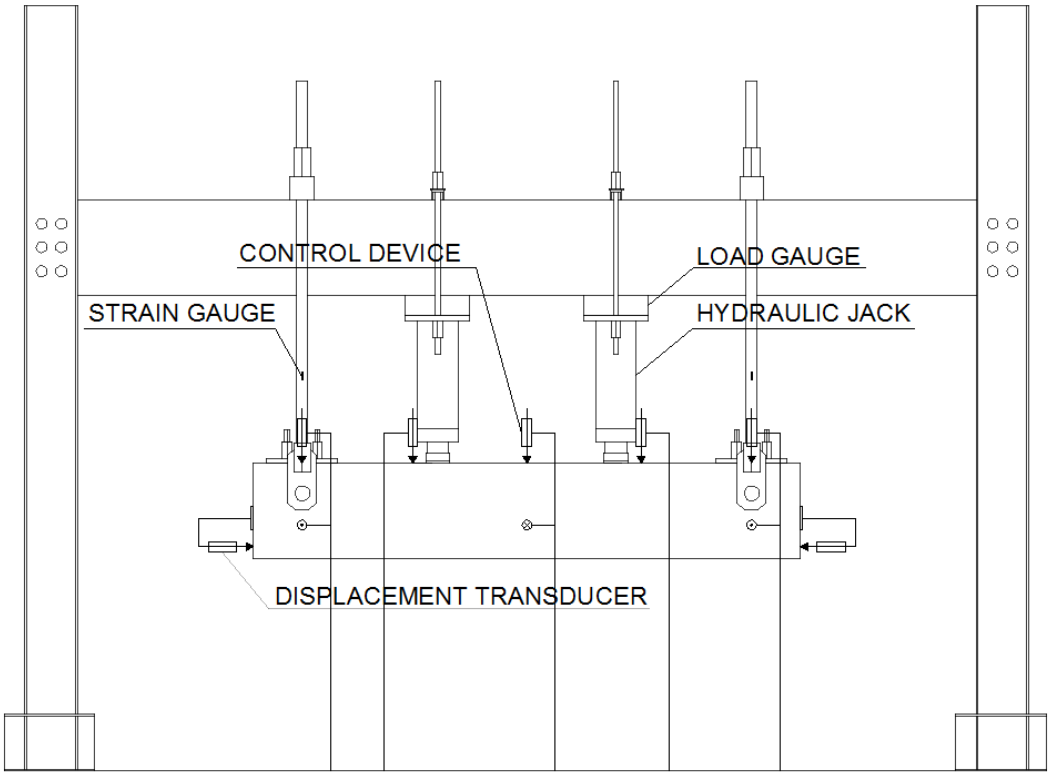


*Figure 5.5 The loading arrangement and the instrumentation of the second beam test.*

The details, with some reservation regarding the location of the suspension hole, are given in Figure 5.6. In reality, the suspension hole was placed 30 mm closer to the top surface of the beam. It should be mentioned that one of the main bars was damaged when the holes of the strengthening bars were drilled. The damaged bar was equipped with the displacement transducer named FES 14 in Appendix G.

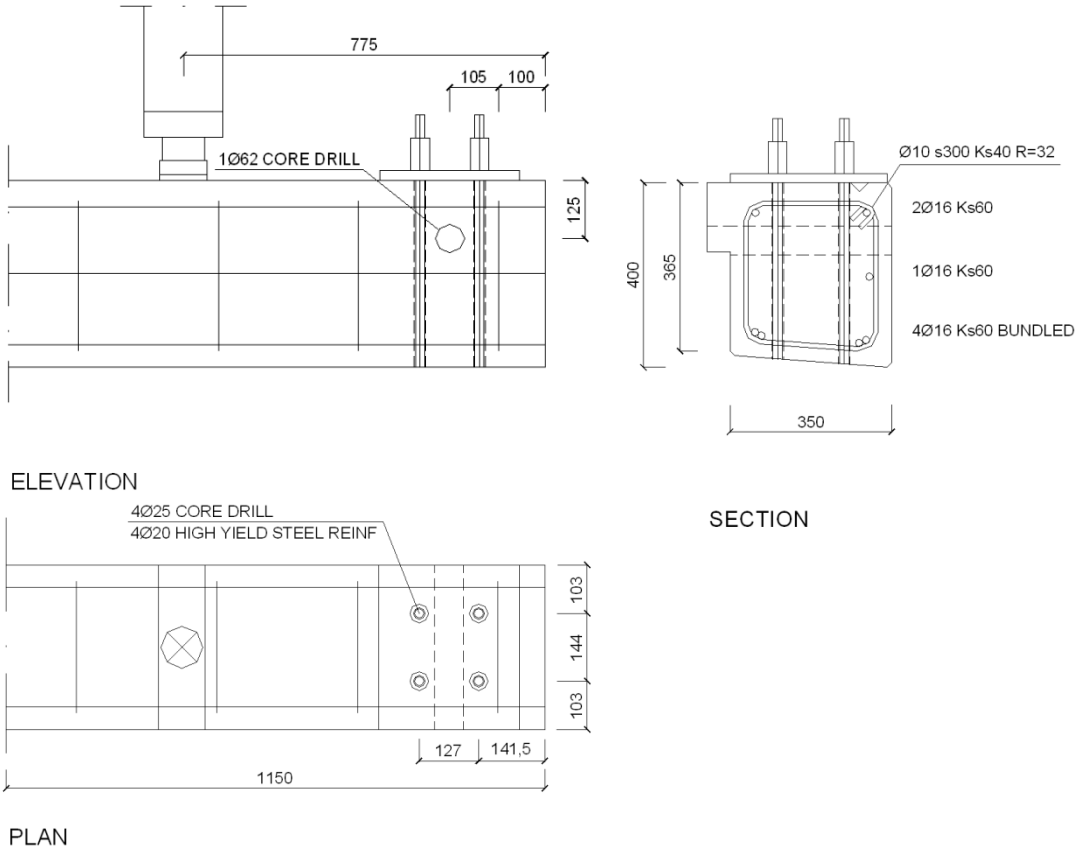


*Figure 5.6 Details of potential test set-up with improved strengthening.*

### 5.3.1 Results

The second beam test resulted in anchorage failure and had a good correspondence to the three-dimensional simulation.

The initial crack pattern and the crack pattern after loading are given in Appendix J and Appendix K respectively. The critical cracks are marked with continuous bold solid lines. The anchorage length from the experiment is considerably shorter in comparison to the length distinguished in the simulation; hence, the critical shear crack propagated closer to the section of the support, i.e. the critical shear crack was less inclined.

The average load of the two hydraulic jacks were plotted against the mid-span displacement, see Figure 5.7. The maximum load was about 270 kN, the same load that was received in the simulation. The three-dimensional simulation showed though a stiffer behaviour in the pre-peak stage. Unlike the simulation, the experiment showed a considerable residual load-bearing capacity of about 70-75%. The sudden drop in the post-peak stage, from the maximum load down to the more or less constant branch representing the residual capacity, indicates that the failure was not completely stable. The recognizable small increase of average load in the post-peak stage depended on an increase of loading rate, from 0.1 mm/minute to 0.5 mm/minute.

The change of stiffness indicates crack appearance. The difference in mid-span displacement for maximum load was only 0.5 mm when comparing the results received from the experiment with the results from the simulation.

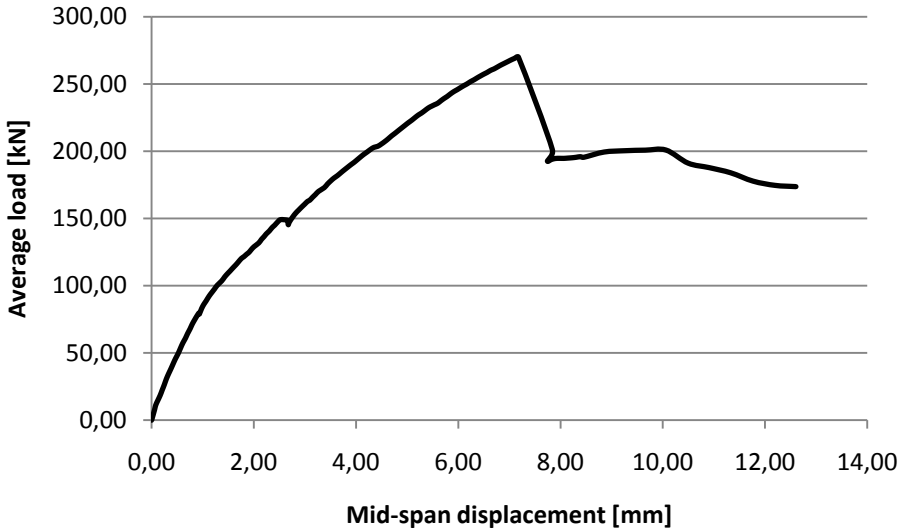


*Figure 5.7 Average load vs. mid-span displacement.*

All the main bars had a considerable slip of 0.1 mm in the pre-peak stage, see Figures 5.8-5.9, which speaks for an anchorage failure. The discontinuous descending branch in the post-peak stage, together with the discontinuous behaviour of the residual load bearing capacity, indicates though that the failure is not completely stable. Considering the structural behaviour, the failure mode was after all designated to be a splitting induced pull-out failure, just as in the three dimensional simulation.

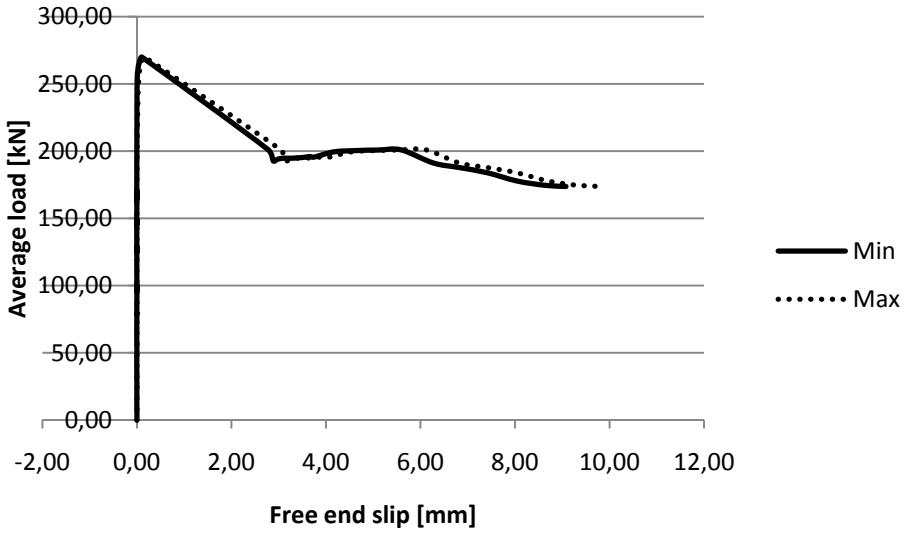


*Figure 5.8 Average load vs. free end slip. Min and Max are represented by the upper and lower pair of bundled main bars respectively.*

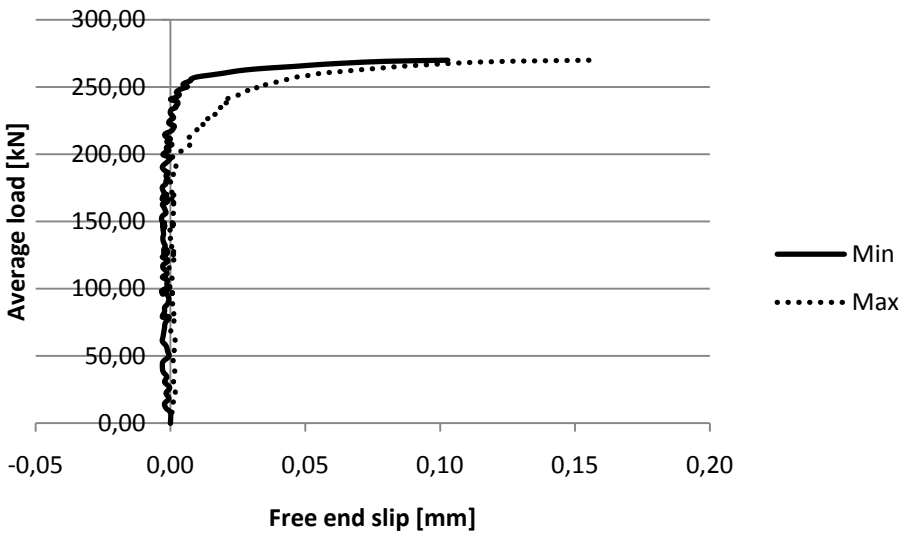


*Figure 5.8 Average load vs. free end slip;magnification. Min and Max are represented by the upper and lower pair of bundled main bars respectively.*

# 6 Conclusions

The aim of this master's thesis was to design a test set-up for naturally corroded edge beams from Stallbackabron, in which anchorage failure was captured. A four point bending test indirectly supported with suspension hanger was considered to be the best test set-up with its least disturbance and influence of the natural damages. Details of the final test configuration is depicted in Figure 5.6. The detailed design was done by using a non-linear finite element method. Two dimensional simulations of the test set-up indicated anchorage failure but were considered to be unreliable and insufficient in describing anchorage failure. In more advanced three-dimensional simulations, the test set-up was developed and a potential test configuration was established. It was seen that the edge beams needed to be strengthened with transverse reinforcement, else they would have failed in a local failure at the suspension hole or in shear. The technique adopted for the strengthening was an internal mounting of steel reinforcement using epoxy as adhesive.

In order to validate the test set-up, a first beam test was conducted. The beam failed in a local failure at the suspension hole due to insufficient anchorage of the strengthening bars. This could not be foreseen in the numerical simulation. With experience gained from the first beam test, the strengthening was improved. The new establishment of the test set-up was validated in a second beam test. This time the beam failed in a, not completely stable, splitting induced pull-out failure, i.e. anchorage failure was captured and the aim of this thesis was achieved.

Hopefully, this work has opened for further experiments on edge beams from Stallbackabron. With a large number of experiments on the naturally corroded concrete structures, a considerable amount of data would be obtained. Data that could be used in order to validate and develop the empirical bond models of today, which are based on investigations of artificially corroded concrete members. Those state-of-art models are at the moment used with great caution, but after have determined their reliability and how well they represent field conditions, perhaps they will be used in a larger extent in the assessment of residual load-bearing capacity of corrosion-damaged concrete structures and in the assessment of remaining service lifetime. Thereto, they may be used in the establishment of enhanced and more effective repair and maintenance strategies.

# 7 Further research

The two –and three dimensional simulations gave different results. The bond behaviour is obviously a three dimensional phenomenon why the three-dimensional simulation is considered to be more reliable in comparison to the two-dimensional simulation. It would be of interest to investigate how the simulation in various dimensions, analytically and numerically, differs and to compare their accuracy under certain conditions.

The numerical model established within this work can be developed further in order to improve the accuracy and precision. The material properties can be updated by carry out material tests. Recommended tests are: modulus of elasticity and tensile splitting strength of the concrete, together with tensile test of the steel reinforcement, both the main bars and the stirrups. Inserting a corrosion model would also improve the structural model. This requires though that the corrosion level, with respect to both uniform and pitting corrosion, of the edge beams can be estimated. The main uncertainties of the existing structural model concerns the epoxy injected steel bars. It was modelled as embedded in the concrete, which proved a poor correspondence to the real behaviour. To develop a sufficient model that describes the bond behaviour of the epoxy injected steel bars is not easy, since few studies have been made dealing with the bond behaviour and the corresponding anchorage capacity of steel reinforcement bars, assembled to concrete structures using epoxy adhesive. It is therefore worth to consider injecting the strengthening steel bars with cement mortar in the future tests on the edge beams from Stallbackabron. The strengthening bars could then be modelled with the same technique used for the longitudinal tensile reinforcement. As more tests on edge beams from Stallbackabron are conducted, the structural model can be configured by adjustments and modifications so that it correspond better to the real measurements received from the experiments.

Recommendations for further tests on the edge beams from Stallbackabron: the tests should be conducted in a laboratory with similar heat and moisture conditions as conventional field conditions; a sudden change of the conditions could else result in cracking. The initial crack pattern, before loading, needs to be documented. It is of interest to distinguish the different cracks from each other regarding the crack width and their origin such as effects of frost and corrosion, or from loading during its service life time. It is also of interest to investigate whether the vibrations, from the time when the specimens were cut and removed from the bridge, have had any effects on the initial crack pattern of the concrete specimens. Throughout the tests, the crack development should be documented in detail by studying the occurrence and the load level at which the cracks initiated and propagated; the resulting crack pattern should subsequently be examined.

The failure of the second beam test, designated to be a splitting induced pull-out failure, showed to be instable; this undesired behavior need to be investigated further. A possible explanation of the instable behavior could be that the anchorage of the strengthening steel bars fails locally, just as in the first beam test, but this time in the bottom of the beam. When the critical shear crack developed and crossed the strengthening steel bars, the anchorage probably became more stressed and the transmission length, between the critical crack and the bottom of the beam, was probably not sufficient in resisting and withstand the bond stresses. A local failure of the strengthening reinforcement could have influenced and interfered with the structural failure of the longitudinal tensile reinforcement. Local failure of the

strengthening steel bars can be investigated by measuring their free end slip during loading, using displacement transducers. If it could be determined that local anchorage failure was the cause of the instable behavior in the second beam test, a solution to this problem could be to attach threaded expandable fasteners to the strengthening steel bars in the bottom of the beam. Securing the anchorage with the same technique as in the top of the beam would have had too much of a disturbance on the confinement in the anchorage region. An alternative solution to the problem of instability could be to cut a thin slot in front of the strengthening, in the shear span, so that the critical inclined shear crack never crossed the strengthening bars; hence, the critical crack then do not risk to influence or interfere with the transmission length.

The notch of this type needs to be simulated in three dimensions, using non linear finite elements method. The influence of notches were never simulated in three-dimensions within this thesis, since all simulations with notches in two dimensions ended up in unwanted shear failure and it was assumed that three dimensions would show the same response, if tried out. Throughout the work, it has later been concluded that the response from two and three dimensional simulations significantly differ from each other and therefore it is relevant to reevaluate the importance of notches.

If the problem with instable failure cannot be overcome, there are arguments to reconsider the entire test set-up. One potential test configuration is suggested: a type pull-out test at a structural level, where an internal rod is pulled in longitudinal direction of the edge beam, see Figure 7.1.

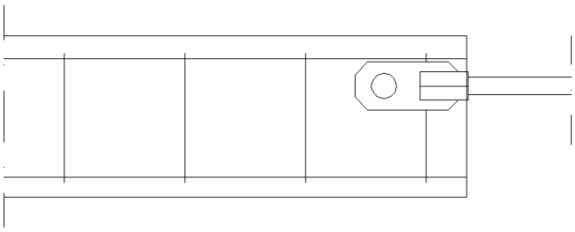

*Figure 7.1 Alternative test set-up.*

# 8 References


Al-Emrani, Mohammad, Engström, Björn, Johansson, Marie & Johansson, Peter (2008a). *Bärande konstruktioner –Del 1*. Göteborg: Chalmers tekniska högskola, Institutionen för Bygg –och miljöteknik, Avdelningen för konstruktionsteknik, CTH.(Rapport 2008:12)

Bigaj, A.J. (1995): *Bond behaviour of Deformed Bars in NSC and HSC: Experimental Study*. Department of Civil Engineering, Delft University of Technology, Publication no. 25.5-95-II, Delft, Netherlands.

Bohlin, A. and Olofsson, K. (2010): *Strengthening of Concrete Slab Bridges with Regard to Shear Capacity*. MSc Thesis, Concrete Structures, Division of Structural Engineering, Department of Civil and Environmental Engineering, Chalmers University of Technology, Publication no. 2010:44, Göteborg, Sweden, 80 pp.

CEB (1993): *CEB-FIP Model Code 1990*. Bulletin d'Information 213/214, Lausanne, Switzerland.

CEB (2000): *Bond of reinforcement in concrete.* Bulletin 10, Lausanne, Switzerland.

DIANA (2010): *DIANA Finite Element Analysis, User's Manual, release 9.4.3.* TNO Building and Construction Research, Delft, Netherlands.

Eligehausen, R., Popov, E. P. and Bertero, V. V. (1983): *Local Bond Stress-Slip Relationship of Deformed Bars under Generalized Excitations*. Earthquake Engineering Research Centre, University of California, Report no. UCB/EERC 82/23, Berkley, California, USA, 169 pp.

EN1992-1-1 (2004): Eurocode 2: Design of Concrete Structures- Part 1-1: General rules and rules for buildings, CEN European Committee for Standardization, Brussels, 225 pp.

Engström, B. (1992): *Ductility of Tie Connections in Precast Structures*. Ph. D. Thesis, Division of Concrete Structures, Chalmers University of Technology, Publication no. 92:1, Göteborg, Sweden, 452 pp.

Engström, B. (1995): *Beräkning av betong- och murverkskonstruktioner: Del II – Beräkningsmodeller* (In Swedish). Division of Concrete Structures, Chalmers University of Technology, Publication no. 94:2B, Göteborg, Sweden.

Huang, Z., Engström, B., Magnusson, J. (1996): Experimental and analytical studies of the bond behaviour of deformed bars in high strength concrete. 4th International Symposium on Utilization on High Strength/High Performance Concrete-BHP 96, Paris, pp. 1115-1124.

Lundgren, K. (1999*): Modelling of Bond: Theoretical Model and Analyses*. Concrete Structures, Division of Structural Engineering, Department of Civil and Environmental Engineering, Chalmers University of Technology, Publication 99:5, Göteborg, Sweden.

Lundgren, K. (2001): *Bond between Corroded Reinforcement and Concrete.* Concrete Structures, Department of Structural Engineering, Chalmers University of Technology, Göteborg, Sweden, Report 00:3, 31 pp.

Lundgren, K. (2007): Effect of corrosion on the bond between steel and concrete: An overview. *Magazine of Concrete Research*, Vol. 59, No. 6, pp. 447-461.

Lundgren, K. and Gylltoft, K. (2000): A model for the bond between concrete and reinforcement. *Magazine of Concrete Research*, Vol. 52, No. 1, pp. 53-63.

Magnusson, J. (2000): *Bond and Anchorage of Ribbed Bars in High-Strength Concrete.* Ph. D. Thesis, Division of Concrete Structures, Chalmers University of Technology, Publication 00:1, Göteborg, Sweden, 300 pp.

RILEM 50-FMC Committee (1985): Determination of the Fracture Energy of Mortar and Concrete by Means of Three-point Bend Tests on Notched Beams. *Materials and Structures*, Vol. 18, pp. 285-290.

Sæther, I. (2010). *Structural Behaviour of Deteriorated and Retrofitted Concrete Structures*. Ph.D. Thesis, Department of Structural Engineering, Norwegian University of Science and Technology, Trondheim, Norway, 218 pp.

Shima, H., Chou, L-L. and Okumura, H. (1987a): Bond-slip-strain Relationship of Deformed Bars Embedded in Massive Concrete. Concrete Library of JSCE, No.10.

Shima, H., Chou, L-L. and Okumura, H. (1987b): Bond Characteristics in the Post-yield Range of Deformed Bars. Concrete Library of JSCE, No.10.

Shima, H., Chou, L-L. and Okumura, H. (1987c): Micro and Macro Models for Bond in Reinforced Concrete.J. of the Faculty of Engrg., University of Tokio, Publication no. 39 (2).

Swedish Standards Institute (2002): Betongprovning med svensk standard (In Swedish). SIS Förlag AB, Stockholm, Sweden.

Tepfers, R. (1973): A Theory of Bond Applied to Overlapped Tensile Reinforcement Splices for Deformed Bars. Ph.D Thesis, Division of Concrete Structures, Chalmers University of Technology, Publication no. 73:2, Göteborg, Sweden, 328 pp.

Zandi Hanjari, K. (2010): *Structural Behaviour of Deteriorated Concrete Structures.* Ph. D. Thesis, Concrete Structures, Division of Structural Engineering, Department of Civil and Environmental Engineering, Chalmers University of Technology, Göteborg, Sweden, 64 pp.

# APPENDIX A

## Stress- strain relationships of steel rebars

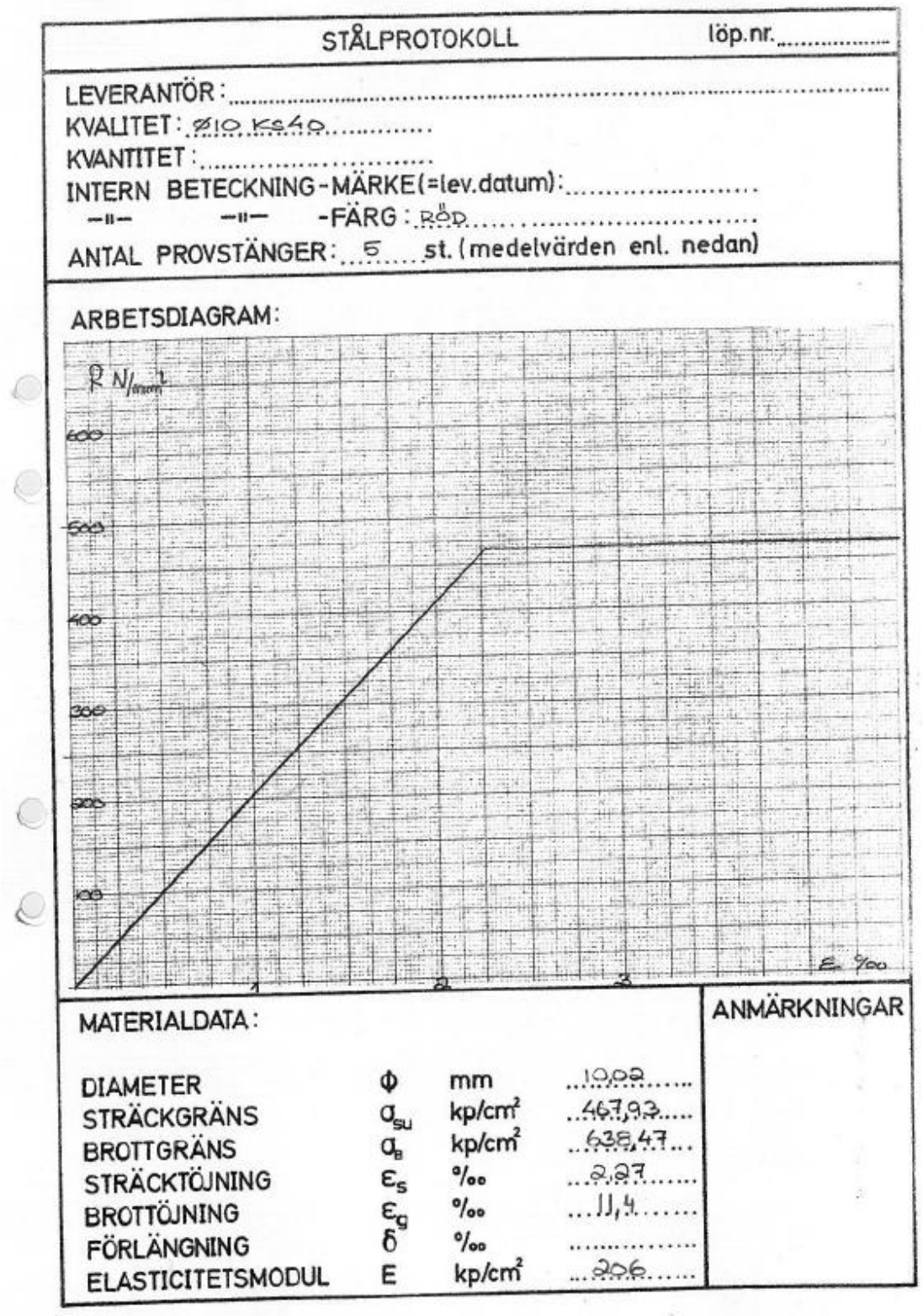


*Figure A1. Stress- strain relationship of reinforcement Ks40.*

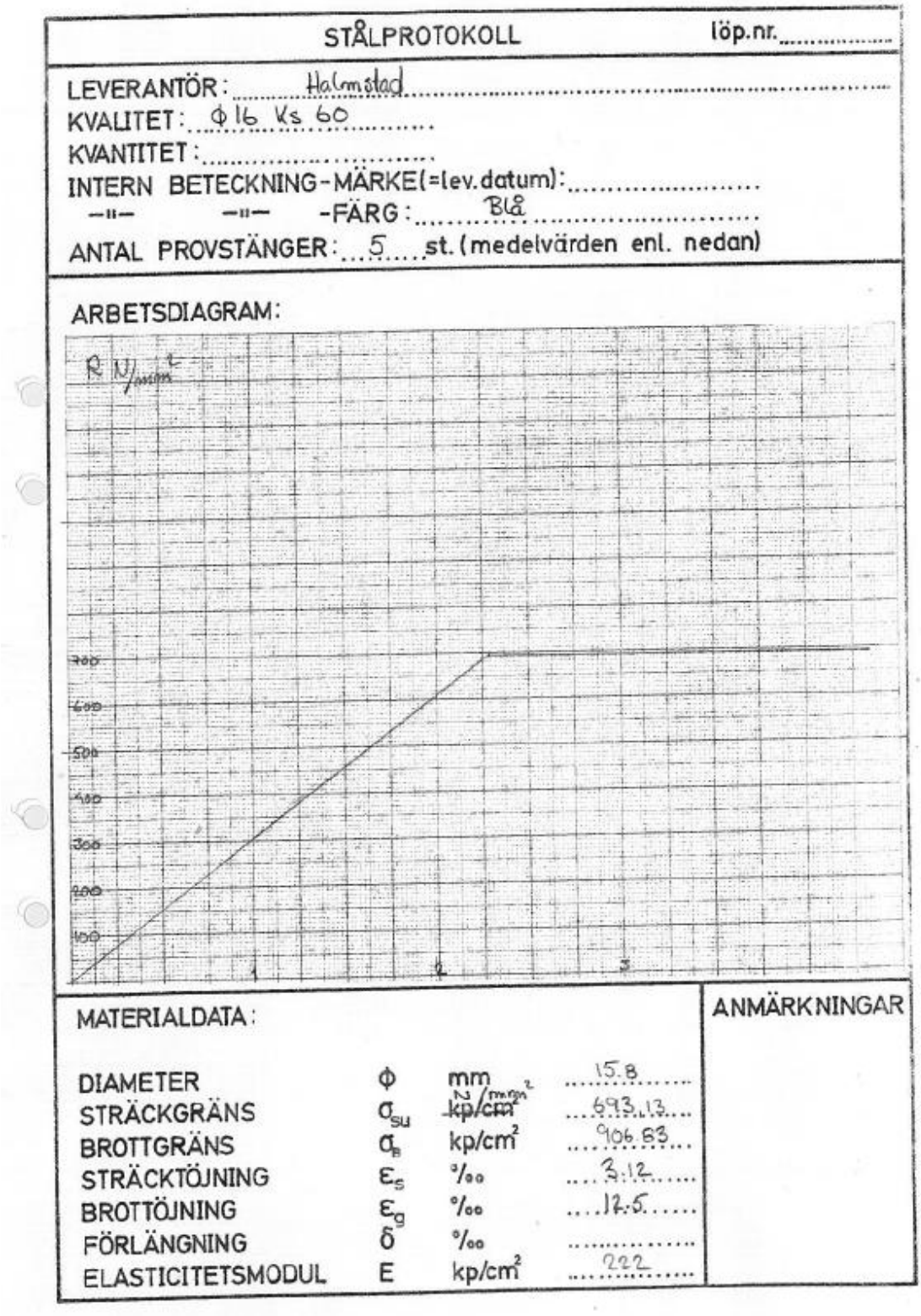


*Figure A.2. Stress- strain relationship of reinforcement Ks60.*

# APPENDIX B

## Data file for two-dimensional simulation

```
Translated from FX+ for DIANA neutral file (version 1.2.0).

'UNITS'
FORCE N                  }
LENGTH MM                }        2D analysis works best with mm and MPa
MASS  1.00000E+003       }

'DIRECTIONS'
   1  1.00000E+000  0.00000E+000  0.00000E+000
   2  0.00000E+000  1.00000E+000  0.00000E+000
   3  0.00000E+000  0.00000E+000  1.00000E+000

'COORDINATES'
   1  9.75600E+002  2.55000E+002  0.00000E+000
   2  9.87800E+002  2.52500E+002  0.00000E+000
   3  1.00000E+003  2.50000E+002  0.00000E+000
            .
            .
'ELEMENTS'
CONNECT
4351 L8IF   508 155 4525 4524          }
4352 L8IF   3505 508 4526 4525         }        Interface elements
4353 L8IF   4081 3505 4527 4526        }
            .                          }
            .                          }
4466 L2TRU  4524 4525                  }
4467 L2TRU  4525 4526                  }        Reinforcement elements
4468 L2TRU  4526 4527                  }
            .                          }
            .                          }
5127 L6BEN  91 4836      ————————————————       Dummy suspension
   1 Q8MEM  1 4 5 2                    }
   2 Q8MEM  2 5 6 3                    }        2D elements
   3 Q8MEM  4 7 8 5                    }
            .                          }
            .                          }
```

**Material properties' input**

```
'MATERI'
   1 NAME   "Concrete"
     YOUNG   3.30000E+004                    Young's modulus
     POISON  2.00000E-001                    Poisson's ratio
     DENSIT  2.40000E-006                    Density
     TOTCRK ROTATE                           Rotating total strain model
     TENCRV HORDYK                           Tensile curve
     TENSTR  2.90000E+000                    Tensile strength
     GF1     7.92000E-002                    Fracture energy
     CRACKB  1.00000E+001                    Crack band width
     COMCRV THOREN                           Compressive curve
     COMSTR  3.80000E+001                    Compressive strength


   2 NAME   "Interface"
     DSTIF   4.00000E+001  4.00000E+001      Dummy stiffness
     BONDSL 3                                Multilinerar bond-slip curve
     SLPVAL  0.00000E+000  0.00000E+000  5.48194E+000  1.00000E-001
             7.23346E+000  2.00000E-001  8.50712E+000  3.00000E-001
             9.54460E+000  4.00000E-001  1.04357E+001  5.00000E-001
             1.12252E+001  6.00000E-001  1.19391E+001  7.00000E-001   *
             1.25942E+001  8.00000E-001  1.32017E+001  9.00000E-001
             1.37700E+001  1.00000E+000  1.37700E+001  3.00000E+000
             5.50800E+000  5.80000E+000  5.50800E+000  1.00000E+001

                                          * Values for bond-slip curve


   3 NAME   "Reinforcement"
     DENSIT  7.80000E-006
     YOUNG   2.22000E+005
     POISON  3.00000E-001
     YIELD  VMISES                           Yield criterion
     HARDEN STRAIN                           Strain hardening
     HARDIA  6.93130E+002  0.00000E+000  9.06830E+002  1.25000E-001

   4 NAME   "Stirrup"
     DENSIT  7.80000E-006
     YOUNG   2.06000E+005
     POISON  3.00000E-001
     YIELD  VMISES
     HARDEN STRAIN
     HARDIA  4.68000E+002  0.00000E+000  6.38000E+002  1.40000E-001

   5 NAME   "Strengthening"
     YOUNG   2.06000E+005
     POISON  3.00000E-001
     DENSIT  7.80000E-006
     YIELD  VMISES
     HARDEN STRAIN
     HARDIA  4.68000E+002 0.00000E+000  6.38000E+002 1.14000E-001

   6 NAME   "DummySuspension"
     DENSIT  0.00000E+000
     YOUNG   1.95600E+011
     POISON  3.00000E-001
```

```
   7 NAME   "WoodBoard"
     YOUNG   1.60000E+003
     POISON  3.50000E-001
     DENSIT  6.00000E-007

   8 NAME   "SteelPlate"
     YOUNG   2.10000E+005
     POISON  3.00000E-001
     DENSIT  7.80000E-006
     YIELD  VMISES
     HARDEN STRAIN
     HARDIA  4.90000E+002 0.00000E+000  6.30000E+002 1.14000E-001
```

**Geometry and Data properties' input**

```
'GEOMET'
   1 NAME   "Interface"
     THICK   5.02000E+001
     CONFIG BONDSL
   2 NAME   "BotBar"
     CROSSE  8.04000E+002
   3 NAME   "MidBar"
     CROSSE  2.01000E+002
   4 NAME   "DummySuspension"
     CIRCLE  1.50000E+002
   5 NAME   "Concrete"
     THICK   3.50000E+002
   6 NAME   "WoodBoard"
     THICK   3.50000E+002
   7 NAME   "SteelPlate"
     THICK   3.50000E+002
   8 NAME   "Stirrup"
     CROSSE  1.57000E+002
   9 NAME   "TopBar"
     CROSSE  4.02000E+002
  10 NAME   "Strengthening"
     CROSSE  6.28000E+002

'DATA'
  12 NAME   "DummySuspension"
   1 NAME   "Concrete"
  13 NAME   "WoodBoard"
  14 NAME   "SteelPlate"
   3 NAME   "BotBar"
   4 NAME   "MidBar"
   2 NAME   "Interface"
   6 NAME   "Stirrup"
   8 NAME   "TopBar"
  10 NAME   "Strengthening"
```

## Assignment of material, data and geometry for 2D elements

```
MATERI
/ 1-4350 / 1
/ 4351-4465 4581-4695 / 2
/ 4466-4580 4696-4810 / 3
/ 5127 / 6
/ 5142-5169 / 7
/ 5170-5199 / 8
DATA
/ 5127 / 12
/ 1-4350 / 1
/ 5142-5169 / 13
/ 5170-5199 / 14
/ 4466-4580 / 3
/ 4696-4810 / 4
/ 4351-4465 4581-4695 / 2
GEOMET
/ 4351-4465 4581-4695 / 1
/ 4466-4580 / 2
/ 4696-4810 / 3
/ 5127 / 4
/ 1-4350 / 5
/ 5142-5169 / 6
/ 5170-5199 / 7
```

## Definition of embedded reinforcement

```
'REINFORCEMENTS'
LOCATI
   1 BAR
     LINE   1101 1100
     LINE   1100 954
     LINE   954 1816
      .
      .
   2 BAR
     LINE   3737 2754
     LINE   2754 3204
     LINE   3204 2371
      .
      .
   3 BAR
     LINE   934 933
     LINE   933 932
     LINE   932 931
      .
      .
   4 BAR
     LINE   2597 4539
     LINE   4539 2268
     LINE   2268 2592
      .
      .
   5 BAR
     LINE   126 479
     LINE   479 3456
     LINE   3456 2543
      .
      .
   6 BAR
     LINE   4756 4757
     LINE   4757 4758
     LINE   4758 4759
      .
      .
   7 BAR
     LINE   4795 4796
     LINE   4796 4797
     LINE   4797 4798
      .
      .
```

## Assignment of embedded reinforcement

```
MATERI
/ 5 / 3
/ 1-4 / 4
/ 6 7 / 5
GEOMET
/ 1-4 / 8
/ 5 / 9
/ 6 7 / 10
DATA
/ 1-4 / 6
/ 5 / 8
/ 6 7 / 10
```

**Definition of loads**

```
'LOADS'
CASE 1
WEIGHT
2 -9.81000E+000

:CASE 2
:DEFORM
:4892 TR 2 -1.00000E+000
```

Phased analysis

**Element groups**

```
'GROUPS'
ELEMEN
  12 "ConcreteBeam" / 1-4350 /
  18 "BotBar" / 4466-4580 /
  23 "MidInterface" / 4581-4695 /
  24 "MidBar" / 4696-4810 /
  25 "BotInterface" / 4351-4465 /
  34 "DummySuspension" 5127
  36 "WoodBoard" / 5142-5169 /
  37 "SteelPlate" / 5170-5199 /
```

**Boundary conditions and constraints**

```
'SUPPOR'
/ 121-159 4524 4640 / TR 1
/ 121-159 4524 4640 / TR 3
/ 91 / TR 2
:/ 4892 / TR 2
```

Phased analysis

```
'TYINGS'
ECCENT TR 2
/ 94 88 97 85 100 82 103 79 76 106 / 91
'END'
```

Link between slave- and master nodes

# APPENDIX C

## Command file for two-dimensional simulation

```
*FILOS
 INITIA                                  First phase
*INPUT
*PHASE

INPUT                                    }
READ TABLE LOADS                         }  Second phase
READ TABLE SUPPORTS                      }
*PHASE                                   }

BEGIN ACTIVE                             ——— Common for both phases
 ELEMENT ALL
 REINFO ALL
END ACTIVE
*NONLIN

  BEGIN TYPE
    BEGIN PHYSIC
    END PHYSIC
  END TYPE

BEGIN OUTPUT                             }
   FXPLUS                                }  Output saved in file ”1” for first phase
   FILE "1"                              }
 END OUTPUT                              }

BEGIN OUTPUT                             }
   FXPLUS                                }  Output saved in file “2” for second phase
   FILE "2"                              }
 END OUTPUT                              }

BEGIN EXECUTE
   BEGIN LOAD                            ———
    LOADNR=1                                 First load; self weight
     BEGIN STEPS
      BEGIN EXPLIC
      SIZES 1.0(1)                       ——— First load applied in one step
     END EXPLIC
     END STEPS
    END LOAD
    BEGIN ITERAT
      METHOD NEWTON REGULA               ——— Iteration method
:      METHOD SECANT BFGS
      MAXITE=100
:      LINESE
      BEGIN CONVER                       }
        ENERGY CONTIN TOLCON=0.0001      }
        FORCE CONTIN TOLCON=0.01         }  Convergence criterion
        DISPLA CONTIN TOLCON=0.01        }
      END CONVER
    END ITERAT
    SOLVE GENEL
  END EXECUT
```

```
  BEGIN EXECUTE
   BEGIN LOAD
    LOADNR=2
     BEGIN STEPS
      BEGIN EXPLIC
      SIZES 0.05(200)
     END EXPLIC
     END STEPS
    END LOAD
    BEGIN ITERAT
      CONTIN
      METHOD NEWTON REGULA
:      METHOD SECANT BFGS
      MAXITE=350
:      LINESE
      BEGIN CONVER
        ENERGY CONTIN TOLCON=0.0001
        FORCE CONTIN TOLCON=0.01
        DISPLA CONTIN TOLCON=0.01
      END CONVER
    END ITERAT
    SOLVE GENEL
  END EXECUT
*END
```

Only for second phase

Step size and number of steps

Iteration method

Convergence criterion

# APPENDIX D

## Data file for three-dimensional simulation

```
Translated from FX+ for DIANA neutral file (version 1.2.0).

'UNITS'
FORCE N
LENGTH M

'DIRECTIONS'
   1  1.00000E+000  0.00000E+000  0.00000E+000
   2  0.00000E+000  1.00000E+000  0.00000E+000
   3  0.00000E+000  0.00000E+000  1.00000E+000

'COORDINATES'
   1  0.00000E+000 -1.75000E-001  1.81000E-001
   2  0.00000E+000 -1.56000E-001  2.00000E-001
   3  0.00000E+000 -1.30538E-001  2.00000E-001
            .
            .
'ELEMENTS'
CONNECT
74952 T18IF 3545 59 58 14711 14579 14578
74953 T18IF 3454 3545 58 14615 14711 14578
74954 T18IF 3454 58 65 14615 14578 14595
            .
            .
79001 L6BEN 1348 16814
79002 L6BEN 5856 16815
79003 L6BEN 5857 16816
            .
            .
79172 TP18L 670 925 671 16829 16830 16831
79173 TP18L 671 925 672 16831 16830 16832
79174 TP18L 937 670 949 16833 16829 16834
            .
            .
    1 TE12L  7438 3168 3123 7307
    2 TE12L  6923 7590 9086 6975
    3 TE12L  12847 12819 11841 12656
            .
            .
```

3D analysis works best with m and Pa

Interface elements

Dummy beam elements

3D elements, Wood board and Steel plate

3D elements; Concrete and reinforcement

**Material properties' input**

```
'MATERI'
   1 NAME   "Concrete"
     YOUNG   3.30000E+010   ————————   Young's modulus
     POISON  2.00000E-001   ————————   Poisson's ratio
     DENSIT  2.40000E+003   ————————   Density
     TOTCRK ROTATE          ————————   Rotating total strain model
     TENCRV HORDYK          ————————   Tensile curve
     TENSTR  2.90000E+006   ————————   Tensile strength
     GF1     7.92000E+001   ————————   Fracture energy
     CRACKB  2.50000E-002   ————————   Crack band width
     COMCRV THOREN          ————————   Compressive curve
     COMSTR  3.80000E+007   ————————   Compressive strength

   2 NAME   "Top_bar"
     YOUNG   2.22000E+011
     POISON  3.00000E-001
     DENSIT  7.80000e+003
     YIELD  VMISES          ————————   Yield criterion
     HARDEN STRAIN          ————————   Strain hardening
     HARDIA  6.93130E+008 0.00000E+000  9.06830E+008 1.25000E-001

   3 NAME   "Stirrups"
     YOUNG   2.06000E+011
     POISON  3.00000E-001
     DENSIT  7.80000E+003
     YIELD  VMISES
     HARDEN STRAIN
     HARDIA  4.68000E+008 0.00000E+000  6.38000E+008 1.14000E-001

   5 NAME   "Bot_bar"
     YOUNG   2.34000E+011
     POISON  3.00000E-001
     DENSIT  7.80000e+003
     YIELD  VMISES
     HARDEN STRAIN
     HARDIA  7.30000E+008 0.00000E+000  9.57000E+008 1.25000E-001

   6 NAME   "Dummy_beam"
     DENSIT  0.00000E+000
     YOUNG   1.95600E+017
     POISON  3.00000E-001

   7 NAME   "Strengthening"
     YOUNG   2.06000E+011
     POISON  3.00000E-001
     DENSIT  7.80000E+003
     YIELD  VMISES
     HARDEN STRAIN
     HARDIA  4.68000E+008 0.00000E+000  6.38000E+008 1.14000E-001
```

```
   9 NAME   "Interface"
     DSTIF       1.1E+13   1.2E+12
:Rust+bond , corrosion penetration 0 micrometer on fi 20 for 38 MPa
and 2.9 MPa concrete
      USRIFC   BOTH
      USRVAL  0   0.4    0.06    4.00E-03
                     0   3.800E+07    1.00  2.90E+6
              1.35E-04   3.800E+07    0.86  290
              2.80E-04   3.789E+07    0.78  0
              4.11E-04   3.770E+07    0.72  0
              6.21E-04   3.663E+07    0.65  0
              8.30E-04   3.568E+07    0.59  0
              1.07E-03   3.306E+07    0.56  0
              1.51E-03   2.877E+07    0.52  0
              1.90E-03   2.675E+07    0.52  0
              2.60E-03   2.440E+07    0.52  0
              4.71E-03   2.056E+07    0.52  0
              1.21E-02   2.569E+06    0.52  0
              1.50E+20   0.000E+00    0.52  0

: At time 0 is the rust thickness=0 and at time 1E6 is the rust
: thickness also= 0.0
                  0 0
                  1E6 0.0
                  14E9 2.0  8.00E-3  0E-6 7.0
      USRSTA  0.0  0.0  0.0  0.0  0.0  0.0  0.0
                1.10E+13   0.0 0.0 0.0 0.0 0.0
      USRIND  0 13 2

  10 NAME   "WoodBoard"
     YOUNG   1.60000E+009
     POISON  3.50000E-001
     DENSIT  6.00000E+002

  11 NAME   "Steel"
     YOUNG   2.10000E+011
     POISON  3.00000E-001
     DENSIT  7.80000E+003
     YIELD  VMISES
     HARDEN STRAIN
     HARDIA  4.90000E+008 0.00000E+000  6.30000E+008 1.14000E-001
```

Parameters for the bond model

**Geometry and Data properties' input**

```
'GEOMET'
   1 NAME   "Int8"
     XAXIS   0.00000E+000  6.015179E+000  -1.81487471E+000 } *
   2 NAME   "DummyBeam"
     CIRCLE  1.50000E-004
   3 NAME   "WoodBoard"
   4 NAME   "SteelPlate"
   5 NAME   "Concrete"
   6 NAME   "Reinforcement"
   7 NAME   "Stirrups"
     CROSSE  7.90000E-005
   8 NAME   "TopBar"
     CROSSE  2.01000E-004
   9 NAME   "Strengthening"
     CROSSE  3.14000E-004
  10 NAME   "Int1"
     XAXIS   0.00000E+000  5.536681E+000  2.97006014E+000
  11 NAME   "Int2"
     XAXIS   0.00000E+000  1.814874E+000  6.015174049E+000
  12 NAME   "Int3"
     XAXIS   0.00000E+000  -2.97006E+000  5.536680571E+000
  13 NAME   "Int4"
     XAXIS   0.00000E+000  -6.015174E+000  1.81487471E+000
  14 NAME   "Int5"
     XAXIS   0.00000E+000  -5.53668E+000  -2.97006014E+000
  15 NAME   "Int6"
     XAXIS   0.00000E+000  -1.814875E+000  -6.01517405E+000
  16 NAME   "Int7"
     XAXIS   0.00000E+000  2.97006E+000  -5.53668057E+000
```

* Definition of local coordinate axis for interface elements

```
'DATA'
   2 NAME   "Concrete"
   3 NAME   "Reinforcement"
  14 NAME   "WoodBoard"
  15 NAME   "SteelPlate"
  12 NAME   "DummyBeam"
   5 NAME   "Interface"
  13 NAME   "Int1"
   6 NAME   "TopBar"
   8 NAME   "Stirrups"
  17 NAME   "Strengthening"
  18 NAME   "Int2"
  19 NAME   "Int3"
  20 NAME   "Int4"
  21 NAME   "Int5"
  22 NAME   "Int6"
  23 NAME   "Int7"
  24 NAME   "Int8"
```

Definition of data

## Assignment of material, data and geometry for 3D elements

```
MATERI
/ 1-67218 / 1
/ 68467-74951 / 5
/ 79001-79015 / 6
/ 74952-78631 / 9
/ 79172-79483 / 10
/ 79588-79899 / 11

DATA
/ 1-67218 / 2
/ 68467-74951 / 3
/ 79172-79483 / 14
/ 79588-79899 / 15
/ 79001-79015 / 12
/ 74961 74963 74968 74986 74987 74989 75003 75005 75029 75030 75284
            .
            .
  78285-78351 78357-78362 78377-78380 / 13
/ 74962 74964 74969 74970 74978 74981 74983 74999 75004 75031 75285
            .
            .
  78073 78074 78081 78083 78084 78087 78088 78095-78098 / 18
/ 74957 74958 74967 74971 74979 74980 74982 74993 75000 75010
            .
            .
  78082 78085 78086 78089 78090 78092 / 19
/ 74955 74956 74965 74966 74992 74994 75009 75011 75022 75023 75999
            .
            .
  78094 78099-78162 78166-78175 78179-78183 78190-78193 / 20
/ 74972 74977 74984 74985 74995 74996 75008 75016 75017 75019
            .
            .
  78178 78184-78189 78194-78257 78260-78265 78269-78273 78282-78284 /
  21
/ 74954 74973 74975 74976 74997 74998 75018 75020 75021 75026
            .
            .
  78381-78444 78450 78460 78461 78464 78465 78469 78470 / 22
/ 74952 74953 74974 74991 75001 75002 75012 75013 75024 75025
            .
            .
  77845-77847 78539-78543 78545-78547 78550-78631 / 23
/ 74959 74960 74988 74990 75006 75007 75014 75015 75027 75028 75177
            .
            .
  78451-78459 78462 78463 78466-78468 78471-78538 78544 78548 78549 /
  24
```

```
GEOMET
/ 79001-79015 / 2
/ 79172-79483 / 3
/ 79588-79899 / 4
/ 1-67218 / 5
/ 68467-74951 / 6
/ 74961 74963 74968 74986 74987 74989 75003 75005 75029 75030 75284
            .
            .
  78285-78351 78357-78362 78377-78380 / 10
/ 74962 74964 74969 74970 74978 74981 74983 74999 75004 75031 75285
            .
            .
  78073 78074 78081 78083 78084 78087 78088 78095-78098 / 11
/ 74957 74958 74967 74971 74979 74980 74982 74993 75000 75010
            .
            .
  78082 78085 78086 78089 78090 78092 / 12
/ 74955 74956 74965 74966 74992 74994 75009 75011 75022 75023 75999
            .
            .
  78094 78099-78162 78166-78175 78179-78183 78190-78193 / 13
/ 74972 74977 74984 74985 74995 74996 75008 75016 75017 75019
            .
            .
  78178 78184-78189 78194-78257 78260-78265 78269-78273 78282-78284 /
  14
/ 74954 74973 74975 74976 74997 74998 75018 75020 75021 75026
            .
            .
  78381-78444 78450 78460 78461 78464 78465 78469 78470 / 15
/ 74952 74953 74974 74991 75001 75002 75012 75013 75024 75025
            .
            .
  77845-77847 78539-78543 78545-78547 78550-78631 / 16
/ 74959 74960 74988 74990 75006 75007 75014 75015 75027 75028 75177
            .
            .
  78451-78459 78462 78463 78466-78468 78471-78538 78544 78548 78549 /
  1
```

## Definition of embedded reinforcement

```
'REINFORCEMENTS'
LOCATI
   1 BAR
     LINE   16454 16455
     LINE   16455 16456
     LINE   16456 16457
            .
            .
   2 BAR
     LINE   16504 16505
     LINE   16505 16506
     LINE   16506 16507
            .
            .
   3 BAR
     LINE   16554 16555
     LINE   16555 16556
     LINE   16556 16557
            .
            .
   4 BAR
     LINE   16604 16605
     LINE   16605 16606
     LINE   16606 16607
            .
            .
   5 BAR
     LINE   16654 16655
     LINE   16655 16656
     LINE   16656 16657
            .
            .
   6 BAR
     LINE   16701 16702
     LINE   16702 16703
     LINE   16703 16704
            .
            .
   7 BAR
     LINE   17235 17236
     LINE   17236 17237
     LINE   17237 17238
            .
            .
   8 BAR
     LINE   17251 17252
     LINE   17252 17253
     LINE   17253 17254
            .
            .
   9 BAR
     LINE   17268 17269
     LINE   17269 17270
     LINE   17270 17271
            .
            .
  10 BAR
     LINE   17284 17285
     LINE   17285 17286
     LINE   17286 17287
            .
            .
```

### Assignment of materials, data and geometry for embedded reinforcement

```
MATERI
/ 5 6 / 2
/ 1-4 / 3
/ 7-10 / 7

GEOMET
/ 1-4 / 7
/ 5 6 / 8
/ 7-10 / 9

DATA
/ 5 6 / 6
/ 1-4 / 8
/ 7-10 / 17
```

### Definition of loads

```
'LOADS'
CASE 1
WEIGHT
3 -9.81000E+000

:CASE 2
:DEFORM
:17167 TR 3 -1.00000E-003
:DEFORM
:17168 TR 3 -1.00000E-003
:DEFORM
:17173 TR 3 -1.00000E-003
:DEFORM
:17176 TR 3 -1.00000E-003
:DEFORM
:17177 TR 3 -1.00000E-003
:DEFORM
:17183 TR 3 -1.00000E-003
:DEFORM
:17209 TR 3 -1.00000E-003
:DEFORM
:17210 TR 3 -1.00000E-003
:DEFORM
:17211 TR 3 -1.00000E-003
:DEFORM
:17212 TR 3 -1.00000E-003
:DEFORM
:17215 TR 3 -1.00000E-003
:DEFORM
:17216 TR 3 -1.00000E-003
:DEFORM
:17222 TR 3 -1.00000E-003
:DEFORM
:17223 TR 3 -1.00000E-003
```

Phased analysis

## Element groups

```
'GROUPS'
ELEMEN
 506 "ConcreteBeam" / 1-67218 /
 509 "Reinforcement #1" / 68467-69760 /
 510 "Reinforcement #2" / 69761-71105 /
 511 "Reinforcement #3" / 71106-72407 /
 512 "Reinforcement #4" / 72408-73716 /
 513 "Reinforcement #5" / 73717-74951 /
 515 "Int1" / 74961 74963 74968 74986 74987 74989 75003 75005 75029
            .
            .
78285-78351 78357-78362 78377-78380 /
 516 "Int2" / 74962 74964 74969 74970 74978 74981 74983 74999 75004
            .
            .
78095-78098 /
 517 "Int3" / 74957 74958 74967 74971 74979 74980 74982 74993 75000
            .
            .
78069 78070 78072 78075-78078 78082 78085 78086 78089 78090 78092 /
 518 "Int4" / 74955 74956 74965 74966 74992 74994 75009 75011 75022
            .
            .
78091 78093 78094 78099-78162 78166-78175 78179-78183 78190-78193 /
 519 "Int5" / 74972 74977 74984 74985 74995 74996 75008 75016 75017
            .
            .
78284 /
 520 "Int6" / 74954 74973 74975 74976 74997 74998 75018 75020 75021
            .
            .
78381-78444 78450 78460 78461 78464 78465 78469 78470 /
 521 "Int7" / 74952 74953 74974 74991 75001 75002 75012 75013 75024
            .
            .
77847 78539-78543 78545-78547 78550-78631 /
 522 "Int8" / 74959 74960 74988 74990 75006 75007 75014 75015 75027
            .
            .
78548 78549 /
 534 "DummySuspension" / 79001-79015 /
 536 "WoodBoard" / 79172-79483 /
 538 "SteelPlate" / 79588-79899 /
```

**Boundary conditions and constraints**

```
'SUPPOR'
/ 14401-14403 14581-14591(5) 14592 14593
14605-14611(3) 14334-14336 14580 14583-14585
14587-14590 14276-14278 14574-14579 14594
14595 1-65 67-86 88-594 14582 14596-14604
14606 14607 14612 14613 14609 14610 14521-14523
14460-14462 / TR 1
/ 1348 2124 5856-5868 / TR 3
:/ 17167 17168 17173 17176 17177 17183
:17209-17212 17215 17216 17222 17223 / TR 3
/ 1348 2124 5856-5868 / RO 1
/ 1348 2124 5856-5868 / RO 3
1348 TR 2
```

Phased analysis

```
'TYINGS'
ECCENT TR 2
/ 1347 1349 / 1348
ECCENT TR 2
/ 5894 5869 / 5856
ECCENT TR 2
/ 5893 5870 / 5857
ECCENT TR 2
/ 5892 5871 / 5858
ECCENT TR 2
/ 5891 5872 / 5859
ECCENT TR 2
/ 5890 5873 / 5860
ECCENT TR 2
/ 5889 5874 / 5861
ECCENT TR 2
/ 5888 5875 / 5862
ECCENT TR 2
/ 5887 5876 / 5863
ECCENT TR 2
/ 5886 5877 / 5864
ECCENT TR 2
/ 5885 5878 / 5865
ECCENT TR 2
/ 5884 5879 / 5866
ECCENT TR 2
/ 5883 5880 / 5867
ECCENT TR 2
/ 5882 5881 / 5868
ECCENT TR 2
/ 2125 2123 / 2124
'END'
```

Link between slave- and master nodes

# APPENDIX E

## Command file for three-dimensional simulation

```
*FILOS
 INITIA
*INPUT
*FORTRAN
 TAKE "usrifc.f"
*PHASE

*INPUT
READ TABLE LOADS
READ TABLE SUPPORTS
*FORTRAN
 TAKE "usrifc.f"
*PHASE

BEGIN ACTIVE
 ELEMENT ALL
 REINFO ALL
END ACTIVE
*NONLIN

 BEGIN TYPE
    BEGIN PHYSIC
    END PHYSIC
  END TYPE

BEGIN OUTPUT
   FXPLUS
   FILE "1"
 END OUTPUT

BEGIN OUTPUT
   FXPLUS
   FILE "2"
 END OUTPUT

  BEGIN EXECUTE
   BEGIN LOAD
    LOADNR=1
     BEGIN STEPS
      BEGIN EXPLIC
      SIZES 1.0(1)
     END EXPLIC
     END STEPS
    END LOAD
    BEGIN ITERAT
      METHOD NEWTON REGULA
:      METHOD SECANT BFGS
      MAXITE=100
:      LINESE
      BEGIN CONVER
        ENERGY CONTIN TOLCON=0.0001
        FORCE CONTIN TOLCON=0.01
        DISPLA CONTIN TOLCON=0.01
```

First phase

Second phase

Common for both phases

Output saved in file ”1” for first phase

Output saved in file “2” for second phase

First load; self weight

First load applied in one step

Iteration method

Convergence criterion

```
      END CONVER
    END ITERAT
    SOLVE GENEL
  END EXECUT
*END

BEGIN EXECUTE                                  Only for second phase
   BEGIN LOAD
    LOADNR=2
     BEGIN STEPS
      BEGIN EXPLIC
      SIZES 0.15(60)                           Step size and number of steps
     END EXPLIC
     END STEPS
    END LOAD
    BEGIN ITERAT
      CONTIN
      METHOD NEWTON REGULA                     Iteration method
:      METHOD SECANT BFGS
      MAXITE=350
:      LINESE
      BEGIN CONVER
        ENERGY CONTIN TOLCON=0.0001
        FORCE CONTIN TOLCON=0.01               Convergence criterion
        DISPLA CONTIN TOLCON=0.01
      END CONVER
    END ITERAT
    SOLVE GENEL
  END EXECUT
*END
```

# APPENDIX F

## Arrangement of LVDTs in the first beam test

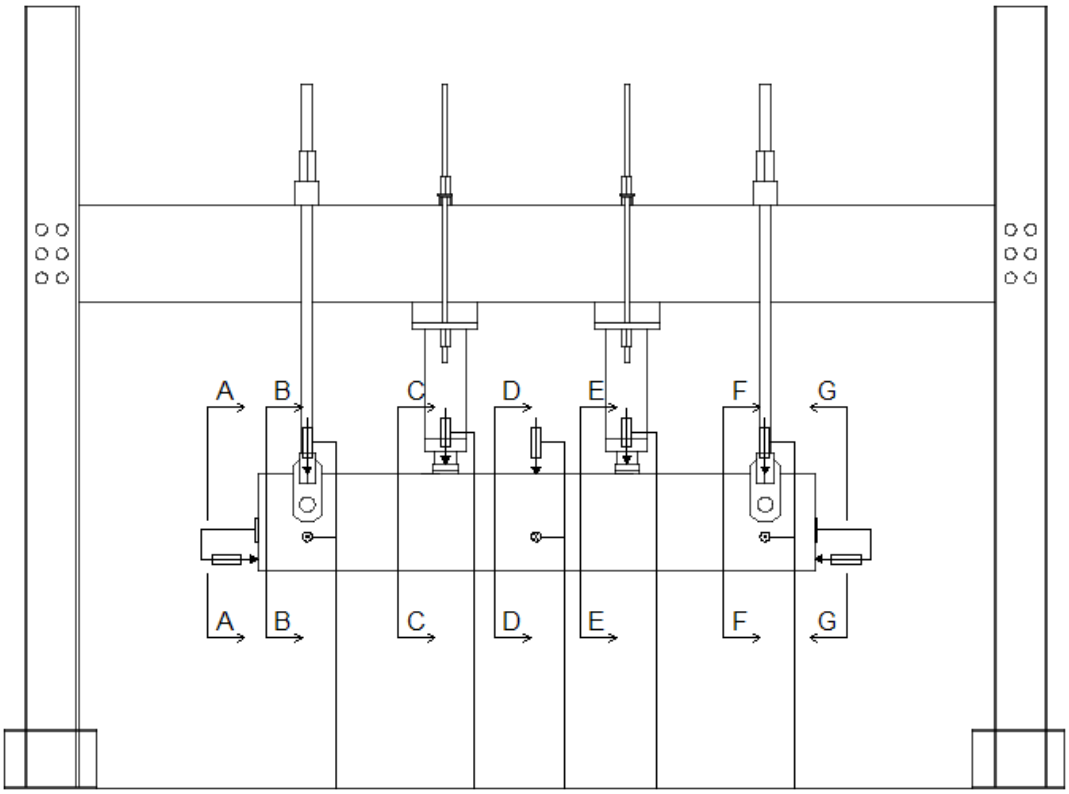


*Figure F.1. Arrangement of LVDTs and their reference points.*

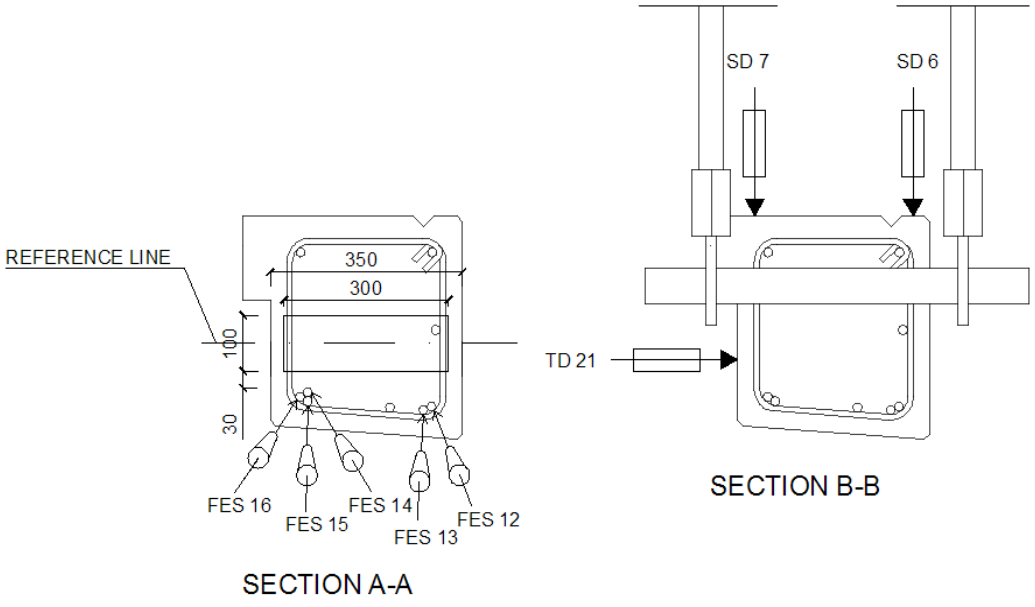

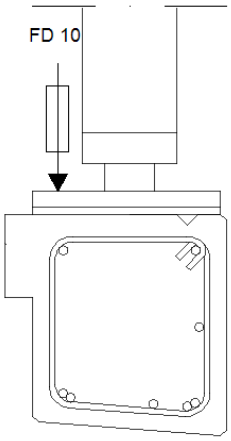


SECTION C-C

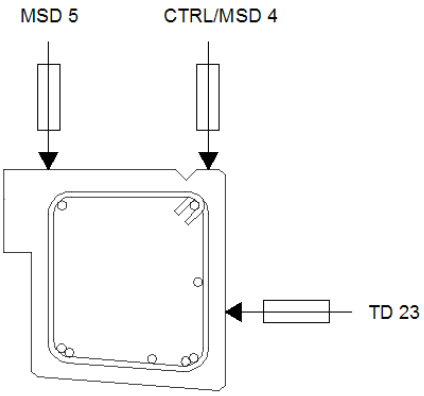


SECTION D-D

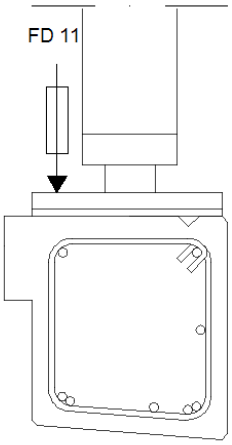


SECTION E-E

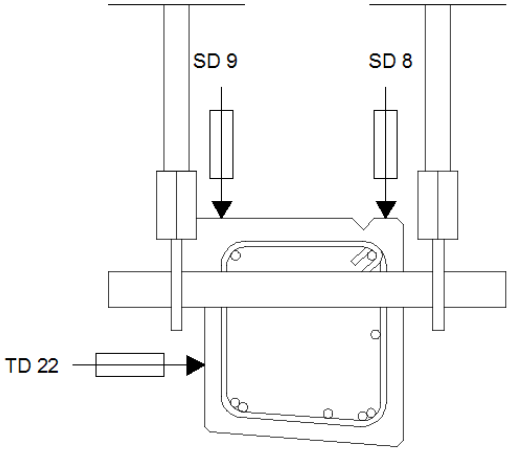


SECTION F-F

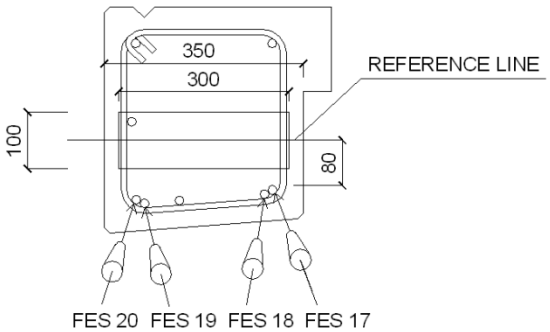


SECTION G-G

*Table F.1. Tolerances of LVDT*

| LVDT | Tolerance [mm] |
|---|---|
| CRTL/MSD 4 | ±50 |
| MSD 5 | ±50 |
| SD 6-9 | ±5 |
| FD 10-11 | ±22.5 |
| FES 12-20 | ±5 |
| TD 21-23 | ±20 |

*Figure F.2. Detailed arrangement of LVDTs.*

# APPENDIX G

## Arrangement of LVDTs in the second beam test

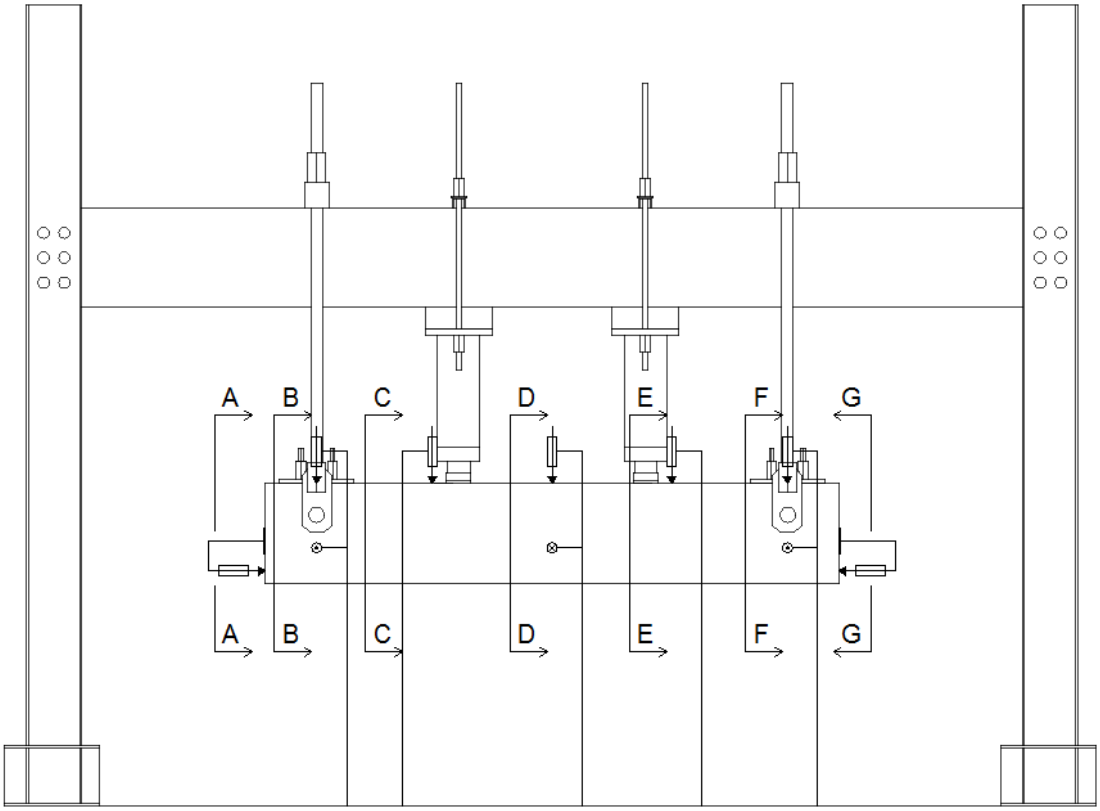


*Figure G.1. Arrangement of displacement transducers and their reference point.*

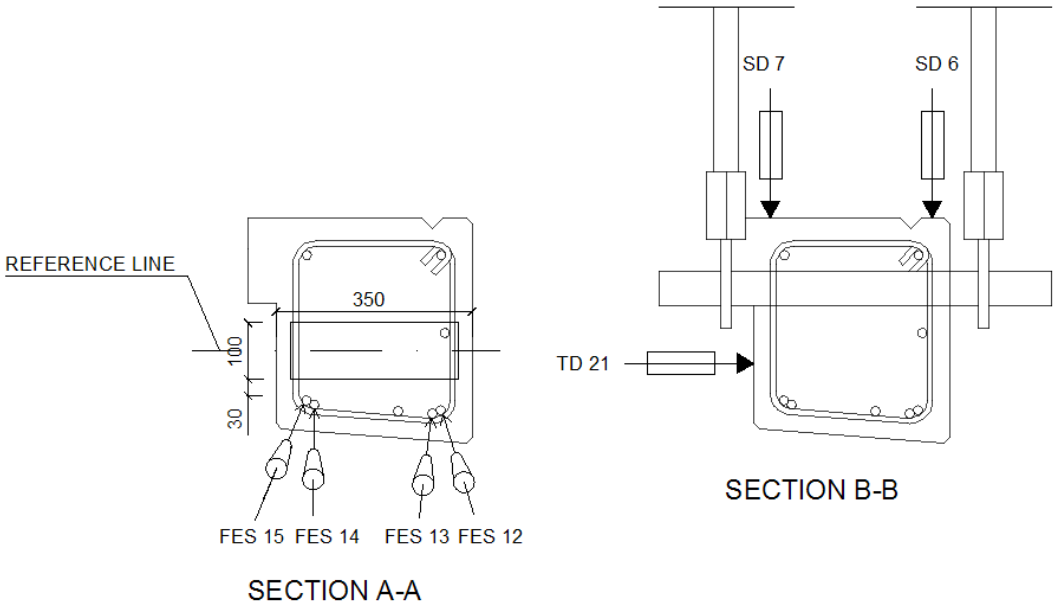

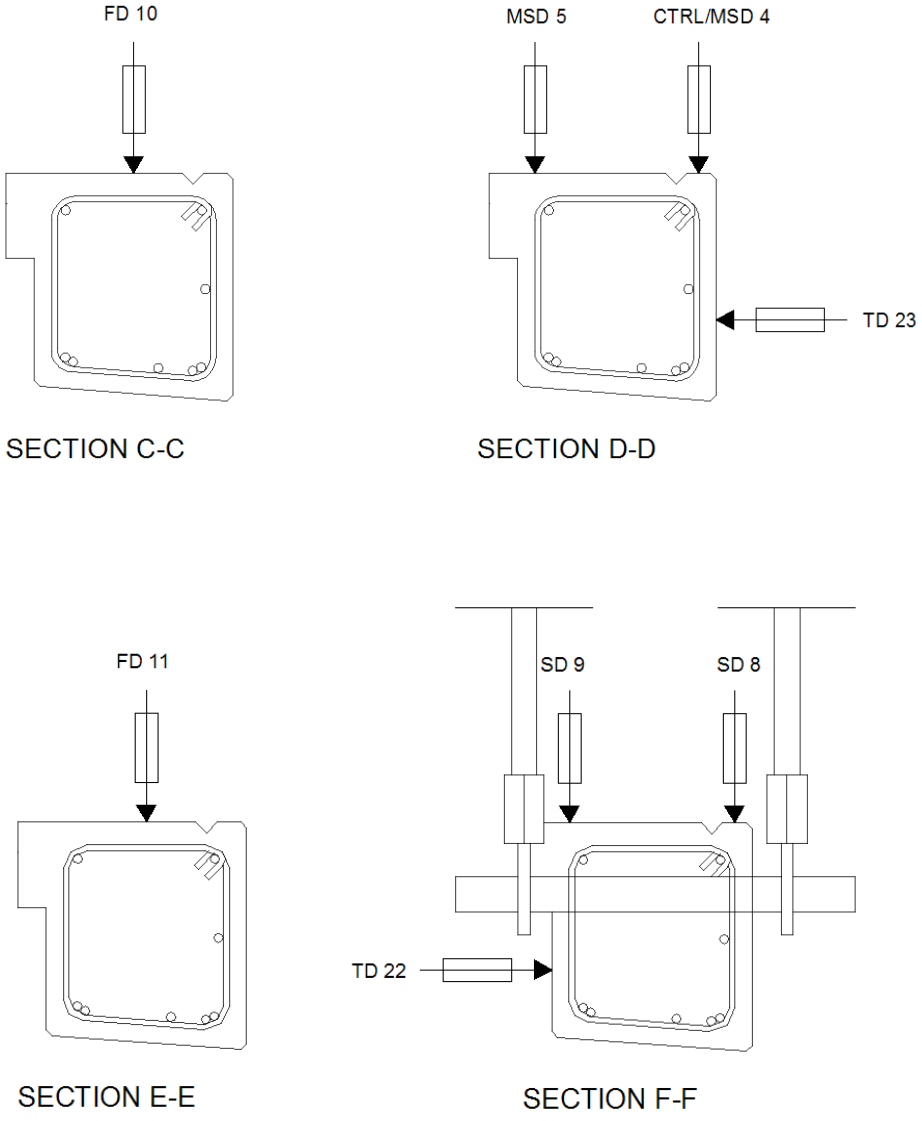


*Figure G.2. Detailed arrangement of LVDTs.*

*Table G.1. Tolerances of LVDT*

| LVDT | Tolerance [mm] |
|---|---|
| CRTL/MSD 4 | ±50 |
| MSD 5 | ±50 |
| SD 6-9 | ±5 |
| FD 10-11 | ±22.5 |
| FES 12-20 | ±5 |
| TD 21-23 | ±20 |

# APPENDIX H

## Initial crack pattern of the first beam test

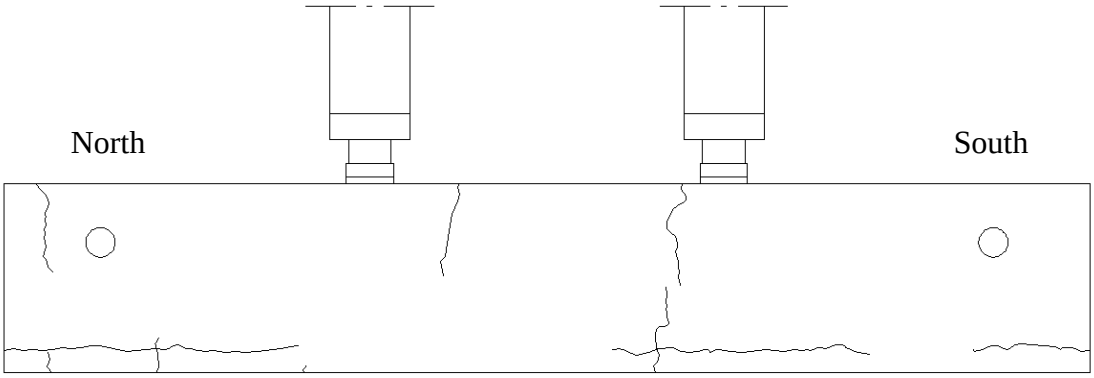


*Figure H.1. Elevation: West (front).*

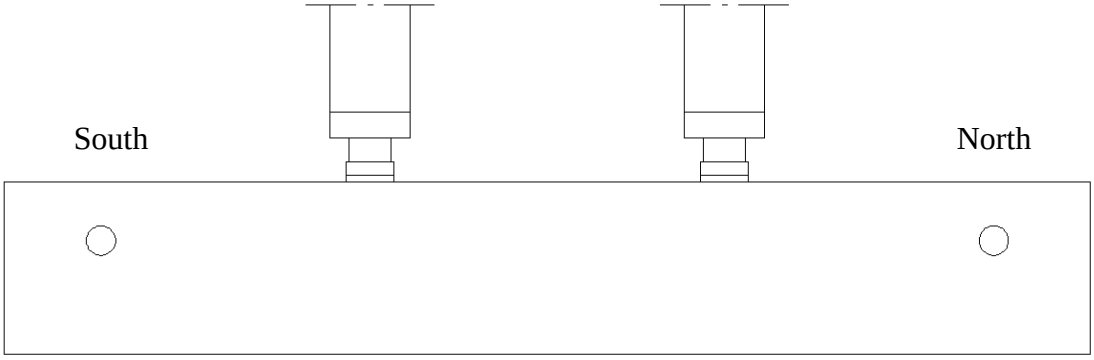


*Figure H.2 Elevation: East (back).*

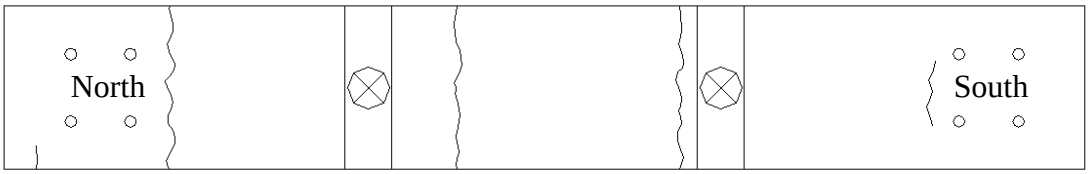


*Figure H.3. Plan:Top.*


*Figure H.4. Plan: Bottom.*

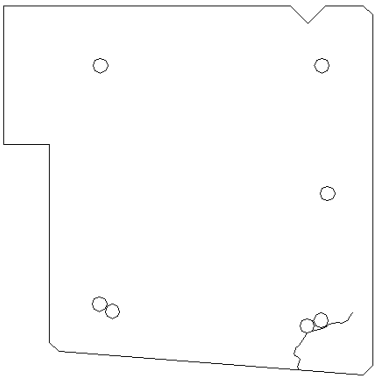

*Figure H.5. Section: North short face.*

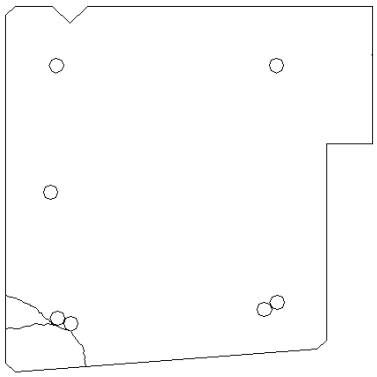

*Figure H.6. Section: South short face.*

# APPENDIX I

## Final crack pattern of the first beam test

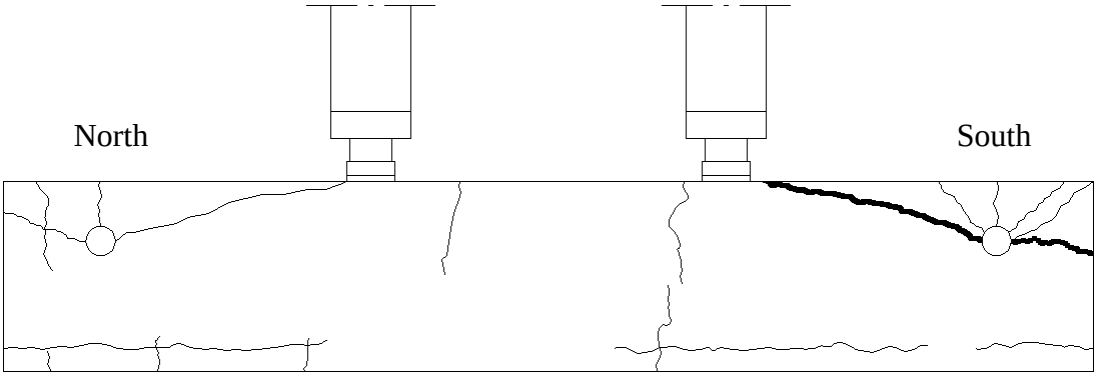


*Figure I.1. Elevation: West (front).*

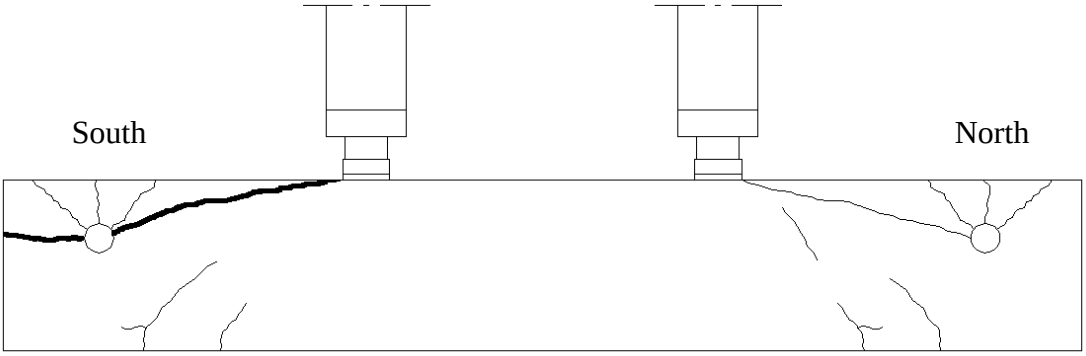


*Figure I.2. Elevation: East (back).*

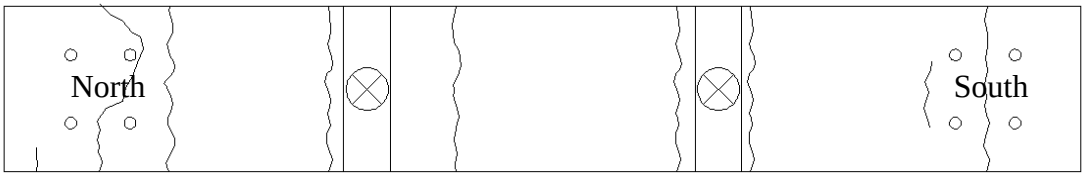


*Figure I.3. Plan: Top.*

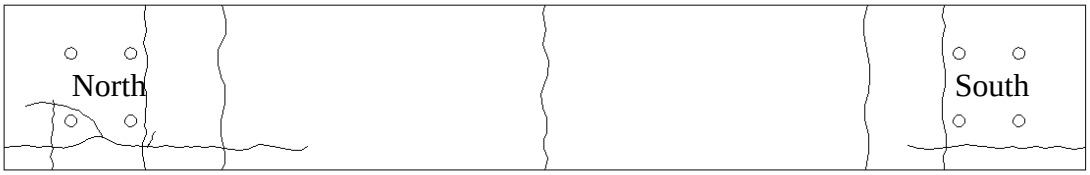


*Figure I.4. Plan: Bottom.*

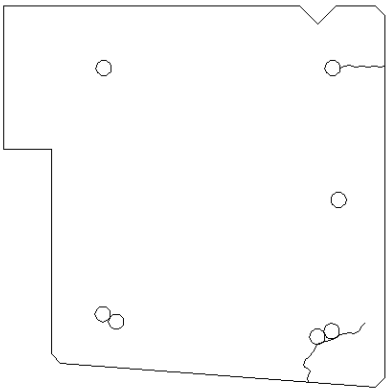

*Figure I.5. Section: North short face.*

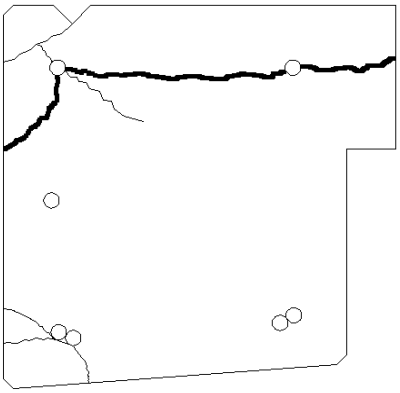

*Figure I.6.Section: South short face.*

*Figure I.7. Elevation: West (front). Critical inclined shear crack.*

*Figure I.8. Elevation: East (back). Critical inclined shear crack.*

*Figure I.9. Section: South short face. Critical splitting cracks radiating out from the compressive reinforcement.*

# APPENDIX J

## Initial crack pattern of the second beam test

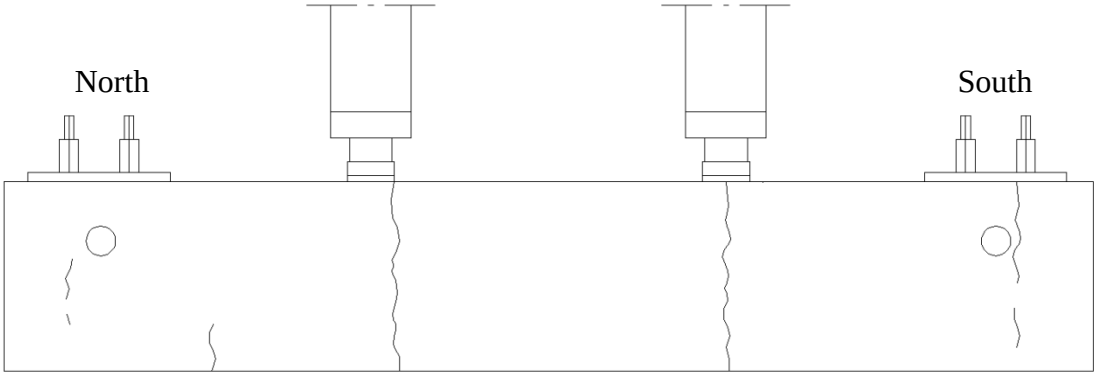


*Figure J.1. Elevation: West (front).*

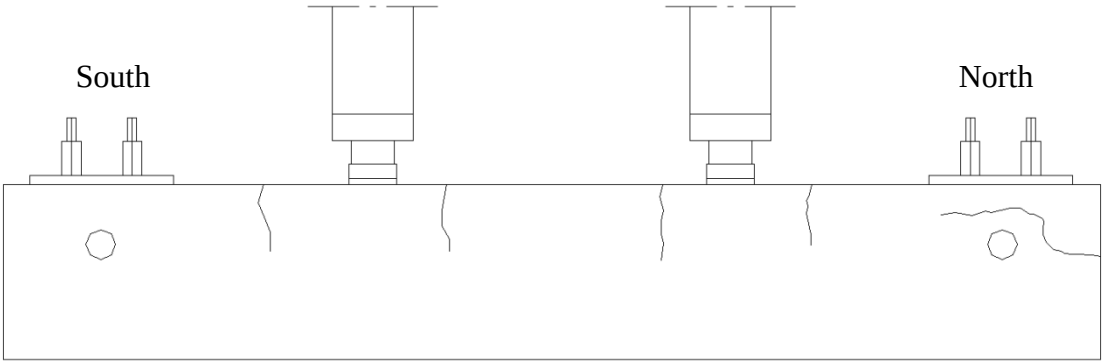


*Figure J.2. Elevation: East (back).*

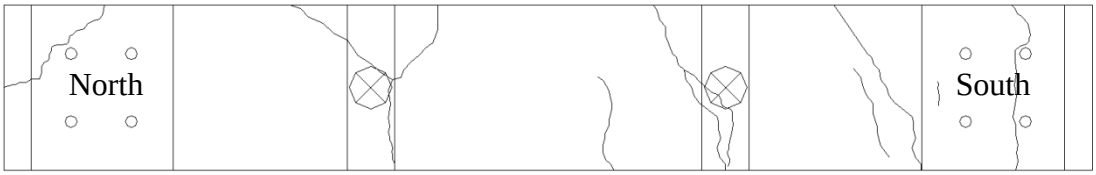


*Figure J.3. Plan: Top.*


*Figure J.4. Plan: Bottom.*

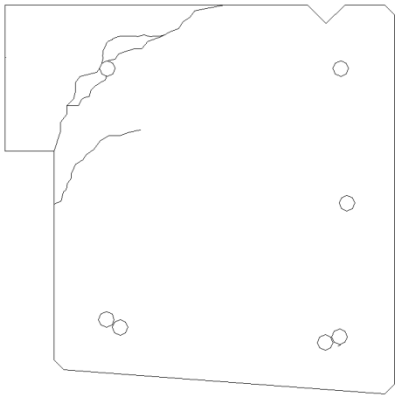

*Figure J.5. Section: North short face.*

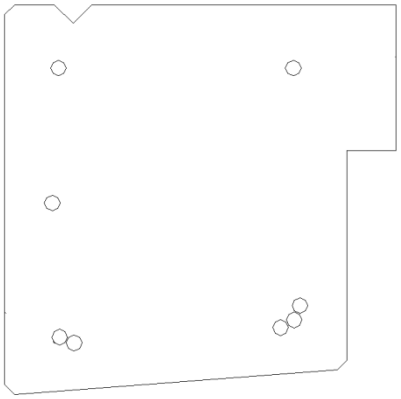

*Figure J.6. Section: South short face.*

# APPENDIX K

## Final crack pattern of the second beam test

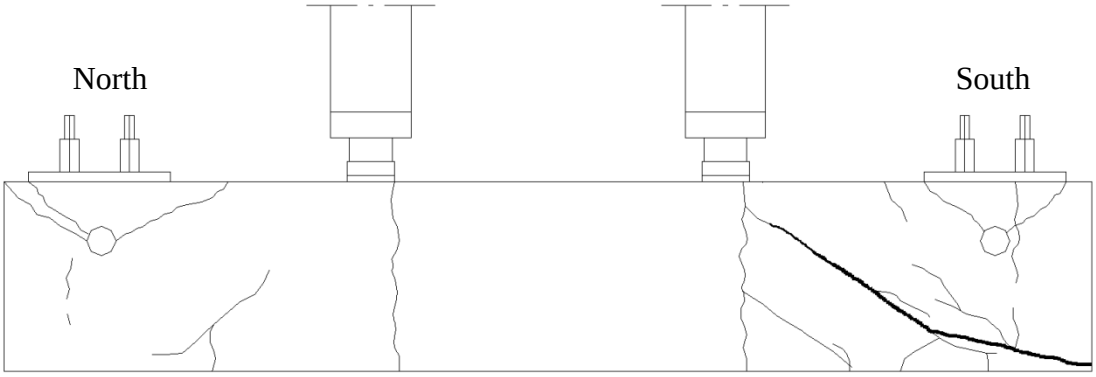


*Figure K.1. Elevation: West (front).*

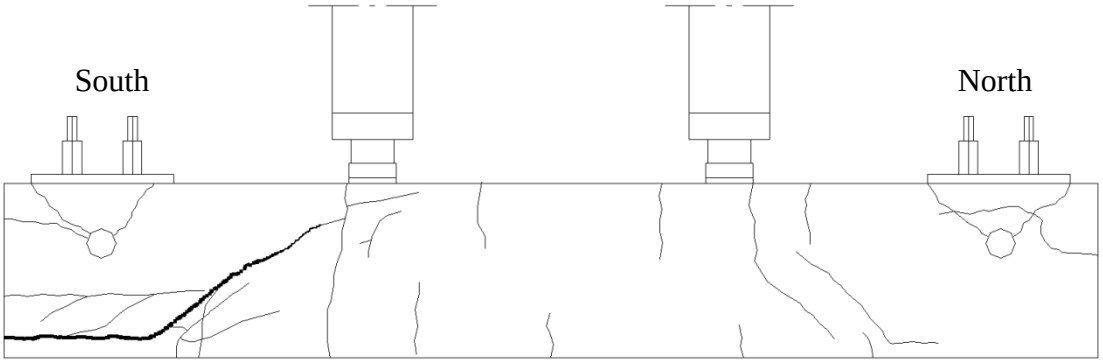


*Figure K.2. Elevation: East (back).*

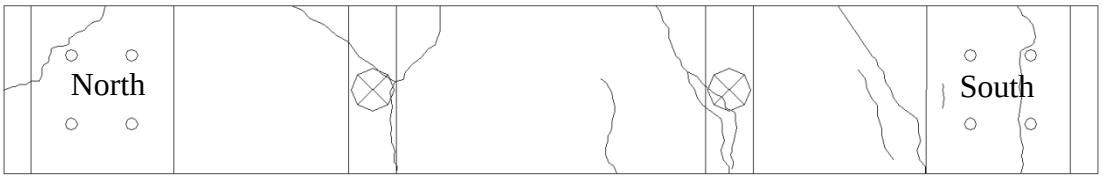


*Figure K.3. Plan: Top.*

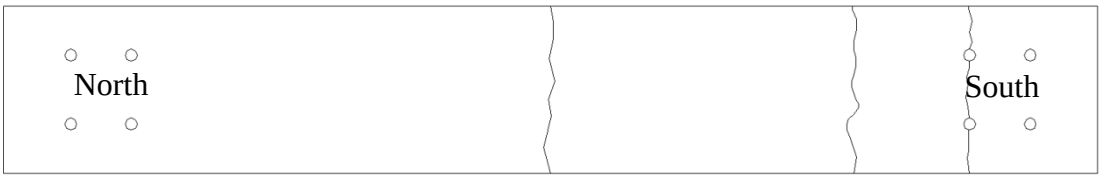


*Figure K.4. Plan: Bottom.*

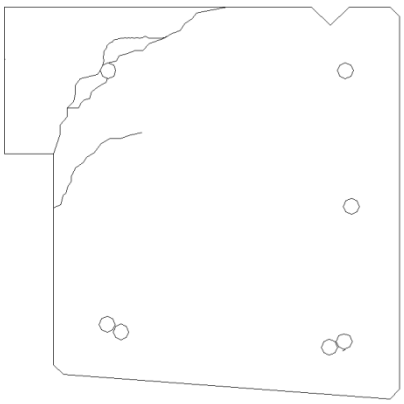

*Figure K.5. Section: North short face.*

*Figure K.6. Section: South short face.*

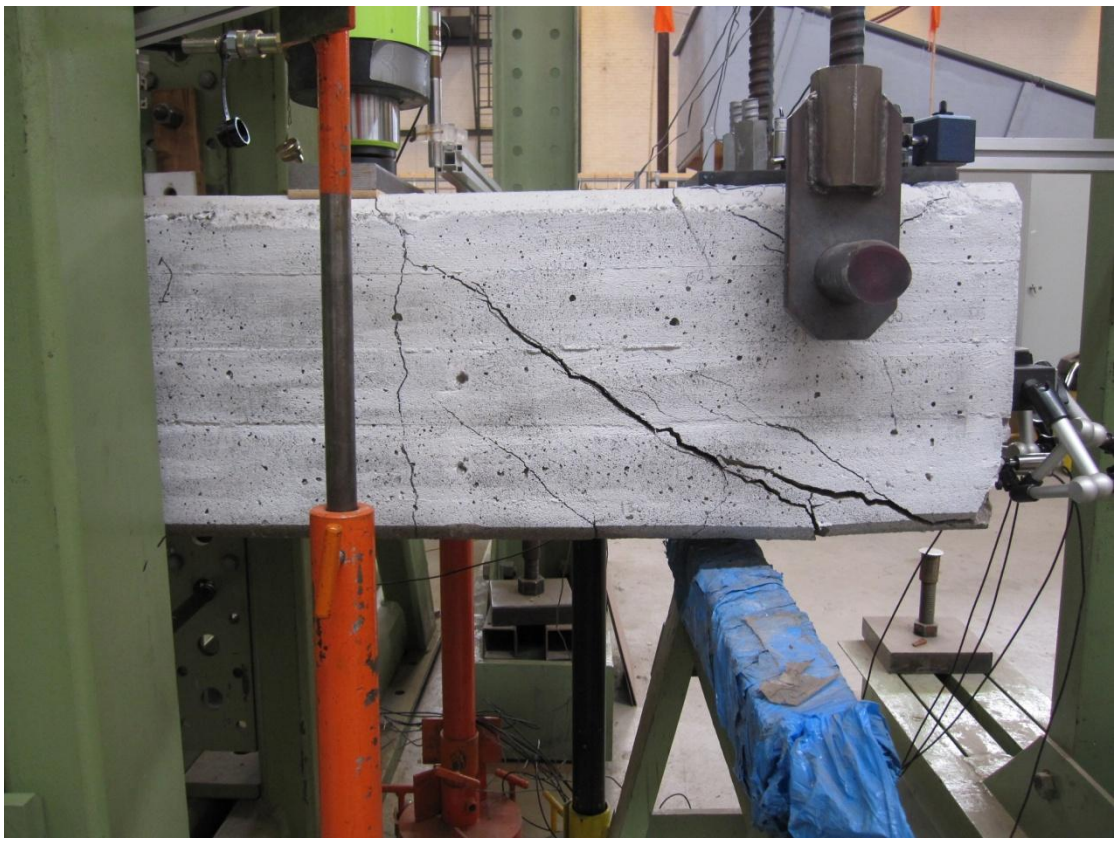

*Figure K.7. Elevation: West (front). Critical inclined shear crack.*

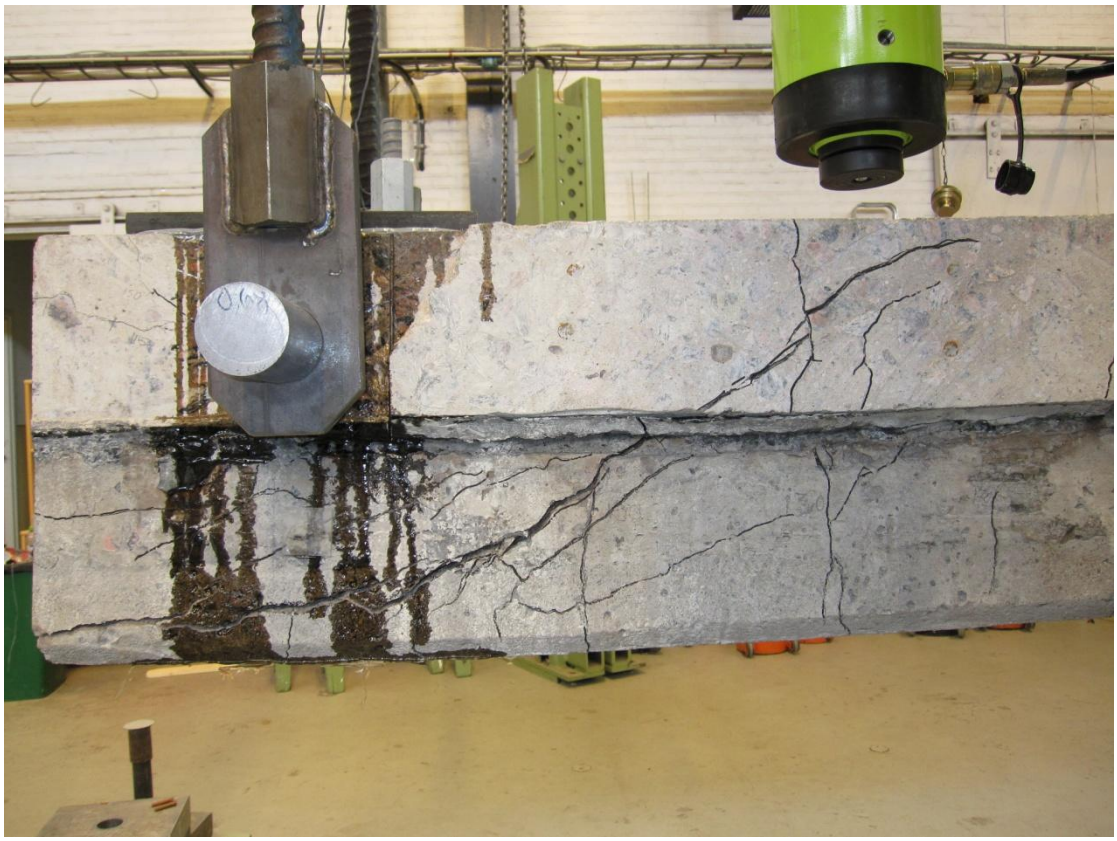

*Figure K.8. Elevation: East (back). Critical inclined shear crack.*

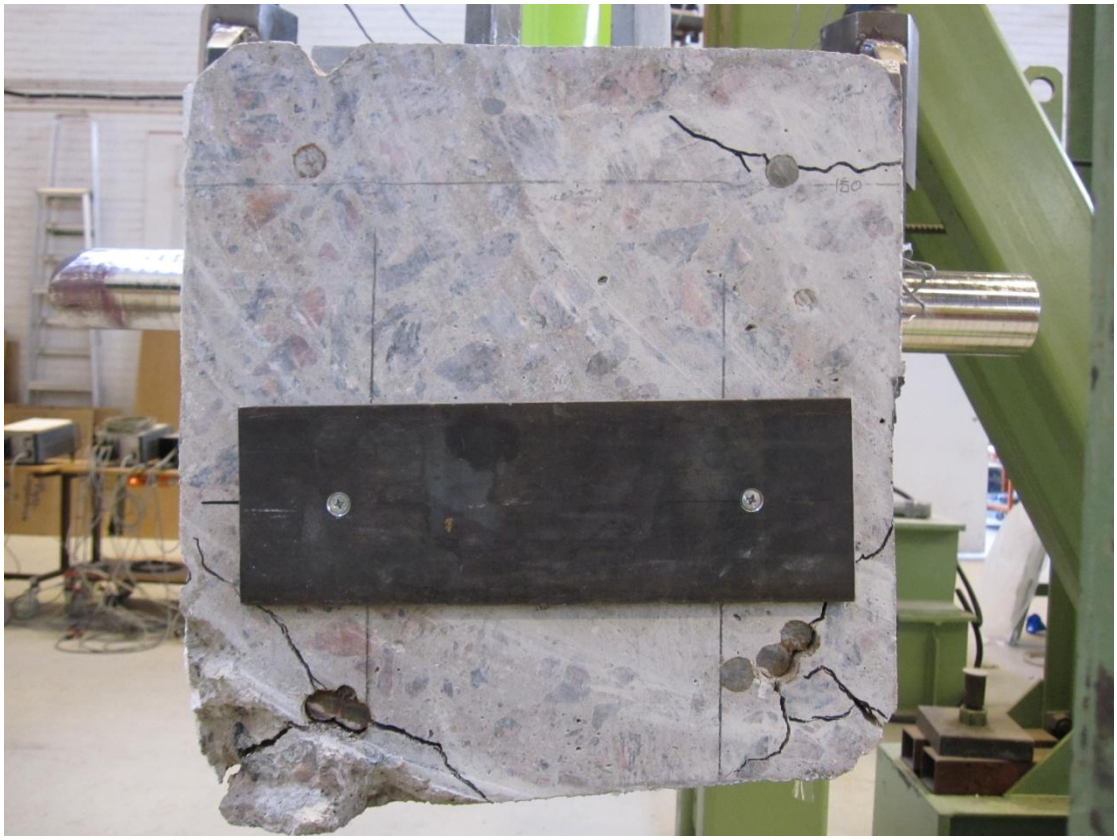

*Figure K.9. Section: South short face. Critical splitting cracks.*